Structural evaluation of a novel box beam system of Pultruded Fibre Reinforced Polymer shapes

Mark Evernden
MEng(Hons)

This report is submitted as partial fulfilment

of the requirements for the PhD Programme of the

School of Engineering

University of Warwick

2006

AUTHOR: Mark Evernden   DEGREE: PhD

TITLE: Structural evaluation of a novel box beam system of Pultruded Fibre Reinforced Polymer shapes

DATE OF DEPOSIT: ....

I agree that this thesis shall be available in accordance with the regulations governing the University of Warwick theses.

I agree that the summary of this thesis may be submitted for publication.

I **agree** that the thesis may be photocopied (single copies for study purposes only).

Theses with no restriction on photocopying will also be made available to the British Library for microfilming. The British Library may supply copies to individuals or libraries. subject to a statement from them that the copy is supplied for non-publishing purposes. All copies supplied by the British Library will carry the following statement:

> "Attention is drawn to the fact that the copyright of this thesis rests with its author. This copy of the thesis has been supplied on the condition that anyone who consults it is understood to recognise that its copyright rests with its author and that no quotation from the thesis and no information derived from it may be published without the author's written consent."

AUTHOR'S SIGNATURE: ....

USER'S DECLARATION

1. I undertake not to quote or make use of any information from this thesis without making acknowledgement to the author.

2. I further undertake to allow no-one else to use this thesis while it is in my care.

DATE   SIGNATURE   ADDRESS

....

....

....

....

....

Abstract

Presented in this thesis is an evaluation of a novel box beam system of Pultruded Fibre Reinforced Polymer (PFRP) shapes. The flat-pack modular beam system consists of separate PFRP flange and web shapes joined together with a new method of mechanical fastening. It is based on the first generation Startlink building system, conceived by UK engineers in 1999. The Startlink building system is introduced, and classified within the scope of Modern Methods of Construction (MMC), and its merits are discussed. In the context of MMC a critical review by the author finds that, although the proposed 1999 generation Startlink system offers design flexibility, it will probably have a limited market potential.

The novel use of the steel M10 Unistrut connection method as a means of fastening distinct PFRP shapes in a building system is characterised. Individual connector design parameters for joint stiffness and resistance are identified and determined, under pure shear loading. The results of a series of physical tests show no significant loss of stiffness or strength with long term environmental exposure. Values of key mechanical properties for design calculations are recommended.

A 400×200×2848 mm prototype PFRP box beam assembly is fabricated from two flange and two web panel-type shapes, cut from existing off-the-shelf PFRP shapes. This is 60 mm deeper than the largest single PFRP shape that could

be used as a beam. The assembly is joined at the web-flange junction with M10 Unistrut connectors set at various spacing's, in the range 50 to 400 mm. These connectors carry the longitudinal shear that is generated between the joined shapes when the modular assembly is in flexure. Theoretical deflections, calculated using a modified form of a partial-interaction analysis model developed for composite concrete and steel structures, are predicted for the assembly accounting for the finite shear stiffness of the web-flange connection. A series of 16 four-point bending load tests on the beam assembly, across two load arrangements, show that its performance is linked to the designated spacing of the M10 Unistrut connections. The flexural rigidity and degree of interaction present in the assembly are determined from analysis of vertical deflections and longitudinal strains, as the beam is deformed. The influence of secondary effects, due to the poor tolerances achieved in the hand fabrication of the beam's assembly, are found to greatly affect the ability of the deflection analysis to give the required measured deflections. Comparison of the effective joint shear rigidities obtained from theory and testing indicates a higher individual connection stiffness in the prototype beam than previously determined by way of the individual Unistrut connector characterisation.

It is found through the combined analytical and physical testing research that the M10 Unistrut connection method can only provide the necessary joint shear stiffness and resistance to the 400 mm deep beam if the connector spacing, along the four joints, is $\leq$ 50 mm. The total number of connectors this represents in the beam is likely to make this modular construction approach too expensive for it to be commercially viable. Although the M10 connector could be used to fabricate beams of lesser depths, since the number of connectors will then be reduced, these beams would find it difficult to compete with the available off-the-shelf PFRP beam shapes, of up to 300 mm deep. There is however scope to use the Unistrut

method of connection to provide longitudinal shear resistance in building systems where, for example, a floor panel is to be stiffened by a channel shaped beam and the overall depth is ≤ 300 mm.

The research work contained in this thesis has contributed to a radical change in the PFRP product offerings now proposed in the 2006 generation Startlink building system.

List of Publications

Conferences Publications

- Evernden, M. C. (2004). Structural performance of a new demountable PFRP box beam, *Oral presentation at the Institution of Structural Engineers 2004 Young Researchers Conference* 17th March 2004, London.

- (Peer-Reviewed) Evernden, M. C., Mottram, J. T. and Delhees, P. (2004). Characterisation of Uni-strut connectors for pultruded fibre reinforced plastic channels, *Proc. 1st International Conference on Innovative Materials and Technologies for Construction and Restoration (IMTCR04)*, Liguori Editore, Naples, Vol. 1, 620-632. ISBN 88 207 3678 0

- Evernden, M. C. and Mottram, J. T. (2005). Structural Performance of a Modular Box Beam Concept of Pultruded Fibre Reinforced Polymer Shapes, *3rd International Conference on Composite in Construction*, Lyon July 11-13th 2005, pp. 8.

Journal papers

- (Invited) Evernden, M. C., and Mottram, J. T. (Accepted March 2005). Characterisation of Unistrut connection method with pultruded fiber reinforced polymer channels, Special Issue of *Journal of Materials in Civil Engineering*, American Society of Civil Engineers. ISSN 0899-1561

Acknowledgements

I would like my family, friends, and colleagues to know that I greatly appreciate the assistance and support that they have provided me with during the course of my studies. I would also like to thank the following:

- Mark Singleton, of Startlink for his time and effort, I wish him all the best for the future.

- Geoff Calvert, of VisEng for his guidance and use of the photo-elastic equipment.

- Peter Delhees, of Mita Ltd. for supplying PFRP channel sections for the connection characterisation work.

- Fiberline Composites, for supplying PFRP materials for further work on the subject on modular PFRP beams.

- Colin Banks, for all his advice and help in the laboratory.

Above all I must thank Toby Mottram, without whose support and guidance much of the research work would not have been possible.

Contents

List of Tables

List of Figures

CHAPTER 1

Introduction

Fibre Reinforced Polymer's (FRP)'s are a group of composite materials that consists of brittle fibres embedded in a polymer matrix. The fibres provide stiffness and strength for the material, the role of the polymer matrix is to transfer load into the fibres and protect them. Unless stated otherwise the abbreviation FRP in the discussion to follow refers to a fibre reinforced polymer with the reinforcing glass fibres of type E. The manufacturing process of pultrusion (Starr, 2000) offers the most cost effective method of continuous production of constant cross section shapes suitable for use in the construction industry in similar way to which rolled steel sections are presently used.

Pultruded Fibre Reinforced Polymer (PFRP) shapes and systems offer distinct advantages over their steel competitors, which allow the designer to increase the efficiency and sustainability of the finished structure (Head, 1994). PFRP structures can be erected with less energy because shapes and systems are lightweight. Since the material also requires less energy to manufacture these factors lower the embodied energy of the structure. Since PFRP's can have a greater corrosion resistance than structural steels they are often used in aggressive environments such as marine, chemical and industrial situations.

In terms of manufacturing costs, a PFRP section can cost 50% more than the

equivalent steel product (Head, 1996). Higher costs are primarily due to tooling costs incurred in producing complex hollow or intricately detailed sections. Head (1995) recognized that complex optimized and modular PFRP systems of profiles could be produced without high labour costs using automated production such as pultrusion. Through the application of modularization in the detailing of such optimised systems, significant reductions in the manufacturing costs can be made, through reduction in the complexity of individual pultruded shapes. The use of such concepts with PFRP materials has increased the flexibility of the designer and opened new markets for PFRP components in construction away from its traditional role as an alternative material to structural steel sections. Most pultruded sections and shapes are used outside the construction sector (e.g. ladders).

The aims of this thesis are to introduce the concept of the Startlink PFRP building systems (Byers & Singleton, 1999)(Fig. 1.1) and to evaluate the flexural performance of a novel modular box beam assembly (Fig. 1.2). The new beam is based on the Startlink concept, and is assembled from separate PFRP flange and web shapes with mechanical fastenings by the Unistrut connection method (Unistrut, 2006)(Fig. 1.3). Throughout the thesis the term *composite-construction* is used to refer to the interaction between the individual structural shapes in a beam assembly in flexure.

The Startlink building system and the concepts of pre-fabrication, mass-production and modularisation in terms of house building systems are reviewed in Chapter 2. A brief review of the present state of the UK house building industry is given and the future role of Modern Methods of Construction (MMC) identified. A number of examples are given, detailing the evolution of these MMC's, and a discussion given on the intended application of PFRP systems as an alternative material to steel and timber for house construction.

An in-depth characterization of the strength and stiffness of the M10 Unistrut connection method with specific PFRP channel sections is detailed in Chapter 3. Design guidance, for the use and application of this connection method with beam assemblies, is proposed, and design values of SLS resistance and connection stiffness for the M10 Unistrut are determined for the Startlink building system.

Within Chapter 4 the application of modularisation to the design of a 400 mm deep structural PFRP box beam, consisting of off-the-shelf shapes is considered. The requirements of full-interaction between the shapes in the assembly, are discussed, in relevance to the Startlink beam system, and the advantages of such a building system presented. Chapter 5 details the experimental set-up and research methodology used to determined the performance, and the level, of composite-action achieved for a prototype modular PFRP box beam. The beam of span 2848 mm is tested under four-point bending with a constant moment length of between 800 - 400 mm. The maximum span was limited by the availability of off-the-shelf PFRP standard shapes. Two separate partial-interaction theoretical models predicting the load-deflection response of the prototype assembly accounting for the finite stiffness of the discrete shear connections (the Unistrut connectors) are presented.

Salient results from a series of full-scale four-point bending tests are presented in Chapter 6. The effectiveness of the Unistrut mechanical fastening method, as a means of supplying shear connection between the distinct web and flange shapes is assessed, based on the experimentally determined flexural rigidity attained at various degrees of shear connection supplied to the web-flange connections. Comparisons are made with the results of the theoretical analysis for partial-interaction developed in Chapter 5. The effect of the low stiffness inherent with the Unistrut connection and PFRP channel, on the flexural performance of the assembly is discussed in context of the comprehensive series of physical tests with

the prototype beam.

In Chapter 7 conclusions are given from research studies that have considered:

- the potential of the Startlink building system as a MMC,

- the performance of the M10 Unistrut connection method with its PFRP channels,

- and the performance of a modular PFRP box beam built of mechanically fasteners shapes,

- and the effect of low stiffness, discrete fasteners in flexural assemblies.

1.1 Figures
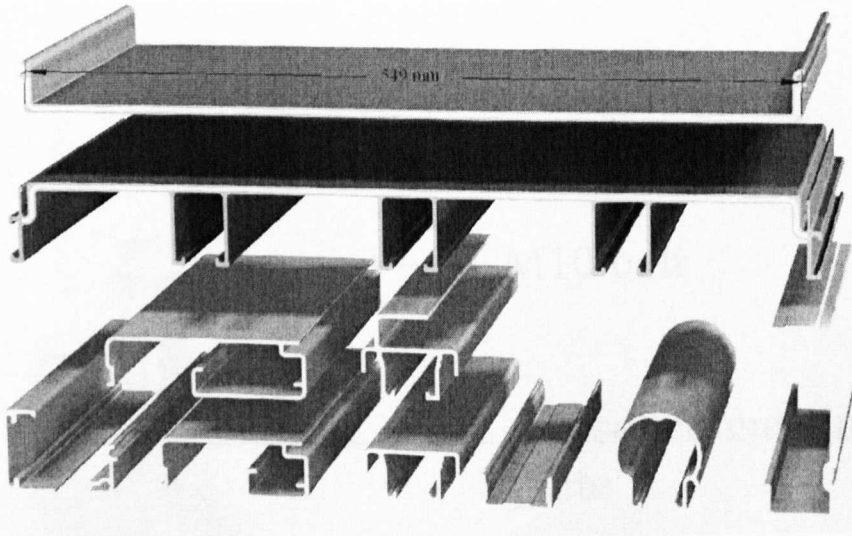
Figure 1.1: Startlink building system
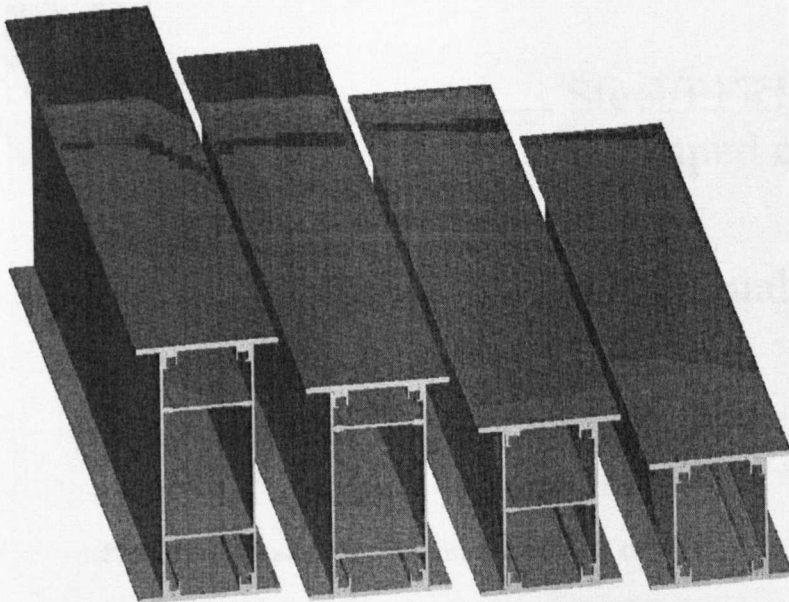
Figure 1.2: Proposed Startlink box beam system
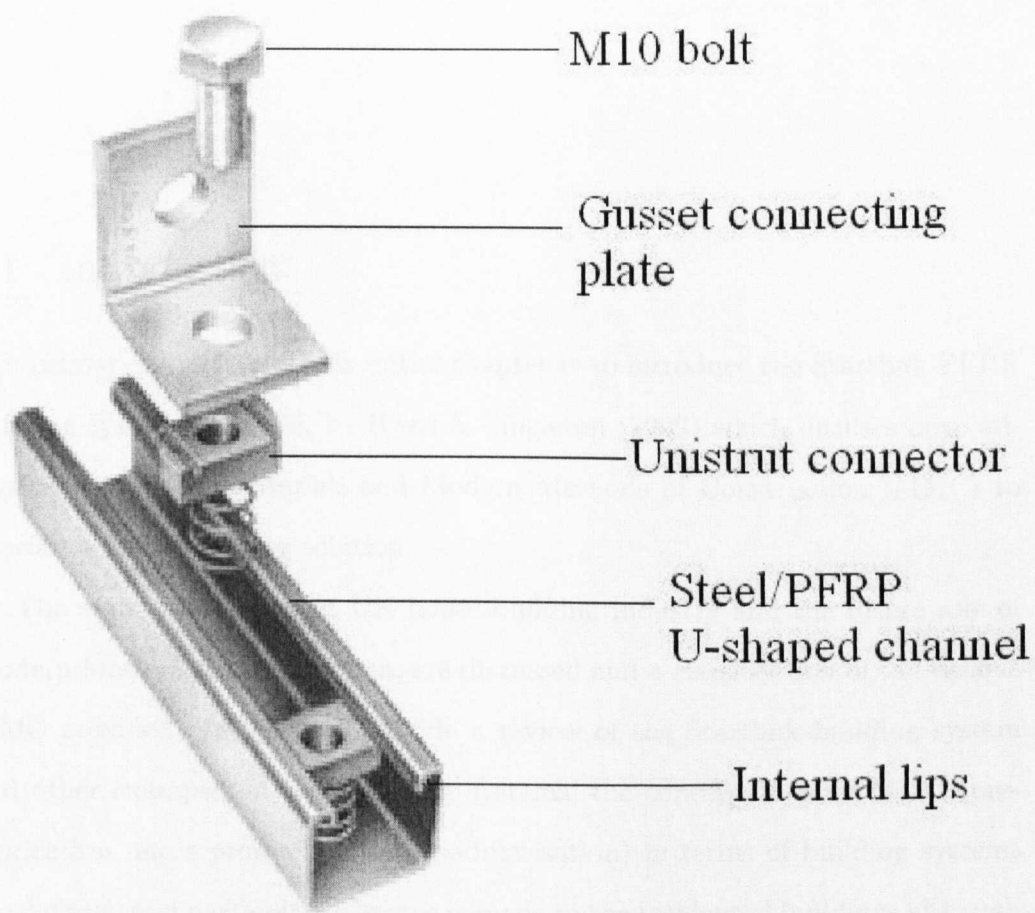
Figure 1.3: Standard Unistrut connection method

The labels in the figure point to the following parts:

- M10 bolt
- Gusset connecting plate
- Unistrut connector
- Steel/PFRP U-shaped channel
- Internal lips

CHAPTER 2

Modern Methods of Construction

2.1 Introduction

The primary objective of this initial chapter is to introduce the Startlink PFRP building system proposed, by Byers & Singleton (1999) which ultilises both advanced composites materials and Modern Methods of Construction (MMC) to provide a future housing solution.

The state of the present UK house building industry and the future role of Modern Method of Construction, are discussed and a classification of the various MMC provided. In order to provide a review of the Startlink building system and other examples of FRP housing systems, the concepts behind MMC (prefabrication, mass production and modularisation) in terms of building systems are defined, and particular reference is made to the residential buildings although the concepts apply equally to industrial applications. A brief review following the evolution of these manufacturing concepts in housing with the use of several noteworthy examples, indicate the ancestry of MMC, the bounds in which the concepts are fixed, and, the possible shortcomings of using these concepts in residential structures.

2.2 The present demand for Modern Methods of Construction (MMC)

A century after Henry Ford showed the world the true power that mass-production and pre-fabrication brought to the manufacturing industries, the same concepts are now embraced by the manufacturing industries as purveyors of quality and efficiency (LeCuyer, 2003). However, when these concepts are used in reference to a dwelling, it becomes synonymous with images of inadequate sub-standard factory style hut houses, reminiscent of military shelters.

Few of these manufacturing concepts have been absorbed into the house-building and construction industry, due to a decline in private investment in new materials and methods in the industry, following the growth of the more lucrative automotive and aerospace industries (Head, 1994) in the mid 19th Century. The present result is a low-technology and labour-intensive construction industry (SERC, 1994) particularly evident in the house building sector where traditional methods and styles prevail.

Following the long history of the UK construction industry in failing to satisfy the expectations of many of its clients, and the increased concern for 'value for money' during the advent of the 1990's, (Green, 1996), the nature of the construction industry came under review. The resulting UK government reports, including the Latham report (1994) and the Egan Report Rethinking Construction (1998) produced by the DETR, discussed the need for performance improvements in the UK construction industry and identified supply chain partnerships, and standardization and pre-assembly as having critical roles in improving construction processes. Both reports called for

> ..a culture of cooperation and with improvements in the design and construction to provide savings to the clients and benefits to society

at large. (Lawson *et al.*, 2005)

The pressures on the UK government to house the growing population, stems from the mismatch of the existing housing stock with the changing demographic the new post war low in house building and stricter EU design regulations on modern living. These factors along with the significant changes in lifestyle over the past 50 years indicate that traditional methods of house building and the existing housing stock will become unsuitable.

The Government's Barker Review (2003) highlighted the combination of these growing pressures on the present-day government to home the growing population indicating the possible economic and social consequences of the present house building policies. The combination of these reports have influenced the UK Government and local authorities, to embrace modern construction techniques and the concept of pre-assembly in house building, to provide the estimated 3 million new homes by 2016 (Anon., 2003).

The term pre-assembly covers the manufacture and assembly (usually off-site) of buildings or parts of buildings or structures earlier than they would traditionally be constructed on site, and their subsequent installation into their final position. The following four techniques fall under this broad heading.

- Modular Construction

- Volumetric Pre-assembly

- Non-volumetric Pre-assembly

- Component Manufacture and Sub-assembly

Gibb & Goodier (2005) ranked these construction techniques by their degree of off-site production as shown in Table 2.1. MMC's may be assumed to exist in Levels 3 and 4, which involve high levels of pre-fabrication.

Perhaps the greatest concern to the UK house building industry, is the forth-coming skills shortage. Presently 80% of house builders are experiencing recruit-ment problems (Anon., 2003). Although this problem has been addressed by the Construction Industry Training Board in recent years, through the advocating of apprentice style training schemes in both MMC and traditional skills, the next generation of skilled labour may still be in training as the demand for housing of higher quality rises.

Unlike automotive manufacture where the man-hour has almost been replaced with the automated robot-hour, it still takes approximately 1 man-year to pro-duce the average 3 bed semi-detached house, (Hutchings, 1998), of which 80% of this time is required by skilled labour in the finishing and outfitting of the structure with utilities.

These combined pressures of increased demand, improvements in quality and the forthcoming skills-shortage, all identified in the Government reports, have boosted the interest in the use of MMC to produce high volumes of quality housing at an acceptable cost.

The industrial production of building components suitable for MMC requires significant capital investment in the infrastructure of machinery and factory pro-duction, design development, product testing and certification. To overcome these capital costs a highly repetitive product is desirable. Presently more than 30 house building factories operate in the UK, (Anon., 2003) producing a great number of generic lightweight steel or timber framed, pre-fabricated, modular housing systems. These systems have been successfully used in the construction of cellular type dwelling structures, typically hotels and student accommodations, which offer a great repetition in design. It is acknowledged by Miles (2003) that whilst the techniques used in these highly repetitive structures provide archi-tectural and functional showcase pieces, they cannot be applied to small scale

residential structures unless a significant reduction in cost was available.

The various forms and techniques of pre-fabricated building systems most suitable for use in house building are shown below. These are based on the categories developed by Lawson *et al.* (2005) for lightweight steel framing systems.

- Lightweight steel framing, elemental and panel systems: Constructed using linear elements (Steel, FRP, Timber), walls are pre-fabricated in storey high assemblies and floors are attached as elemental pieces on site.

- Modular/Volumetric construction: Manufactured from 2D panels and floors, assembled into load bearing boxes, which are equipped with utilities and transported to site. The maximum dimension of each unit is limited to around 4 m due to transportation legalization.

- Hybrid (modular and panel) and (panel and elemental) systems: By combining the use of elemental, 2D and 3D components the greatest savings can be made in terms of manufacturing costs. The highly serviced areas, such as bathrooms, are modular units (greatly reducing the on-site wet trades), whilst 2D components are used for the wall and floor components creating designer flexible open space structures.

- Open Building Systems: Open building technology is a general term used to describe systems which provide flexibility in space planning and in interchange of components (Lawson *et al.*, 2005). The previously mentioned forms of MMC achieve some low level of open building technology, but are constrained in their spatial flexibility by the limited number and size of components. A true open building system will offer unlimited flexibility to the designer, through the use of standardized units.

According to the recent report by the National Audit Office (2005), a Volu-

metric building approach can reduce on-site construction time for a housing development to 16 weeks compared to 39 weeks for traditional methods, with intermediate time savings for other MMC. Other advantages of MMC include reduced on-site labour and time to provide a weather tight condition (Anon., 2005b). Although such time savings would indicate a reduction in the overall cost, Fig 2.1 (Anon., 2005b) indicates that on average MMC tends to be more expensive than more established techniques. It is believed, that this cost gap between MMC and traditional techniques will be closed in the near future as the level of competition increases. However, where cost saving can be made, depends on the nature of the MMC product; Volumetric products will only become more competitive if the off-site costs are reduced. For other MMC approaches saving can be made in either on-site or off-site costs. It is estimated that 15% reduction in off-site costs is sufficient to close the gap between Volumetric approaches and traditional methods (Anon., 2005b).

At present the MMC market consists of a number of manufacturers with well established products, in lightweight cold rolled steel, precast concrete and timber all capable of supplying low-cost residential housing systems at less than £60,000 for a completed dwelling. In 2002 MMC accounted for only 1% of all UK house construction, this is predicted to grow to 6% by 2008 presenting established companies with significant growth (Anon, 2005a). The highest growth rates are expected in the light-weight steel MMC sector. In 2000 approximately 2,000 lightweight steel units were fabricated, this rose to 30,000 in 2004, a further 180% increase in production is expected by 2011 (Pearce, 2006).

According to the survey of the top 100 UK house builders by Pan *et al.* (2005), the use of Volumetric bathroom and kitchen units represents the greatest growth in the use of MMC. The use of complete modular buildings was not considered as having the same potential. The most significant barriers to the use of complete

modular buildings were considered to be the high capital investment, the lack of standardisation between different systems, and, the inability to alter design as the build progresses. The restriction on cash-flow and the possible issues involved in arranging a mortgage are also quoted as barriers to the use of complete modular buildings (Milburn & Bowler, 2005).

2.3 Pre-fabrication in the history of the house-building and construction industries

Although the concepts akin to pre-assembly are presently being marketed as a MMC, their use and development into the 'modern' form can be charted through the history of house building and construction.

The advantages of standardisation and pre-fabrication in construction were known to the ancient Sumerians , 4000BC, who using burnt clay bricks manufactured off-site built the first great cities (Farstad, 1982).

This raises the question. Can the Sumerian Clay brick or even the present day house brick be considered a part of a pre-fabricated building system? According to the modern definitions given below, the building technique used by the ancient Sumerians almost 6000 years ago, contains the same conceptual elements of a modern pre-fabricated building system:

Mass-production: The manufacture of goods in large quantities, often using standardized designs and assembly-line techniques.

Pre-fabrication:

1. To manufacture (a building or section of a building, for example) in advance, especially in standard sections that can be easily shipped and assembled.

2. To make up, construct, or develop in an artificial, unoriginal, or stereotypic

manner.

<div align="right">(The Oxford Dictionary of English)</div>

Although bricks are mass produced off-site, using standardized assembly methods in advance of their intended use, the art of bricklaying cannot be considered as a MMC. The construction of a building system from brick alone is a highly labour intensive process, which could easily be optimised to reduce labour costs.

2.3.1 The onset of modern pre-fabrication and mass-production

The development of the modern pre-fabricated and mass produced building systems in modern materials (cast and wrought-iron and later steel and concrete) started with the Industrial Revolution of the 1800's. The beginnings of the era, which may be termed the machine age, were realized with the harnessing of steam power allowing the industrial production of iron by 1750. New and innovative building methods for the structural use of cast and wrought iron were utilizing the strength of the material to produce structures of greater efficiency and more importantly increased productivity. Examples of the efficient use of iron to increase productivity, include the framing system developed for textile factories in the north of England which is the fore-runner of modern steel construction (Pervsner, 1986) and, to a greater extent, the pioneering all iron bridge built at Coalbrookdale, UK by Abraham Darby in 1780.

These are examples of the concepts of mass-production and pre-fabrication. However, the concept of modularity in building and component design defined below was not embraced until later.

- Modular: Designed with standardized units or dimensions, as for easy assembly and repair or flexible arrangement and use: modular furniture; modular homes.

(The Oxford Dictionary of English)

By 1830, the improvements in the industry production of iron, allowed the trickle down of technology to house building with possibly the world's first metallic house(Fig2.2). Built pre-1830 on the West Bromwich-Birmingham highway, the walls were built from standardized 18 inch wide cast iron flanged panels bolted together (Harrison, 1946). This unobtrusive structure may have been the first truly modern pre-fabricated living structure built of standardized modular panel elements. These cast iron panels can be considered modular in their design and function.

In the years following 1830, great improvements were achieved in the production of cast iron and glass, providing immense prospects to the pioneering engineers of the time. A notable example would be the Great Exhibition Hall in Hyde Park London, known as the Crystal Palace, built in 1851 by Joseph Paxton, the design made good use of large-scale mass-production and carried a degree of modular repetition.

Although the Great Exhibition Hall is a wonderful example of how a mass-produced and pre-fabricated building system can develop into an architectural delight, many thousands of more modest pre-fabricated structures were manufactured destined for export across Europe and into the expanding British Colonial Empire (1820-1900). Sponsors of the colonial settlement encouraged the use of pre-made housing, for obvious economical and utilitarian reasons. The 'Portable Colonial Cottage' (Fig. 2.3), designed and built by Manning of London in the 1830's, was a pioneering effort to the pre-fabricated dwellings issued to settlers in South Australia.

As expected, the way new structures are developed and new materials utilized is sculpted by the economical and architectural constraints placed upon the designer. However, some of the greatest advances in the development of pre-

fabricated housing in the 19th Century are the result of humanitarian pressures.

The engineer Isambard Kingdom Brunel was commissioned by the War Office, to provide a solution to the inadequate provision of field hospitals during the Crimean War (1854 - 1856). Brunel developed a complete system of pre-fabrication, transportation and erection, inventing the portable flat-pack field hospital. Of the modular panel and elemental building system, Brunel wrote:

> The construction of each building has been studied with great care,
> so as to secure the minimum amount of material, the least possible
> work in construction and erection, and the means of arranging all the
> parts in separate packages, capable of being carried by two men.

The 2,200 bed Renkioi Hospital, designed by Brunel using the basic ideas of mass-production and component repetition, excelled as a temporary hospital, being shipped and constructed within 5 months and reducing the fatality rate infection from 40 to 3% through the provision of adequate ventilation. So successful was Brunel's approach to design, the name 'Kingdom' is still used today to refer to modular field hospitals .

2.3.2   The Modernist Movement: The founding of modularity in pre-fabricated housing

By the end of the 19th Century the popularity of gothic influenced architecture had demised with the rise of the Art Nouveau style of design. Several new and innovative approaches in the design and style of buildings were embraced by this new, art influenced, genre of architects. It was during this period that the definitions of mass-production, pre-fabrication and modularization in terms of building are founded.

The work of architects such as Charles Rennie Macintosh (1868 - 1927) and

Le Corbusier (1887 - 1965) broke away from the traditional founding's of Art Nouveau, in favour of a more contemporary appreciation of design. Both architects harnessed the intricacies of free and working space within their designs through the omission of curvature creating a more abstract effect through the use of uprights, horizontals, squares and oblongs as illustrated Fig. 2.4. This use of crisp straight lines and clean planar surfaces to produce a striking, and, clear abstract form contributed to the new Modernist Movement. (Pervsner, 1986).

Whereas the Industrial Revolution had provided the impetus of modern prefabrication through advancements in manufacturing technology, and, the need for improvements in building technology to cope with demand, the Modernist Movement provided the influence for the standardization of pre-fabricated building components. Such standardisation directed pre-fabricated components, into the general housing market by allowing greater design flexibility.

Following the First World War (1914 - 1918), the great economical pressures placed upon those countries deeply involved, and, the urgent need to supply low-cost housing to a returning workforce resulted in a growth in the manufacture of pre-fabricated housing systems. Within the UK alternative methods of house building were sought as it was realized that traditional methods could never meet the demand due to economical constraints and the shortage of skilled labour. During this period, the so called traditional 'English' stick built timber framing system evolved into a more productive method of building low cost timber housing developed in the US.

Traditional timber frame construction is characterized chiefly by the fact that vertical and horizontal members are joined using carpentry techniques, such as tongues, grooves and dovetails, which significantly lower the resistance of the members at the connection. Therefore, requiring members of such dimension to ensure sufficient resistance can be developed at the connection details. Through

the use of nailing and nail plates to produce connection details, a higher degree of material utilization could be achieved reducing the overall cost. This highly cost effective construction method was first realized in the US supplying over 60% of the American population with housing by 1930, and is still widely used.

Design influences were also sought from the Northern European countries whose construction systems offered a higher degree of pre-fabrication and off-site manufacture saving much time and cost compared to the traditional 'English' and the American nail-plate timber framing systems (Yeomans, 1997). The Modernist Movement, flourishing in the expanding industrial inter-war Germany was one such influence. At its core, the movement advocated that contemporary methods of industrial organization and manufacture should be a model for building design and production (Finnimore, 1989).

The work of the Bauhaus School of Design founded by Walter Gropius in 1919, whose motto *'art and technology- a new unity'*, followed Gropius's own belief.

> The creation of standard types for all practical commodities of every-
> day use is a social necessity (Gropius, 1926)

It was the problem of standardization of components and modular co-ordination for a building system that became the subject of study for Gropius and others in the following years. In the same period, Konard Waschmann chief designer for a prominent manufacturer of pre-fabricated wooden buildings in Europe (1920 - 1930) developed a catalogue containing a grid system, on which the client could draw their approximate floor plans. By using such a grid of modules and a number of predefined parts, Waschmann had achieved in practice what Gropius had been seeking in theory.

In 1940 in the US, Gropius and Waschmann worked together to design and

manufacture a timber frame building system based on a cubic module of 3ft 4inch, which itself was based on the original concept, that a 4in cubic module is the largest dimension upon which universal agreement could be obtained. The General Panel System, developed by Waschmann with the aid of Gropius in 1941, shown in Fig. 2.5(a) and (b), relied on complex and intricate connection details to provide the repetition and flexibility required for a modern modular building system. Such a system may be classified using Lawson's categories (Lawson *et al.*, 2005) as an open building system of elemental panels.

The concept of 'system' was the back-bone Gropius and Wachsmann's work, who were able to comprehend the complete structure and still see the significance of the part as reciprocal aspects of the integrated system. For them the satisfaction came from the solution of the problems of designing a panel or jointing system. The General Panel System was developed into a complete 'Packaged House' and the General Panel Corporation was born with the aim of providing 42,000 demountable houses for defence workers following America's entrance into the Second World War in 1941. The General Panel Corporation went into liquidation in 1951 having only produced 150 - 200 houses most of which were sold to the United States Corp. of Engineers and shipped to Alaska (Waschmann, 1939).

The failure of the General Panel System to entice the middle class housing market was not only due to the poor economical situation but more interestingly the psychology of the buying public. The General Panel System was a well designed system, of better quality than traditional housing, but it was perceived as inferior due to the '*pre-fab*' tag (Herbet, 1984).

The following paragraphs briefly introduce pre-fabricated/modular building systems and approaches to house building developed by other influential architects of the period, notably Frank Lloyd Wright (1867-1959) and Richard Buckminster Fuller (1895-1983).

Frank Lloyd Wright's concept of the Usonian house, illustrated in Fig. 2.6, focused on a homogenous building block approach, and is a radical move away from the individuality of Wachsmanns creation. Although Wright's Usonian house was never conceived to be a low-cost demountable housing solution, it was based around the similar concept of modular repetition. Architecturally there are great differences in the utilization of space within the two building systems. The fixed spaces of the Volumetric building block approach, are opposed to the indeterminate fixing of space possible with the building system.

It is within the extremes established by Wachsmann's general panel system and Wrights Usonian houses that pre-fabrication is fixed (Herbet, 1984)

Richard Buckminster Fuller believed pre-fabrication and modularization would play a significant role in the technocratic society of the future (Pawley, 1990), where every detail of day to day living for the masses will be calculated to maximise efficiency and eliminate waste. Although Fullers beliefs were similar to Gropius's own beliefs of a future led by technology and the need for standardization in living, Fuller was critical of this so-called Modernistic influence in architectural design claiming it to be designed entirely for looks. Buckminster Fuller's more radical dream, would be designed by technologists for function.

Buckminster Fuller's first attempt at a pre-fabricated dwelling was inspired by corrugated steel grain silos. By providing doors and windows and fitting a 'Dymaxion' bathroom unit to a 5.5 m drum, he converted the cheap enclosures into small houses. The entire production run of the 'The Dymaxion Deployment Units' (DDU's) (Fig. 2.7(a)), were bought up by the United States Signal Corps as emergency accommodation for radar crews in 1942. (Pawley, 1990).

The DDU provided the basis for the design behind the larger and more so-

phisticated 4D-mass-production house (Fig. 2.7(b)), commonly known as the 'Witcha' house which were constructed from pressed aluminium sheets. Using technology developed in the aircraft industries in the Second World War, the curved cladding sheets were suspended from a central mast, making great use of the structural properties of the new material. The individual parts were to be shipped to the site for on-site assembly; with no component weighing more than 50 kg the structure could be assembled in one day by a team of six men.

With the installation of pre-fabricated Dymaxion bathroom units, the 'Witicha' house is an early example of a hybrid (Volumetric and Panel) construction system. Although the cladding sheets may be classed as modular, the design flexibility of the system is fixed with only one structural form possible, unlike the infinitely variable General Panel System.

The Fuller House Inc. received 37,000 unsolicited orders for the 'Witcha' house in October 1945. By the end of 1946, Fuller House Inc. was in liquidation owing to delays in the onset of full production caused by Buckminster Fuller himself, only four prototypes were ever built.

2.3.3   Social interpretation of factory made housing

Although, the concepts of pre-fabrication and modularisation at the core of the Modernist Movement offered possible solutions to the housing crisis of the period, few of the symbols, and, ideologies of the Movement, were ever embraced by the political powers of the time. Under the totalitarian regimes that grew in power in Germany, Italy and Russia during the interwar period, Modern architecture was open to the charge of being foreign and not grown from national cultural roots and craft traditions: in Germany it was frequently portrayed as an oriental import part of a Bolshevist plot originating in the East. Simultaneously in communist Russia, modern architecture was treated as a commodity from the West.

According to the leaders of the Bauhaus... the new man is no longer a man, he is a geometrical animal. He needs no dwelling; no home only a dwelling machine. This man is not a personality but a collective entity, a piece of mass man. They want to kill personality in men, they want collectivism, for the highest goal of these architects is Marxism, Communism.(Curtis, 1987)

The distaste of all modern influence in art and architecture, evolved from the growing nationalism in Germany. The rise to power of the Nazi party lead to the closure of Bauhaus school in 1933, with many members seeking refugee in the UK and US. Although the present day social climate is far removed from the totalitarian regimes of the mid 20th Century, the notion of living in a prefabricated house in the UK, is easily frowned upon. This modern day distaste of the concept of living in a factory made dwelling, may extend from the triumphant efforts of post-war architects, engineers and planning officers to house the nation. The solutions to the post-war housing crisis in the UK lacked the architectural delight of Wachsman's or Fullers proposals, but none of the functionality. The Aluminium Bungalow of the AIROH (Aircraft Industries and Research Organisation on Housing), exploited the redundant aircraft industries in the UK, to produce a completely industrialised housing system supplying over 69,000 houses in a ten year period.

2.4   FRP housing systems

As a building material FRP's can offer the following several distinct advantages over the more traditional building materials:

- Resistant to warping and distortion due to moisture changes

- Low thermal conductance avoiding the possibility of cold bridging and heat loss

- Due to the relatively low stiffness of FRP the material is acoustically absorbent, reducing noise transmittance throughout the structure.

- With tensile strengths of FRP's comparable to that of steel at only one third the weight, significant reductions in the total weight of material required for a given application can be made.

The following subsections provide examples of pre-fabricated housing systems and living structures constructed of FRP, classified according to the construction technique present. Many other uses of FRP in construction and building can be found in Leggart (1984) and Starr (2000).

2.4.1 Panel and Elemental systems

There exists a great number of PFRP elemental type structures built using commercially available standard I and WF beam sections. The Eye-Catcher building (Fig. 2.8(a)) in Switzerland, is the only known example of a non-industrial building built using this style of construction. The 5 storey, 15 m structure was designed and constructed around the Fiberline standard structural profiles. The use of bolted connections allowed the whole structure to be disassembled transported and reassembled in a new location (Fiberline Ltd., 2006).

The first reference to a complete living structure manufactured of FRP is adeptly titled 'The pre-fabricated plastic house' (Fig. 2.8(b)). Designed by the Henry Kaiser Housing Company, USA in 1946, the single storey panel based structure is similar to the modernistic style of the General Panel System.

2.4.2 Complete, Volumetric and Modular systems

The U.F.O. inspired Futuro House, (Fig. 2.9(a)), designed by Finnish architect Matti Suuronen in 1968, reflected the optimism of the period. Constructed as a single shell type structure entirely of FRP, the lightweight, self-contained structure could be transported by helicopter in one piece making mobile living a new possibility for the future. Only 20 Futuro Houses were ever manufactured as by 1973 oil prices had raised the production costs too high to be profitable.

As an example of Volumetric and Modular construction, the SpaceBox (Fig. 2.9(b)), developed by Holland Composites Industrial and Deflt University Student Housing Service, represents a unique concept in modern-day temporary housing. The style exemplifies the building block approach of Wright's Usonian House, combined with the advantages of modern composites to provide individual self-contained living modules. Owing to their lightweight and modular design, the individual SpaceBox modules can be stacked, to create a small communal dwelling without the need for special foundations. Each of the individual modules are completely pre-fabricated, plumbed, wired, furbished and finished off-site, such that modules may be inhabited within hours of deployment.

2.4.3 Open space systems

The use of open space building systems, which use a greater number of smaller components in comparison to the basic elemental and panel constructions styles, offer greater design flexibility. A well designed building system, will allow the designer to produce a vast number of unique structures each with a high degree of component repetition.

The Advanced Composite Construction System (ACCS), developed by Maunsell Structural Plastics in the early 1980's, is possibly the only successfully applied

PFRP modular system produced. It has been used to produce many world firsts and flagship PFRP structures. Devised in 1981 as an economic system for bridge enclosures, the uniquely designed shape rely on the 'system concept' (Head & Churchman, 1989) to produce an almost infinite number of arrangements of relatively simple plank and connector shapes, as shown in Fig. 2.10.

The modular construction system consists of six interlocking components, including a main (80×605 mm) multi-celled building panel, and, three-way and 45° connection blocks allow the system components to turn corners facilitating the joining wall units. Toggle connectors are used to provide the connection detail between the separate components, the connection detail allows a small amount of adhesive to be supplied to the joint providing a high degree of interaction over the connection.

The first application of the system was the 16,000 m² bridge enclosure constructed on the underside of the Tees Viaduct, UK in 1988. Using a more complex arrangement of the same shapes the world's first all-composite bridge using a multi-panel box beam cross section was constructed and later installed at Bonds Mill, UK. The first building type structure built from the ACCS was constructed at the site of the second Severn crossing. The temporary site building was erected in a short period illustrating the merits of pre-fabrication and has remained in place as a visitor centre. Although not ever used or intended for permanent dwelling the structure is a prime example of the application of a modular PFRP building system to a residential structure.

The Startlink modular PFRP building system proposed by Byers & Singleton (1999) offers two complete construction systems. The first is designed specially for building and residential structures, and, provides almost unlimited designer flexibility from a series of open sectioned pultrusions illustrated in Fig. 2.10(b). The use of snap fit and flat pack assembly offers major advantages over existing

building systems, including the ACCS. Connections between the profiles are also made using the Unistrut connection method (Fig. 1.3). Using this blind fixing technique to join the various pultruded shapes, a great number of housing components can be produced. The various building assemblies illustrated in Figs. 2.11(a) and (b) can be assembled from the twelve open sectioned shapes building into a complete PFRP dwelling (Fig. 2.12) offering the following advantages over existing tradition construction methods:

- Lower total build cost (550 £/m^2), compared to existing MMC and traditional methods (Fig. 2.1)

- Significant reduction in total weight of building material required, for a typical single storey 2 bed structure it is estimated that only 6 tonnes of PFRP profiles are required (Singleton, 2006), which provides considerable reduction in transportation costs when compared to the 28, 64 and 61 tonnes required for similar timber, concrete and steel structures (Buchanan *et al.*, 1994)

- Reduced storage and transportation costs due to flat pack nature

- Reduced on-site labour time due to low weight (≤ 50 kg) of individual components.

The Startlink building system is not confined to residential housing. The flexible system can be used in a variety of industry applications, other intended uses include:

- Industrial applications where a corrosive environment may limit the use of traditional materials, such as in Cooling Tower systems

- Emergency housing that may be required to be transported by helicopter and assembled on-site by semi-skilled operators.

- Retrofitting of existing structural shells to provide temporary work space

The second Startlink system, offers a family of PFRP box beam members illustrated in Fig. 1.2. Each beam is built-up from a series of mechanically fastened open sectioned PFRP shapes. An evaluation of the Startlink beam concept including the performance of the proposed Unistrut connection system are given in the remaining chapters.

2.4.4 Critique of Startlink system

Upon initial inspection the Startlink building system appears a valid concept and suitable for the low-cost housing market. Based on the knowledge gained from research into the use of MMC and the development of factory made housing systems, it is the belief of the author that certain features of the proposed Startlink system, will reduce the viability of the concept.

From a practical perspective, the use of eight separate profiles may offer greater flexibility to the designer than alternative PFRP systems, but will significantly increase the complexity and number of connections required in the finished structure. It is plausible that the intended primary concept, of a PFRP housing system will become second place to an ingenious but overcomplicated connection system, as with the 'Packaged House' concept developed by Waschmann and Gropius.

Technically the Startlink building system employs the concepts of modularity and pre-fabrication in the design of the structural system. However, these basic concepts of modern design have not yet been transferred to the architectural style of the finished structure, shown in Fig. 2.12, which is reminiscent of traditional housing styles. Despite offering a low-cost and sustainable housing solution, the present designs lack the kerb-appeal of other traditional and non-traditional

construction techniques.

As discussed in Section 2.2, there exist many barriers to entry into the MMC housing market, the greatest challenge to the Startlink system may be the growing competition, from the already established lightweight steel manufacturers who offer a robust and almost publically accepted product. Social acceptance of a pre-fabricated *'plastic'* house may prove to be an equally significant barrier to the Startlink system. In conclusion the Startlink system, offers a versatile and lightweight PFRP building system, with many potential advantages over traditional methods of construction, it is the opinion of the author that the Startlink system is over-ambitious in trying to apply this non-traditional material and construction method to a traditional style of housing in a market dominated by more acceptable and established alternatives.

The Startlink system offers clear advantages over existing products in industrial applications, in particular the floor and wall systems could be used in the retro-fitting of existing structural shells to provide temporary durable and flexible working spaces.

The use of Unistrut connections to provide structural connection between load bearing system shapes, may prove to be biggest structural down fall off the proposed system. Although simplicity of the Unistrut quarter turn blind fixings is ideally suited to quick connection of the shapes (Turvey, 2001), the stiffness of the connection details will greatly affect the stability of the structure by providing only intermittent connection between shapes

The work in the following chapters details the following

- Characterisation of the Unistrut connection method for use in PFRP shapes, providing parameters for the design of adequate connections for use in the proposed Startlink systems

- Evaluation of the structural performance of a prototype PFRP box beam, following the same concept of the Startlink beam assemblies shown in Fig. 1.2, relying on the Unistrut connection method to provide continuity between the separate profiles.

2.5 Conclusions

- The proposed use of Modern Methods of Construction (MMC) to provide for the rising shortfall in low-cost housing has been identified and the present classifications of MMC are detailed.

- Steps in the historical evolution of present day MMC have been identified, and the role of social, architectural and economic influences are discussed with reference to several early housing systems akin to present day MMC.

- The advantages of FRP as a material suitable for housing are discussed and various FRP housing systems are classified according to the method of construction.

- The Startlink PFRP construction system has been introduced and the merits of the proposed system discussed. The presented review suggests that although the building system offers design flexibility, it may be over complicated by the number of components, and, some what over-ambitious in its application. It is the opinion of the author, that the intended use of the Unistrut connection method to provide stiffness between system shapes may limit the practicality of the Startlink system.

2.6 Figures & Tables

Construction cost ($£/m^2$)
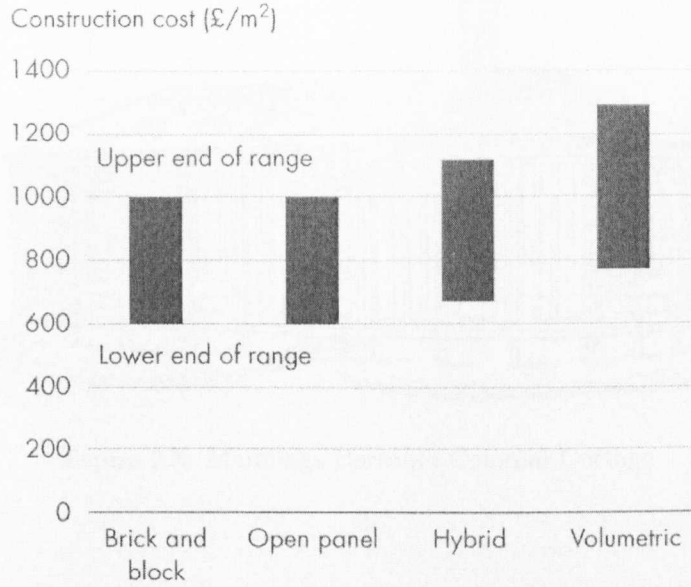
Source: Cost calculations prepared for the National Audit Office by the
Building Cost Information Service using process plans developed by the
Salford Centre for Research and Innovation

Figure 2.1: Comparitive cost of traditional and modern methods construction
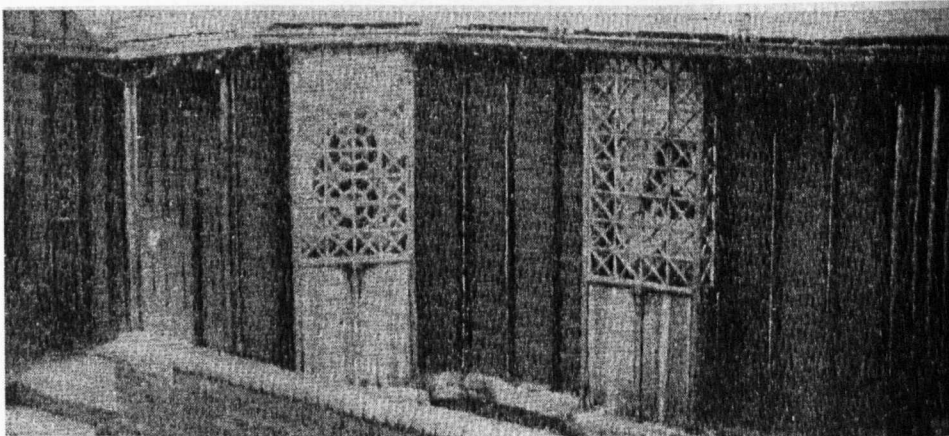
Figure 2.2: West Bromwich Toll House
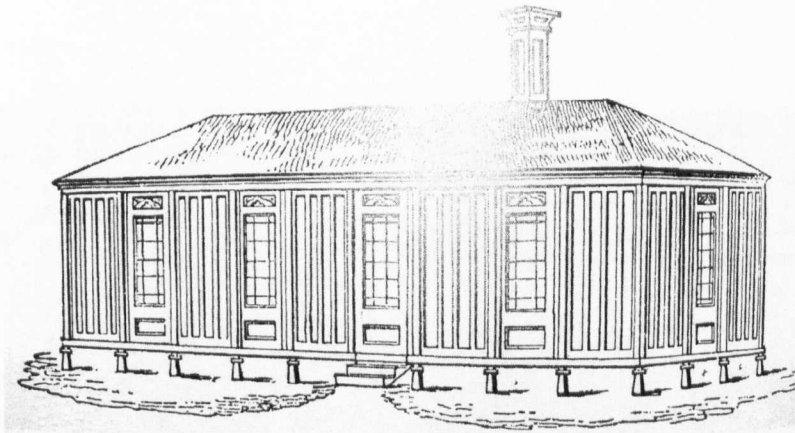
Figure 2.3: Mannings Portable Colonial Cottage
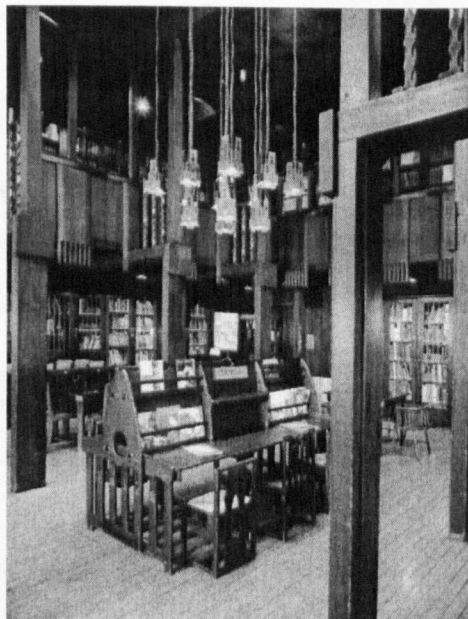
Figure 2.4: Glasgow School of Art
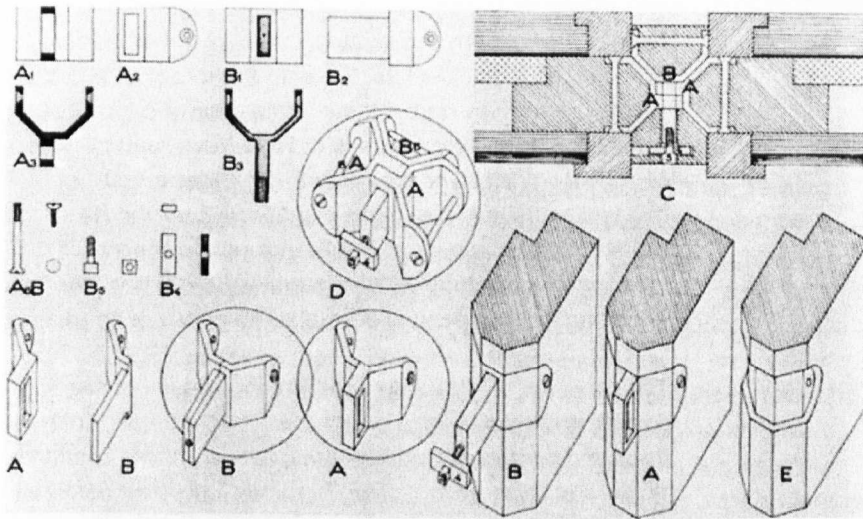
(a)
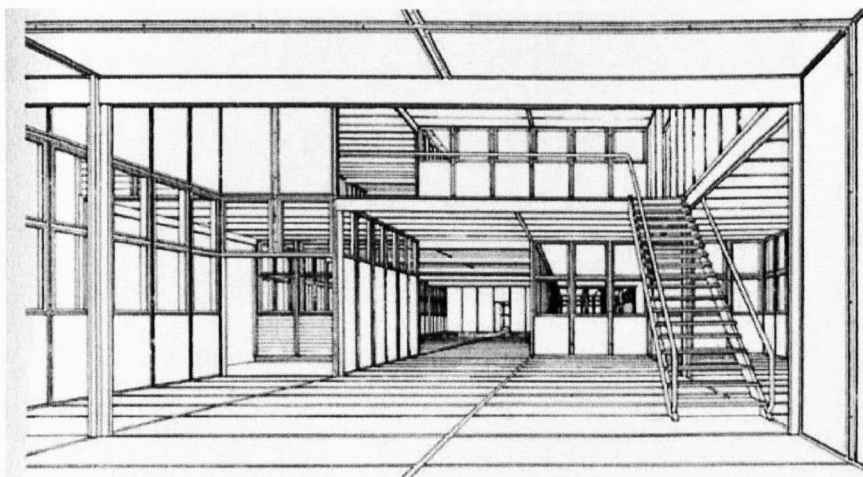
(b)

Figure 2.5: Details of General Panel System (a) Connection system (b) Sectional view
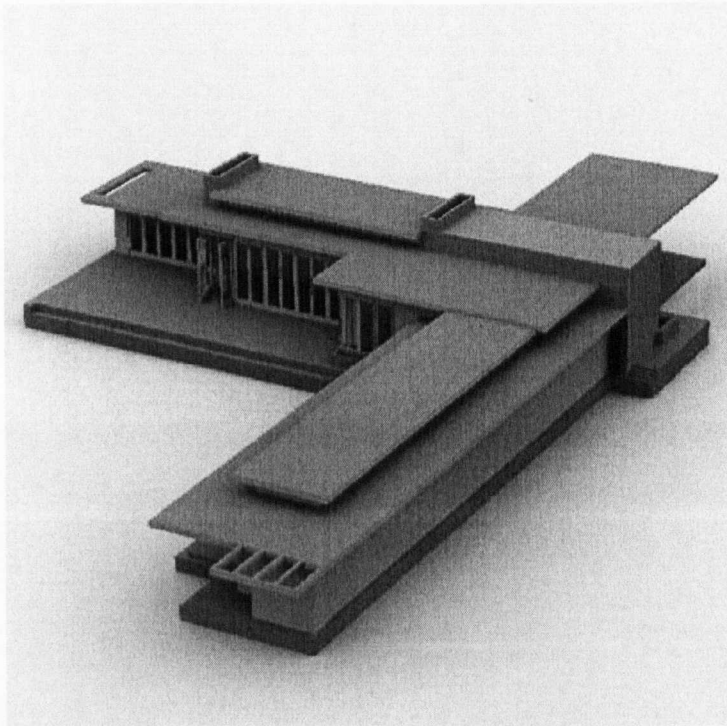
Figure 2.6: Example of Usonian house concept
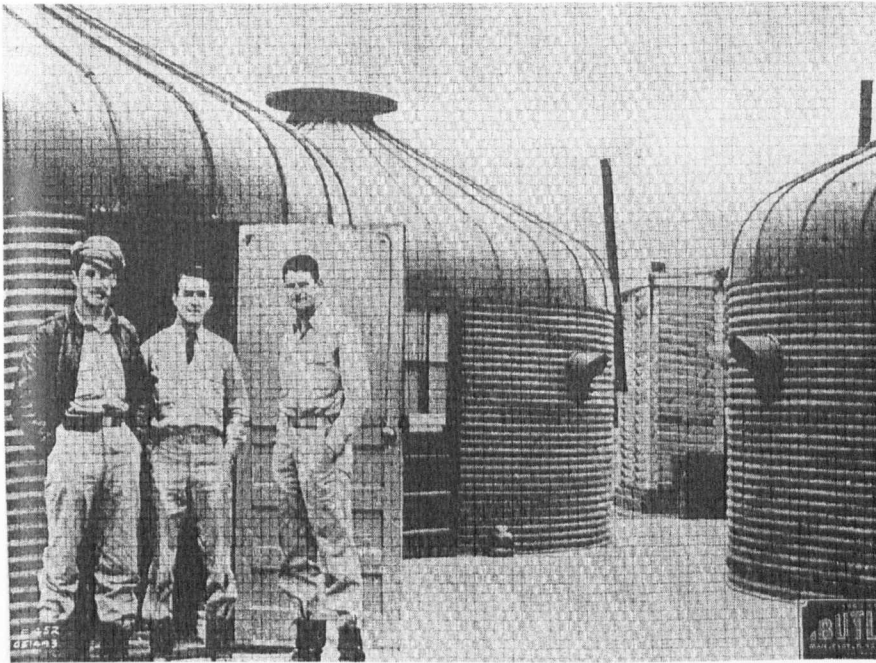
(a)
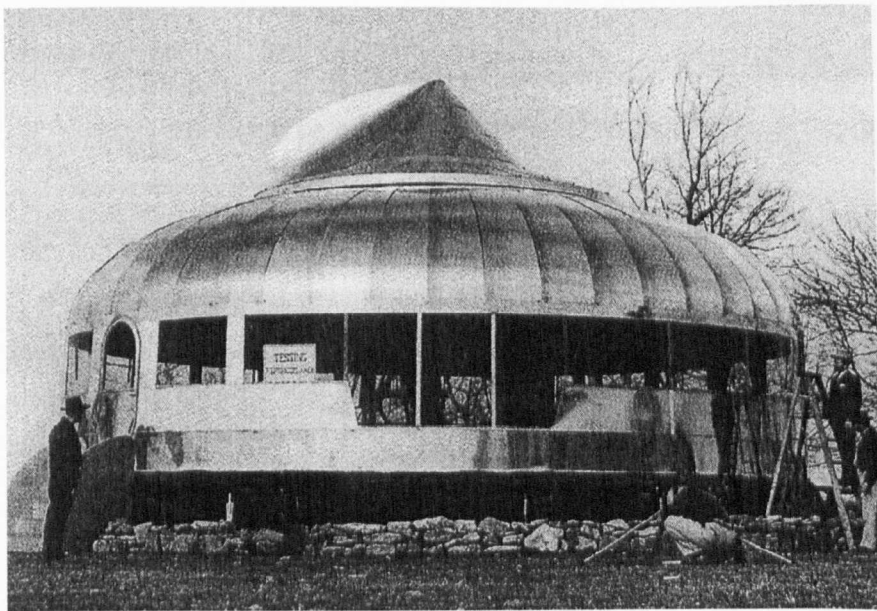
(b)

Figure 2.7: Dymaxion houses (a) The Dymaxion Deployment Units (b)'Witcha' house under field tests.

(a)
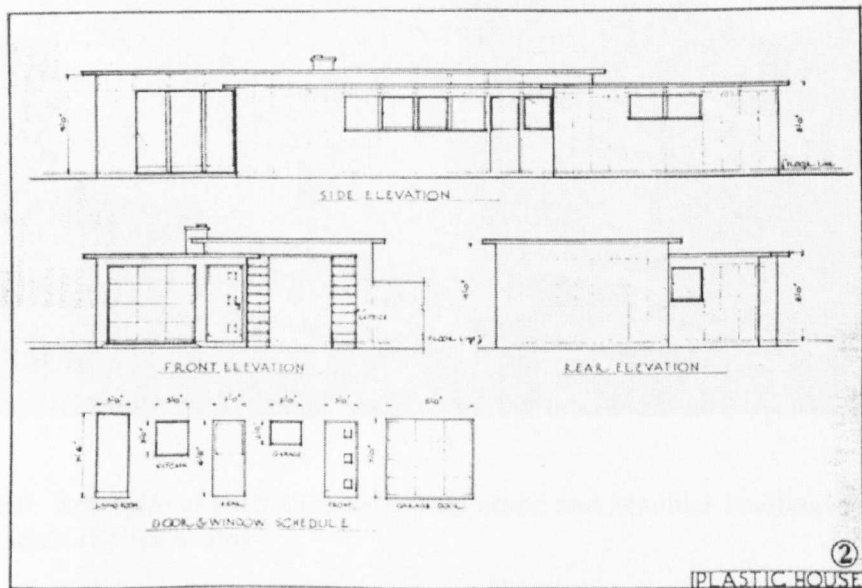
(b)

Figure 2.8: Examples of FRP Elemental building systems (a) Eye-catcher building, Switzerland. (b)Henry Kaiser housing Company 'Pre-fabricated Plastic House' 1945.
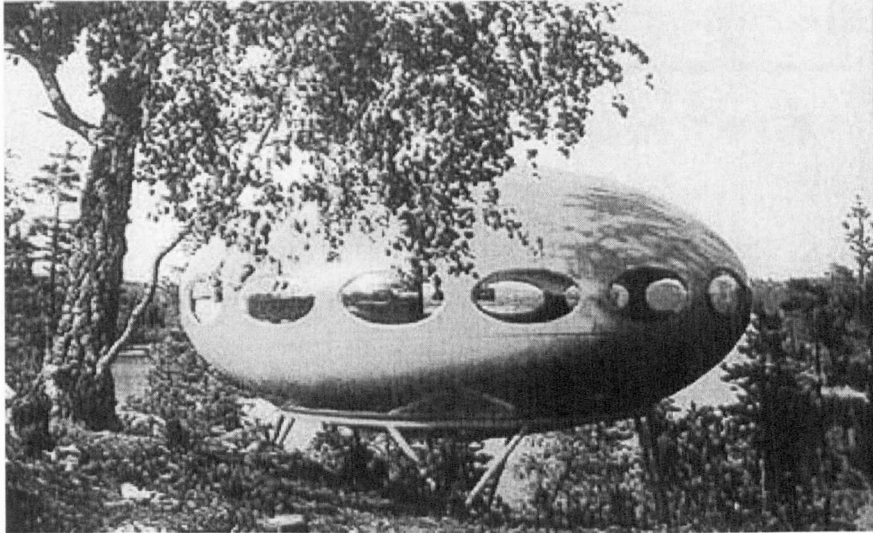
(a)

(b)

Figure 2.9: Examples of FRP Complete, Volumetric and Modular building systems(a) Futuro house (b) Space Box
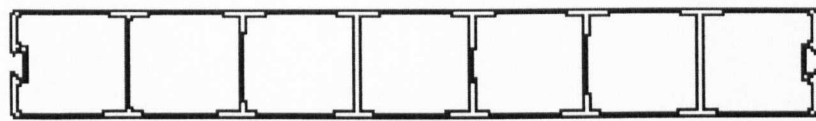
Panel
(3" x 24" nominal size — 80mm x 604.7mm actual)   7.49 lbs/ft
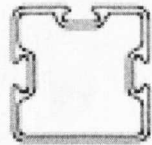
3-Way Connector
1.65 lbs/ft
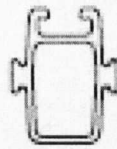
Hanger
1.55 lbs/ft

Toggle
.34 lbs/ft
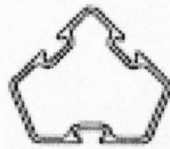
45° Connector
1.65 lbs/ft

End Cap
.57 lbs/ft

(a)
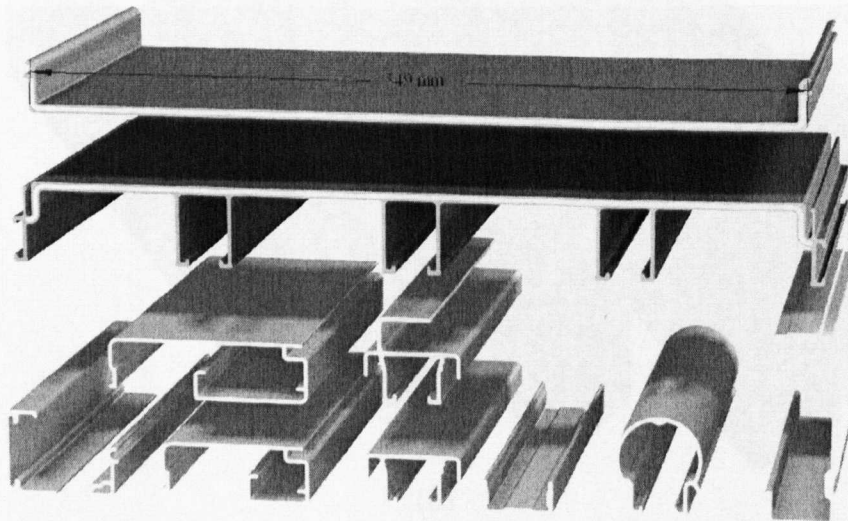
(b)

Figure 2.10: Examples of FRP Open building systems (a) ASSC panel system (b) Startlink building system
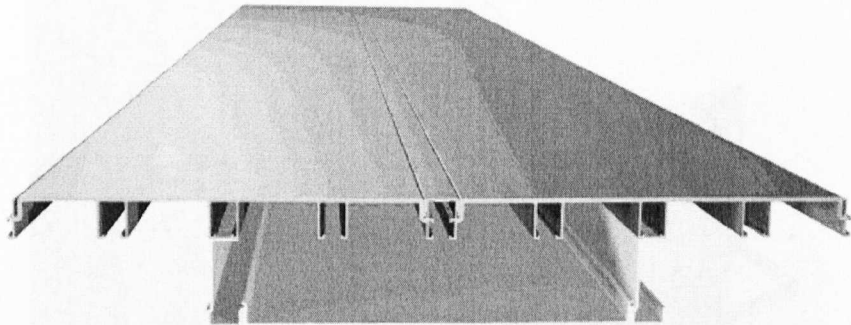
(a)
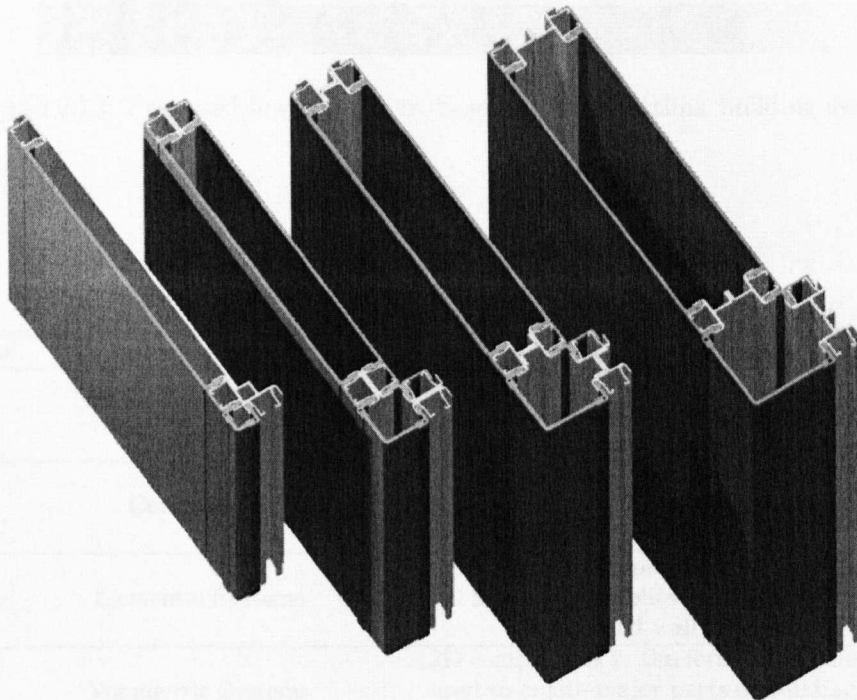
(b)

Figure 2.11: Startlink building system (a) Floor panel system (b) Wall panel system
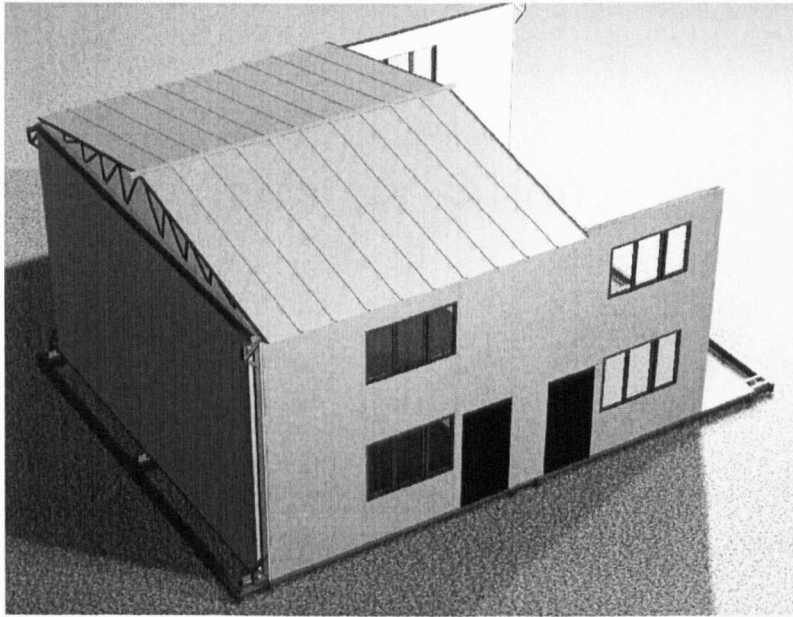
Figure 2.12: Proposed low-cost house based on the Startlink building system

Level	Component	Description of technology
0	Materials	Basic material for site intensive construction e.g. concrete, brick
1	Components	Components that are used as part of a site intensive building assembly e.g. Timber A frames
2	Elemental Systems	Linear or 2D components in the form of assemblies of structural frames and wall panels
3	Volumetric Systems	3D components in the form of modules used to create major parts of buildings which may be combined with elemental systems
4	Complete building systems	Complete building systems which comprise modular components and are essentially fully finished before delivery to site

Table 2.1: Various forms of Pre-fabricated technologies

CHAPTER 3

Connection characterisation

h This chapter presents work to characterise the Unistrut steel connection method for M10 blind fixings using Pultruded Fibre Reinforced Polymer (PFRP) shapes of channel section, representative of the connection detail present in the Startlink building system, Figs. 2.10(b) - 2.12 and the modular beam assembly, Fig. 1.2 proposed by Byers & Singleton (1999).

Both the standard nut and a smooth nut (standard without the serrations), have been used in the testing program to determine the resistance and stiffness via load-slip behaviour, under various applied bolt torques, and pure shear loading. It is shown that the standard nut provides adequate connection shear strength and stiffness, but with severe PFRP material damage that might be detrimental to the connection's structural performance over 30 years or more expected design life. The smooth connection is shown to significantly reduce PFRP material damage. However, this advantage is linked to a 35% reduction in the connection's shear resistance, making it less suitable for the development of composite action. Preliminary hot/wet aging and creep tests are used to estimate the reduction in strength and stiffness with time. Preliminary investigation of the connection method has highlighted several weaknesses in the design of the connection as part of a PFRP building system and recommendations for improvement are given. The

test results are used to establish four Unistrut connection design parameters that are required for the development of lightweight modular systems of PFRP such as the system proposed by Byers & Singleton (1999).

3.1   The Unistrut connection method

The cable management industry in the UK has traditionally used small cold-rolled light steel channels to produce modular systems with blind fixings (Mita Ltd., 2006). The typical cross-sectional size of a channel is 41×41×2.75 mm. This is shown in Fig. 1.3 with typical Unistrut connection details. In recent years, the market has moved towards replacing steel channel with PFRP channels because the composite material allows the installation of cable management systems in chemically aggressive environments, where metallic products are not ideally suited. The load bearing elements of a cable support system consist of U-shaped channel shapes (see Fig. 3.1(a) and 3.2(b)) having connections made between members using gusset plates secured by M10 steel bolts and specific steel channel nuts. This connection method, referred to as the Unistrut method, is shown in Fig. 1.3. The nut has a spring on one side. To insert the nut its longer sides are aligned with the channel's opening. The nut is then pushed into the opening such that the spring is fully compressed. Rotating the nut through 90° and releasing the pressure allows the spring to uncoil. The two lips of the channel are then mated with the grooves in the nut. The compressed spring provides sufficient pre-load to prevent the nut from moving while the M10 bolt is put through the hole in the gusset plate, threaded into the nut and tightened to the required bolt torque. This produces a quick and simple connection method for blind fixings.

The Unistrut nuts are designed to provide a secure means of attachment when

they are positioned anywhere along the opening of a channel. The standard nut is formed, or stamped, such that in its two grooves there are, evenly spaced, five serrations of 2 mm height. Under compression, following bolt tightening these 'teeth' impress themselves into the channel lips. In this way the connection can resist shear loading. A mean peak shear force of 3.8 kN has been measured for the M10 standard Unistrut connection with a steel channel, at a torque of 20 Nm (Evernden & Mottram, 2005). According to BS 6946:1998, the force required to give continuous slip shall be not less than three times the safe working load given by the manufacturer. The design working shear force when the channel is of steel is therefore under 1.3 kN per connection. Such specification is for the steel channels used in electrical installations. To determine the safe working load when the channel material is of PFRP it is important to characterise the load-slip behaviour by physical testing.

3.2 Requirements of characterisation rationale

Turvey (2001) has, via a series of three-point flexural tests with a prototype beam for the Startlink modular system (similar to the beam concept shown in Fig. 1.2), highlighted the potential of the Unistrut connection method. Connections were used in the 4.8 m span beams to fasten two flange shapes to two web shapes that formed a large box of overall size 35×120 mm. Turvey (2001) noted that the simplicity of these quarter turn fasteners is fully exploited with these shapes to allow blind fixing and to eliminate the problem of hole alignment in predrilled components. The results of his flexural tests gave conflicting findings. On the one hand, the connection concept was found to be promising, while on the other hand the structural performance of the prototype Startlink beams was adversely affected by an inadequate number of connections along its length (Turvey, 2001).

Such a finding indicates the need for the characterisation of the PFRP/Unistrut nut connection approach for application in modular systems.

Presented in this chapter are the results of tests characterising the structural performance of the Unistrut connection method using PFRP material. Two PFRP channels from Mita Ltd. (2006) are used. GS1 (General Strut 1) channel, shown in Fig. 3.1(a), has the size and shape of the standard steel channel (Fig. 1.3). The GS2 (General Strut 2) channel, shown in Fig. 3.1(b), has, where the standard nut makes contact, a shape and reinforcement arrangement more suited to the change in material. The test program has been planned to cover expected in-service conditions. Based on the test results and observations of the failure modes, etc., the following four connection design parameters are established:

- The initial bolt torque for the M10 bolting.

- The shear force per connection at ultimate limit state (ULS).

- The short-term connection stiffness (or modulus) for serviceability limit state (SLS).

- The long-term connection stiffness (or modulus) for SLS.

Knowledge of these connection parameters will enable modular systems, such as shown in Fig. 1.3, to be designed with an adequate number of Unistrut connections to provide the necessary composite action between connected PFRP shapes.

The characterisation of any structural component should be conducted in a manner that is most fitting to the intended and proposed in-service conditions of use. The in-service conditions might include exposure to the natural environment. Durability is an aspect of performance that embraces physical, as well as mechanical and aesthetic properties and is therefore one of the most important

qualities to be considered when using FRP's (Hollaway, 1993). From the civil engineering perspective the physical and mechanical properties of the material are of particular interest. Primary load bearing structures of FRP (Clarke, 1996) can be expected to be in-service, without substantial inspection or maintenance, for 75 or more years (Karbhari & Xie, 1998). The Advanced Composite Construction System designed by Maunsell Structural Plastics Ltd., UK, has been employed in many civil engineering structures in both load and non-load bearing applications (Head, 1994; Head, 1995). This PFRP second-generation modular system has a design working life to first maintenance of 30 to 40 years, and this provides major benefits in whole life costing over traditional construction materials (Head, 1994).

3.2.1 Durability of PFRP components and connections

The durability of FRP expressed as the material's resistance to water, light and chemicals (Leggart, 1984), is of significant importance in the characterisation rationale of the FRP components. As reported in Section 3.5, the indentation of the serrations of the Unistrut standard nut into the PFRP material will expose glass fibres as they cut into the channel's lips (Figs. 3.2(a) and (b)). The presence of this localised zone of material damage is of concern to the use of the standard nut since the durability of FRPs (as measured by loss in residual strength) may be impaired when E-glass fibres are exposed to the natural 'aggressive' environment. Having an understanding of the possible degradation mechanisms on exposure to an 'aggressive' environment (Liao, 1989; Khennane & Melchers, 2000), and being able to make long-term predictions of the changes in mechanical properties is essential in evaluating the feasibility of using FRP's in an 'aggressive' environment.

E-glass fibre reinforced polymers are known to suffer loss of load carrying capacity after exposure to water due to a variety of stress corrosion mechanisms.

Nanni *et al.* (1992) and GangaRao *et al.* (1995) have investigated the dissolution of glass fibres in alkali solutions, whilst the hydrolytic de-polymerisation of the matrix has been studied through the use of Raman (Prian & Barkatt, 1999) and infrared spectroscopy (Ghorbel & Valentini, 1993). The resulting micro-buckling of fibres and matrix swelling can cause serious macro-scale material damage altering the material's physical and mechanical properties. The rate of material property deterioration has been found to be dependent on the rate of diffusion of water molecules linked by hydrogen bonds to the polymer resin and movement of liquid water due to capillary action through the composite. This, itself is influenced by a number of factors such as: (Khennane & Melchers, 2000; Dutta, 1995; Hofer *et al.*, 1986)

- The FRP section's geometry

- The orientation and packing fraction of the local fibre architecture

- Development of capillary action along the E-glass/matrix interface

- The presence and nucleation of micro-cracks along this interface

- The nature of the resin.

Measurements of various mechanical properties of glass FRP materials exposed to aqueous media have shown the possibility of sudden decrease, after a certain induction period. Of particular relevance to the in-service mechanical properties of the Unistrut connection in PFRP are the effects of stress corrosion mechanisms upon the matrix dependent shear strength of E-glass/vinylester polymers. Prian & Barkatt (1998) showed a drastic decrease in shear properties of an E-glass/vinylester composite after prolonged exposure (224 days) to water at elevated temperatures (80°C). The damage caused by the dissolution of glass

fibres and the breakdown of the resin/fibre interface due to chemical reaction between the fibres and water, are far more detrimental to the composite than that sustained by the resin alone, such damage is increased by the presence of stress and strain (Khennane & Melchers, 2000).

In order to assess the possible loss of durability caused by the localised damage around the indentations the performance of conditioned and un-conditioned samples with the standard nut will be compared. To determine the functional importance to whether or not the serrations are required, the structural performance of the Unistrut connection method having a nut with the serrations removed also needs to be evaluated.

3.3 Material details

3.3.1 Mita PFRP Channels

Two different PFRP channel shapes, supplied by Mita Ltd. UK, are used in the series of experiments. Their dimensions and reinforcement construction are given in Figs. 3.1 and 3.2. Both the GS1 and GS2 shapes have a sandwich construction of E-glass unidirectional (UD) roving core between a outer layers of 450 gm/m^2 E-glass continuous filament mat (CFM), set in Isopthalic thermoset polyester resin. There is also a thin protective polyester veil (the resin rich layer) above the glass reinforcement. The first-generation GS1 shape was originally based on the equivalent steel section shown in Fig. 1.3. This channel's cross-section is shown Fig. 3.1(a). The wall thicknesses are measured to be 3 mm in the sides and 3.4 mm for the base. This shape is an off-the-shelf product from a number of pultruders. The second-generation GS2 shape is shown in Fig. 3.1(b), which has a PFRP specific shape. It has the same wall and base thicknesses as GS1. To increase the connection's structural performance there is more material and UD

fibre reinforcement located in the channel lips. This shape is a product specific to Mita Ltd., UK. The photographs in Fig. 3.2(a) and (b) show the geometries of the lips for the two channel shapes. Note that the 4.5 mm height (Fig. 3.1(a)) of the GS1 lip, which mates with the groove on the nut, is 2.5 mm deeper than the lip for the GS2 channel (Fig. 3.1(b)). Also seen in Fig. 3.2 is the local reinforcement arrangement. Figure 3.2(a) shows that there is a continuous CFM surface where the nut locates. Figure 3.2(b) shows that for GS2 there is no CFM layer over the same surface. In order to accommodate the tight geometrical constraints in the lip region of the GS2 shape this layer has been transposed to the outer face of the channel.

3.3.2   The M10 Unistrut nut and bolting

The standard M10 Unistrut nut is shown in Fig. 3.3(a). It is manufactured from 9.0 mm thick zinc galvanised steel and is approximately 34×20 mm in plan. There are two locating grooves of length 20 mm, width 3.5 mm and depth 3 mm. Each groove has five serrations of maximum height 2.0 mm. The serrations have varying height across the width of the groove and the highest side alternates along the groove from one serration to the next. In this chapter their application is referred to as the *standard* nut. The smooth M10 nut is shown in Fig. 3.3(b). The five serrations in each groove of the standard nut were completely removed by mechanical filing. Throughout this chapter their application is referred to as the *smooth* nut. Grade 8.8 M10 stainless steel bolts and standard washers were used in all tests to make the Unistrut connections. This connection method is shown in Fig. 1.3.

3.4   Preliminary Bolt tension study

As mentioned earlier the characterisation of any component or system must be undertaken in a manner that is befitting of its intended use. also it should identify all possible responses and possible unforeseen weaknesses of the system. The following section contains four separate studies, carried out prior to commencing the series of load-slip tests, in which the individual response to the application of a fastening torque were studied for the various components (PFRP Channel and Bolt plate, Unistrut connector, M10 Bolt) in the connection system.

The response of the PFRP channel lips to the bearing stresses developed by the application of a fastening torque and the bolt torque required to achieve a state of full indentation are considered in the first study.

3.4.1   Qualitative Indentation investigation

Prior to commencing the series of load-slip tests it was necessary to determine the value of bolt torque to be applied. This required knowing the response of the PFRP material to nut compression, by the application of increasing bolt tension (or bolt torque). Initially, a series of purely qualitative tests were conducted in order to ascertain the level of damage caused to the channel's lips. This was achieved by incrementing the torque, thereby increasing in stages the bolt tension. Torque was applied using a 300 mm MHM calibrated torque wrench, which can be read to an accuracy of 1 Nm. Tension in the bolt is reacted by bearing stresses over the contact area of the nut's grooves and the channel lips.

> The effects of over-torquing (excessive bolt tension) could be identified by way of a mode of ultimate failure such as a twisted bolt head, a bent or cracked nut, a crushed channel lip, or a deformed fitting (Anon., 2004).

To assess the damage to the internal lips a set of 15 GS1 channel specimens of length 50 mm were fitted with a single standard nut (Fig. 3.3(a)). A 10 mm diameter centrally notched steel top plate (40×40×6 mm) provided the necessary load path to tighten the M10 bolt against the channel. With the test arrangement similar to that shown in Fig. 3.5, the bolt was torqued incrementally to 10, 15, 20 and 25 Nm. At each torque the connection was disassembled and the PFRP lips inspected for the degree of localised material damage. A further five samples were subjected to continuously increasing torque to determine the over-torque value at the onset of ultimate failure. This over-torquing test procedure was repeated with a second set of five GS1 specimens and the smooth connector, shown in Fig. 3.3(b).

For the five samples fitted with the standard connectors, crushing of the lips occurred at between applied loads of 28 - 38 Nm, yielding an average value of 32 Nm (StD = 3.6 Nm, CoV = 0.11). For the samples fitted with smooth connector, crushing of the lips occurred over the range 36 - 44 Nm, yielding an average value of 40 Nm (StD = 3.0 Nm, CoV = 0.08).

For the standard connector, torques of 10 and 15 Nm were found to cause only minor cracking in the outer veil layer. Increasing the torque to 25 Nm significantly increased the damage to this protective layer and the near surface CFM fibre reinforcement (acoustic emissions were audible during, and after, application of the torque). With the smooth connector the presence of localised PFRP damage was only visible at the much higher torque of 35 Nm.

Bolt torque, T, is dependent on bolt tension, P_o, and the diameter of the bolt shank, D. In accordance with BS 3580:1964 the relationship between these parameters is:

$$T = 0.2P_o D \qquad (3.1)$$

Equation 3.1 can be used to estimate bolt tension for a known bolt torque by assuming 90% of the proof yield strength of the bolt is available for clamping. Such a condition might only be valid for clean fully lubricated threads. The remaining 10% of bolt force is lost through thread friction. For dry and unlubricated threads, only 50% of the yield strength of the bolt should be regarded as available. To determine the coefficient of friction of PFRP on PFRP, Mottram (2004a) used a simple plate-to-plate test arrangement. Via tests he showed that the bolt's preload is significantly reduced when the bolt is torqued by attaching the wrench to the bolt head. Because of this known reduction in bolt tension, on-site practice is always to tighten bolts with the torque wrench on the nut (Kulak *et al.*, 2000), and it is this situation that Equation 3.1, is valid for. Since the Unistrut connector is tightened via the bolt head an extra reduction should be made to the available yield strength.

For M10 bolts the shank diameter D is 9.8 mm. Using Equation 3.1, and accounting for losses, the bolt tension at the point of ultimate material failure in the lip section is predicted to be 9.7 kN, or higher (depending on the condition of the threads). Over the contact area this develops a mean bearing stress between the nut and the internal lips of 120 N/mm^2, or higher. It is to be noted that this stress is above the minimum required transverse pin-bearing strength of 70 N/mm^2 for grade E23 PFRP material (BS EN ISO 13706-2:2002).

3.4.2   Induced bolt tension during indentation

Using a 100 kN Testometric screw-thread testing machine fitted with a 10 kN load cell, the simple experimental/specimen set-up shown in Fig. 3.4 was used to determine the bolt tension during the indentation process up to the point of full indentation of the 2 mm high serrations with the standard connector. The bolt torque was zero in this study. For a set of five tests with the GS1 sections (Fig.

3.1(a)) the force required varied between 2.3 and 6.0 kN, with an average of 4.2 kN (StD = 1.2 kN, CoV = 0.24). Using Equation 3.1, and considering the range of physical conditions that could prevail the predicted minimum torque (T_{min}) for full indentation is in the range 8 Nm to 22 Nm. It is therefore found that the recommended torque of 10 Nm (Mita Ltd., 2006), with dry, non-lubricated, threads, does not necessarily ensure full indentation of the connector into the PFRP material. If the standard connector is to function structurally as designed full indentation is desirable, and for this to be present the author recommends applying a T_{min} of 20 Nm.

3.4.3 Bolt tension relaxation

Mottram (2004a) has conducted preliminary work to investigate the influence of the out-of-plane visco-elastic creep behaviour of PFRP bolted joints on reducing a bolt's preload with time.

With the standard (serrated) Unistrut connector the transfer of shear across the nut/PFRP interface relies on the normal load supplied by the bolt tension, generated by the application of bolt torque to produce *full* indentation of the serrations, the development of surface frictional effects will contribute to this load transfer. The effect on the standard connector of through thickness material creep will be to lower the bolt tension with time, reducing both the frictional and indentation contributions to the shear resistance. If the smooth nut is used there will be no indentation contribution to shear resistance and the detrimental affect of long-term creep on shear strength is going to be worse.

Using the load cell approach described by Sun *et al.* (2002), it is possible to measure the strain-time relationship for a preloaded bolt. As Fig. 3.5 shows the load cell comprises a steel tube of length 25 mm and outer and inner diameters of 22 and 17 mm. The ends of the tube were machined smooth and parallel. Four 6

mm TML strain gauges (type FLA-6-120-11) were placed at 90° intervals around the tube to measure the mean axial strain. The strain response was recorded in real time using an Orion Solartron 3531 data acquisition system. This same load cell used by Mottram (2004a) can be calibrated to relate the mean axial strain directly to the tension in the bolt. To identify the different rates of bolt tension relaxation, as a result of visco-elastic material creep and the presence of PFRP damage, for samples, two each of the GS1 and GS2 channels, were fitted with either the standard or the smooth nut. The initial bolt torque was 20 Nm and the same bolt was used in the four samples to ensure a fair test.

Figure 3.6 shows the proportional decrease of the tension over time (up to 110 hours) for the two channels and two connector combinations. The difference between the samples indicated that the presence of the indentation and material damage alters the time dependent behaviour. As expected, the GS1/standard nut sample exhibited the highest rate of relaxation. The preliminary results indicate that after 100 hours about 50% of the bolt tension will be lost with this combination of channel and nut. This can be compared to a preload loss of 22% in 100 hours, reported Mottram (2004a) for a conventional M16 bolt PFRP joint, which was torqued to 70 Nm. It is believed that the higher rate of bolt tension loss with the standard nut is due to additional stress relieving caused by material damage as well as the visco-elastic material creep. Since the smooth nut does not cause localised material damage the rate of bolt tension shedding was less since only the creep relaxation process will be active. Audible acoustic emissions from the GS1 and GS2 specimens some hours after bolt tightening indicate the presence of a time-dependent indentation process, which will greatly contribute to a reduction in the bolt tension. The increased bearing surface area and resulting lower mean bearing stress with GS2 reduces the rapid loss in bolt tension, possibly by limiting any time-dependent indentation process. The loss

after 100 hours is about 25%, similar to a bolt with standard washer and nut determined by Mottram (2004a), and half that with the GS1 channel. The long-term relaxation in tension for the two samples with the smooth connector are found to be similar and as Fig. 3.6 shows their response gives more than 30% loss in 100 hours. This however cannot be due to any indentation process and is due to the material's visco-elasticity.

3.4.4 Investigation of bolt plate tension zone

To fully characterise the strength and durability of a connection, the response of all components of the connection should be examined.

The application of a fastening bolt torque to the connection not only causes damage to the internal lips of the channel section but also develops significant stresses within the bolt plate, which will tend to act in bending between the supporting channel lips. As it is intended to use lightweight foam cored shapes as the web panels in the building system panels (these are shown in Fig. 2.11(a) and (b)), the effect of such assembly loads on this highly shear flexible component should be examined.

To assess the stress field generated in the PFRP bolt due to the presence of the fastening torque of the M10 connector an instrumented PFRP bolt plate manufactured from Extren© 625 flat sheet material (50 × 200 × 6.35 mm) was fitted to a GS2 channel with the standard serrated connector. A 10.5 mm diameter hole was supplied centrally to the plate providing the necessary load path to tighten the M10 bolt against the channel. Two 2 mm strain gauges (type FLA-2-120-11) were attached to the underside of the PFRP plate in the transverse direction. As Fig. 3.7 shows these gauges were offset at distances of 5 mm and 15 mm from the edge of the bolt hole. The strain response was recorded in real time using an Orion Solartron 3531 data acquisition system.

Figure 3.8 shows the increase in tensile strain on the underside of the bolt plate at the two positions under increasing fastening torque. Strains of up to 5000 $\mu\varepsilon$ were generated under only a moderate fastening torque of 10 Nm, although no cracking and grazing of the veil was noticeable after the removal of the bolt plate, it can be expected that such high strains (0.5%) are likely to affect the serviceability of the bolt plate possibly reducing the bearing resistance of the PFRP plate. As highlighted in Section 3.5.3, the bolt tension can be expected to relax by up to 30% for the standard (serrated) connection over the period of approximately 100 hours; this will have the effect of reducing the flexural strains local to the fastened connection. However the presence of such high and possibly damaging strains developed during the installation of the connection cannot be justified.

Let us now assume that the strain is inversely proportional to the second moment of area and, therefore, to the cube of plate thickness, ie. $\varepsilon \propto 1/h^3$. From this assumpution a plate thickness of at least 11 mm is required to give an acceptable localised strain near the bolt hole of 1000 $\mu\varepsilon$ (for design purposes), for a fastening torque of 10 Nm, as recommend by Mita Ltd.

For a specific PFRP building system, which utilises the Unistrut connection it is recommended by the author that the stiffness of the bolt plate local to the connection be substantial enough to adequately resist, the flexural stresses developed in the application of a suitable fasting torque.

3.5 Principal load-slip test

3.5.1 Specimen details

A pullout type test method is used to determine the shear load-slip characteristics that can be used to establish the four connection design parameters listed in the

Section 3.1. The specimen and load fixture are shown in Figs. 3.9 and 3.10. In order to achieve a state of pure shear at the PFRP/nut interface the specimen has two connections symmetrically placed with respect to the axial loading. Each specimen comprises two 150 mm lengths of PFRP channel bonded back-to-back using a 0.5 mm thick layer of a two-part cold-curing epoxy adhesive. The test arrangement, which minimises secondary moments, is shown in Fig. 3.9. Figure 3.9 also shows the loading yoke comprising two vertical steel plates of thickness 6 mm that are secured by bolting to a central rigid beam. At a distance of 75 mm from the free-end of the channels, a Unistrut connection per side is made to join the steel side-plate to the back-to-back channels. Load was applied using the 250 kN DARTEC 9500 hydraulic testing machine shown in Fig. 3.10. When the specimen is set-up its loading yoke is gripped by the top set of grips in the testing machine. Steel plates at the base, which are bolted through the webs of the bonded back-to-back channels (not shown in Fig. 3.9), are clamped by the bottom set of grips and used to subject the specimen to tensile load. This feature of the test arrangement can be seen in Fig. 3.10.

For the load-slip results presented in this chapter the recommended test procedure given in BS 6946:1998 for steel channels was not followed. The British Standard method requires an eccentric load to be applied to the Unistrut connection. This was deemed inappropriate since the use of this connection method in PFRP modular beams, such as shown in Fig. 1.2, would induce a state of pure shear. Tensile load is applied to a specimen at room temperature at a constant stroke rate of 0.3 mm/s. The load-slip response was recorded in real time using an Orion Solartron 3531 data acquisition system. By dividing the tensile load by two the shear force per connection can be determined.

3.5.2 Experimental procedure

For the preliminary short-term resistance test series sixty load-slip tests were conducted using the standard and the smooth nuts and the first-generation GS1 channel of PFRP. The two connections in a specimen were tightened to a constant torque of 10, 15, 20, 25, 30 or 35 Nm. At each torque value, five nominally identical load-slip specimens were made and tested.

A series of 12 load-slip tests were completed next using the standard nut and the second-generation GS2 channel. Based on the results of the preliminary load-slip tests and the bolt torque characterisation work mentioned in the previous section, it was decided to use a single torque of 20 Nm in all future test series. As Figs. 3.1(a) and 3.2(a) show the 4.5 mm height of the GS1 lip on to which the nut groove locates is greater than the 2 mm depth of the grooves (Fig. 3.3). On achieving full serration indentation there will therefore be an air gap (about 2.5 mm high) between the bottom surface of the nut and the GS1 shape (Fig. 3.2(a)). In the case of GS2 the height of the lip in Fig. 3.2(b) can be assumed to be no more than the 2 mm depth of the grooves on the Unistrut connector. This means that there is potential, before the same depth of serration indentation with shape GS1, for bearing to occur between the flat bottom surface of the nut and the shape. So when compared to GS1, the different boundary conditions where the standard nut and GS2 shape make contact could reduce the zone of localised material damage (by limiting the crushing and shearing failure mechanisms). Based on the different lip designs of the two PFRP channels their Unistrut connection load-slip characteristics can be expected to be different.

3.5.3 Preparation and testing of conditioned samples

To determine if the shear resistance properties change with hygrothermal aging six specimens of both GS1 and GS2 channels were fitted with the standard nut at a fastening torque of 20 Nm and exposed to a hygrothermal environment by placement in Grant Sub-36 tap water baths, at a constant temperature of 40°C for the duration of 1000 hours. Except for the localised PFRP stress fields where the nut made contact, these specimens were unstressed while in the baths. This hot/wet aging test procedure is in accordance with ASTM 5229M for the durability testing of FRP materials, and this can be assumed to be equivalent to two years of exposure to the outside environment. To prevent water ingress, except where the serrations expose fibres, the specimen's surfaces at the cut ends and fixing holes were sealed using Araldite 2015 two-part toughened epoxy resin. After removing the specimens from the baths the load-slip test procedure was the same as that used in the short-term resistance tests.

3.5.4 Preparation and testing of samples under sustained loading

Single specimens of GS1/standard nut and GS2/standard nut were prepared in order to determine the influence of visco-elastic material creep on the connection's stiffness when the shear force is constant for an extended time period. Using the DARTEC 9500 testing machine in load control each specimen was subjected for duration of 200 hours to a constant working load of 70% of the mean ultimate shear force. The ultimate shear force was established on analysing the load-slip results from the short-term and accelerated-aged characteristics. Tensile load was applied at an initial loading rate of 0.05 kN/sec. It took 100 seconds to reach the 5 kN load, which gave a shear force per GS2 connection of 2.5 kN. The constant force for the weaker GS1 connection was 1.8 kN.

3.6   Results and Discussion

3.6.1   Principal load slip tests

The load-slip results will be presented and evaluated to determine the four connection design parameters. If the connection method is to be used in modular construction systems the designer needs to know the relevant connection properties at the serviceability (SLS) and ultimate limit states (ULS). These two states for the Unistrut connection method are as follows. The ULS is given by the ultimate shear force per connection, which according to BS 6946:1998 is the resistance developed in the connection at a continuous slip. Based on the new results presented here this is taken, for PFRP material, to be a slip of 3 mm. To check for the SLS deflection the designer requires knowledge of the connection stiffness (or modulus). For the short-term loading situation this is defined to be the secant stiffness of the linear portion of the load-slip curve up to a slip of 1 mm. If the shear loading on the connection is constant for a long period of time there will be additional slip due to 'creep', which effectively reduces the connection stiffness at SLS. For such a long-term loading situation the stiffness can be redefined to be that determined by dividing the connection load given by either $2/3^{rd}$ of ULS or the initial load at 1 mm slip, which ever is lower, by the initial 1 mm slip plus the increase in slip due to creep. Note that the value of the long-term connection stiffness will change, as it is dependent on the magnitude of the constant load and its time of application. To complete a modular beam design, the recommended bolt torque for the Unistrut connection is required.

In presenting the load-slip test results in Figs. 3.11 to 3.14 the measured stroke by the DARTEC testing machine is taken to be the slip at the PFRP/nut interface. The load is the shear force per connection. To prevent the plots from being overcrowded with curves the mean curve from a batch of five specimens

is often given. Tables 3.1 and 3.2 are given to collate the secant stiffness and strength results, showing per connection the mean and range values for each batch tested. The final entry in the two tables gives the results for the GS1 steel channel using the test procedure developed by the author. It is to be noted that with the standard nut and the GS1 steel channel the mode of failure limiting the peak shear force to 3.8 kN is shearing-off of the serrations. When the material is PFRP the serrations are not damaged and the nut can be used more than once.

Figure 3.11 shows the batch mean shear force-slip for the GS1/standard connection with increasing torque from 10 to 35 Nm, in increments of 5 Nm. The general shape of the short-term resistance test curves can be described as commencing with a linearly increasing shear force, culminating in a peak value at approximately 2 mm slip. A region of pseudo-ductility follows the peak, showing that the connection does not fail in a brittle manner. The slip, at peak shear force, is found not to change significantly with the bolt torque. Prior to full serration indentation, the post-peak force remains constant and this behaviour is associated by a dominant shear failure mechanism in the CFM layer. Under this situation, when the torque is 15 Nm, or less, a high proportion of the shear force is being reacted against by the outer CFM reinforcement. As shown in Fig. 3.2(a), this CFM layer has a thickness of 0.5 mm where the nut is located. This layer and the outer resin rich layer can be expected to be more shear flexible than the much stiffer UD core below.

For bolt torques higher than 15 Nm there will be full indentation of the serrations into the underlying UD. The force at slips >2 mm is now lower than the peak value and it is believed this is due to a shear failure mechanism controlled by the UD core. Intermittent acoustic emissions emanating from the fracturing UD fibres were audible during all the load-slip tests in which the torque was 20 Nm, or higher. The development of this progressive damage growth was found

to coincide with the discontinuities in the load slip measurement (see Fig. 3.12), before the peak load was attained. The actual shape of the curve post-peak might depend on a combination of the various competing failure mechanisms. The PFRP is found to ultimately fail along a shear plane through the UD core and this severe lip failure is shown in Fig. 3.15. As the PFRP material behaviour is controlled by the degree of the serration indentation into the stiffer UD core the secant stiffness at 1 mm slip increases with torque, and this is also why the peak force in Fig. 3.12 increases significantly from 2 to 3.5 kN. The mean secant stiffness is found to increase with applied bolt torque from 1.33 kN/mm at 10 Nm to 2.40 kN/mm at 25 Nm. The measured stiffness then reduces to 1.85 kN/mm at 30 Nm and is then similar to the 25 Nm value when the maximum torque of 35 Nm is applied. These values are given in rows one to six of column seven in Table 3.1.

The standard nut has been designed to grip into the lips of channels (with GS1 dimensions) of structural grade steel. Steel will allow the very high localised stresses of indentation to be redistributed by material plasticity and so allow the Unistrut connection to have a load-slip curve that closely mimics the stress-strain relationship of steel. Such an acceptable structural performance cannot be expected with a PFRP channel and the standard nut, since the increasing zone of localised material damage with increasing bolt torque cannot be relieved by material plasticity.

The short-term resistance test curves plotted in Fig. 3.12 give the individual load-slip results for the 20 Nm connections of the GS1 PFRP channel and standard nut. The curves show that there is significant variation within the batch of five specimens. This is believed to be due to the shape's non-homogeneous reinforcement (e.g., local fibre variation, imperfections, resin rich areas and the presence of micro-cracks), and varying damage zones caused by the serrations

being fully impressed into the PFRP. Peak shear force ranges from 2.2 to 3.7 kN at approximately a constant slip of 2 mm. The presence of a rapid load increase of 1 kN at the start of the test is indicative of an initial very high shear stiffness. After this sudden increase there is a fairly linear load-slip response to the peak load. This is followed by a pseudo-ductile region of slip under a fairly constant shear force of between 2.0 to 3.0 kN per connection.

From visual study of the material damage to the tested specimens fitted with standard connections it has been possible to determine two processes from which the resistance maybe generated. At low applied torques (10 - 15 Nm) the connection resistance is generated via the bearing resistance of the material, in front of the lightly indented serrations, leading to a scraping type of failure. For such a failure mode the ultimate peak load may be limited by the 2.5 mm spacing of the serrations. Consider a standard connection at a slip of less than 2.0 mm, the serrations are acting in 'virgin' material, at a slip of approximately 2.0 mm all the serrations with the exception of the foremost serrations enter a region of degraded material, resulting in a loss of resistance. At slips >2.0 mm only the foremost serrations act in bearing on 'virgin' material the trailing serrations only provide additional resistance in the form of dynamic surface friction, where slip is accompanied by a scraping action removing material from in front of the serrations.

The development of a shear plane in the PFRP material below the indented serrations occurs for the standard connections with a higher applied torque (>20 Nm) providing a greater degree of indentation of the serrations. A shear plane type failure is clearly visible in Fig. 3.15.

Figure 3.13 presents mean results with varying torque when the GS1 connection has the smooth nut. Comparing with the equivalent curves in Fig. 3.11 for the standard nut case it is seen that the common form to the shape of the load-

slip curve suggests a single dominant failure mechanism (i.e. sliding). For the same bolt torque the peak shear force is found to have reduced. For example, at the torque 20 Nm the smooth nut gives a maximum shear force of 1.75 kN, which is 41% lower per connection than with the standard nut. This peak is attained at a slip of <1 mm, which is half the slip for the peak with the standard nut (see Fig. 3.11). The mean secant stiffness is found to linearly increase with applied torque from 1.12 kN/mm at 15 Nm to 2.12 kN/mm at 35 Nm. As found with the standard nut the stiffness at the 30 Nm torque is seen not to fit the increasing trend. These values are given in rows ten to fourteen of column seven in Table 3.1. For slips >1 mm the load transmitted through the connection does not reduce and there is evidence from the curves in Fig. 3.14 to suggest that it might even slightly increase. The 'constant' load to 5 mm slip is believed to be due to the smooth nut sliding along the lips, on overcoming the dynamic frictional force developed by the presence of the normal bearing stress. On completing the load test and disassembling the connection it was observed that the GS1 lips remain virtually undamaged, when the nut is smooth.

The GS1/smooth nut tests were performed within five minutes of the bolts being tightened to the required torque. Knowing that there is a high rate of reduction in bolt tension the short-term results given in Fig. 3.13 are unlikely to be relevant in the long-term; we are requiring lifetimes of 30 years or higher (Head, 1994; Karbhari *et al.*, 2000). One option to compensate for a loss in shear strength from material creep could be to recommend a higher initial bolt torque than is being designed for, however this torque would have to be limited to <40 Nm as crushing of the GS1 lips will occur. With the GS2 shape a higher bolt torque of 60 Nm can be applied without failure of the lips crushing through, it should be noted that the design and transverse stiffness of the bolting plate must be considered if fastening torques of this magnitude are to be chosen.

3.6.2 Hygrothermal effect on connection resistance

Figure 3.14 shows load-slip curves for the GS1/standard nut samples after hot/wet aging. The load-slip characteristics of these five conditioned specimens are found to give less variation up to peak shear force than the equivalent unconditioned specimens (Fig. 3.13). One possible reason for the smoother curves in Fig. 3.14 is that hot/wet aging has altered the properties of the PFRP material in the region of the damage zone. During these tests no acoustic emissions were audible, suggesting an absence of intermittent fracturing of the UD fibres. After aging, the mean response of the GS1/standard nut combination showed little or no sign of a loss in shear resistance. Similar values for mean peak shear force and the mean shear force at continuous slip are given in Table 3.2 for both the conditioned and unconditioned batches. Despite the presence of the damage zone this finding indicates that any changes to the PFRP material after the 1000 hours conditioning under water at 40°C has not affected the bearing and shear resistances that limit the resistance of the Unistrut connector. This observation is not supported by residual tensile strength testing of FRP material, which shows a reduction in strength with aging (Gaur & Miller, 1990; Hofer *et al.*, 1986).

Figure 3.16 gives the batch mean load-slip curves for the conditioned and unconditioned samples of GS2 and standard nut. This shows increased stiffness and strength over the batch mean values in Tables 3.1 and 3.2 for the equivalent tests with the GS1 channel. The secant stiffness at 1 mm slip was found to have reduced from 2.5 kN/mm to 1.9 kN/mm after hot/wet aging. At a slip> 2.5 mm, a pseudo-ductile failure mode is associated with a constant shear resistance of 3.6 kN. This is an 18% decrease in shear load compared with the non-conditioned connection. Based on the work of (Liao, 1989; Gaur & Miller, 1990) the observed loss in interlaminar shear strength in Fig. 3.16 from the environmental

aging could be a result of a number of actions such as, matrix softening, leaching out of the low-molecular weight oligomers from the resin/E-glass interface, and hydrolysing of the coupling agent. Other factors over the 1000 hours of conditioning that could have affected the connection's load-slip characteristics are the relaxation in bolt tension and changes to the nature of the contacting surfaces where the slip between the channel and the nut occurs.

3.6.3   Long-term standard connection response

Figure 3.17 gives single plots for the slip increase with time for the constant load response of the standard nut with the two PFRP channels. The constant shear load per connection is 1.8 kN for shape GS1 and 2.5 kN for shape GS2. At time zero there is an initial slip similar to that given in Figs. 3.11 and 3.13. This is not shown in Fig. 3.17. The two PFRP channels exhibit similar behaviour under sustained loading, showing two distinct time dependent processes. There is an initial linear increase in displacement in the first 2 to 4 hours, followed by a much slower exponential rate of increase for the remaining time to 190 hours. Under the constant load of 2.5 kN the slip for GS2/standard nut increased by 0.2 mm over 4 hours, by an unknown mechanism. Further slip increase occurs due to visco-elastic response and this gives a total increase in slip of 0.28 mm after 190 hours. It can be expected that the slip will continue to increase at a continually reducing exponential rate, and that, if the load remained constant for years, the connection secant stiffness used in design would need to be lower than the short-term values given in Table 3.1.

3.7   Analysis of Results

In accordance with BS 6946:1998 the load at 1 mm slip and under continuous slippage, herein taken to be 3 mm, will be used to evaluate a connection's structural performance. The mean shear force for the three connections types GS1/standard, GS1/smooth and GS2/standard are plotted in Figs. 3.18(a) and (b) at the slips of 1 mm and 3 mm, respectively. The mean values per connection are from a batch of five specimens, the corresponding error bars show the standard deviation asssociated with each data set. In the figures the connection symbols ◇ ,□ and △ are for the channel/nut combinations of GS1/standard, GS1/smooth, and GS2/standard. For each channel/connection combination a linear trendline is fitted to the mean data, indicating the gerenal trend.

Both nuts and the GS1 channel give similar shear forces at the 1 mm slip and both connections exhibit similar linear trends with increasing torque. There is a gradual increase in the force to a torque of 25 Nm. This is followed by a decrease of approximately 20-25% when the torque is increased from 25 to 30 Nm. It is believed this could be due to the onset of crushing of the PFRP lips. On increasing the torque to 35 Nm the shear force at 1 mm slip is found again to increase with the standard nut, but not substantially. The reason(s) why the mean force should change as it does in Fig. 3.18(a) is/are unclear.

On comparing the results in Figs. 3.18(a) and (b) it is found that the shear force carried by the GS1/smooth connection remains unchanged as the slip increases from 1 to 3 mm. This is because the peak force was attained at a slip <1 mm, and for higher slips there is little variation in the load (Fig. 3.14). For the standard connection the shear force at 3 mm is higher than at the 1 mm slip. A slip of more than twice 1 mm is required to attain this GS1 connection's peak load.

Under short-term testing the standard nut gives the GS1 connection with the highest shear force at both the 1 and 3 mm slips. This standard connection might, however, be unsuitable for use in PFRP modular systems (Fig. 2.10(b)) because the severe material damage zone created by the serrations impressing into the PFRP lips could comprise the connection's durability and reduce its long-term strength and stiffness. The preliminary results in Fig. 3.16, from the load-slip tests conducted on the hot/wet aged specimens, suggest otherwise, as the connection's strength and stiffness has increased. Further work is required to obtain the scientific evidence to explain this observation, which is the opposite of what would be expected (Khennane & Melchers, 2000).

Smooth connections, although giving more consistent load-slip results (Fig. 3.13) and minimal PFRP damage, provided a significantly lower mean peak load at only 1.75 kN (bolt torque is 20 Nm). This lower load is due to the limited frictional force that can be generated between the steel nut and GS1 channel. Moreover, the maximum frictional force will reduce with time as the bolt tension relaxes (see Section 3.5.3).

Because the mean shear forces in Figs. 3.18(a) and (b) are given at specified slip values they give a direct measure of the connection stiffness. It can be seen that the GS2/standard nut, at the 20 Nm torque, provides the stiffest and strongest connection. For the batch of five specimens the shear force varies between 1.7 and 3.4 kN at 1 mm slip, and between 3.6 and 4.6 kN at 3 mm slip. The means of the batches are 2.5 and 4.1 kN, (StD = 0.75, CoV = 0.30 and StD = 0.35, CoV = 0.09) respectively. These give on average a 60% increase in the secant stiffness over the standard connection with the GS1 channel at the same applied torque.

Results in Fig. 3.18 show that the GS2 and the standard nut will give the connection with highest shear properties. It is also the connection combination

that gives the least material damage due to serration indentation. It is therefore the most suitable Unistrut connection to be used in PFRP modular systems. However, its application in modular beams will depend on the design accounting for the two long-term effects of environmental aging and creep, which have been shown in Figs. 3.16 and Fig. 3.17, respectively, to reduce structural performance of the Unistrut connection.

Using the test data that is representative of in-service conditions the four connection design parameters listed in Section 3.2 can be established. The test series presented earlier have been used to show that modular beam systems should use the GS2/standard nut connection as it gives acceptable structural properties. The design parameters, which are established using the load-slip characteristics, will be determined for the recommended initial bolt torque of 20 Nm. To take account of strength and stiffness reductions due to in-service conditions the ULS and SLS design parameters for this connection will be based on load-slip data from the conditioned specimens (Fig. 3.14 and Fig. 3.16). The design parameters for stiffness and resistance of the GS2/standard nut connection are determined using mean values. Many more load-slip test results are required to apply reliability analysis and statistical evaluation to determine characteristic values and partial safety factors (Gulvanessian *et al.*, 2002) for the strength and stiffness of this Unistrut connection. However, a justification for giving mean values now is that modular systems require the connections resisting the longitudinal shear force to work as a group.

At the ULS the mean shear force per connection is 3.7 kN. This design parameter is given in row 16 of column eight in Table 3.2. The short-term secant stiffness is 1.8 kN/mm. It is found that the shear force of 1.8 kN at 1 mm slip is less than 2.4 kN, which is $2/3^{rd}$ of ULS. The shear force per connection of 1.8 kN is therefore the maximum force that a connection can transmit at SLS. A

long-term stiffness can be estimated from the results of the preliminary creep test given in Fig. 3.17. From an initial slip of 1 mm the estimated increase is 0.4 mm, for an 'in-service' aging and constant load period of two years. The estimated lower connection stiffness which will account for the connection subjected to its SLS shear force for 2 years is therefore given by 1.8/(1.0 + 0.4) which gives 1.3 kN/mm.

3.8   Conclusions

- A new load-slip test method is presented which can be used to characterise the structural performance of the Unistrut connection method with Pultruded Fibre Reinforced Polymer (PFRP) channels, subjected to a state of pure shear.

- The load-slip characterisations show that the shear properties of strength and stiffness of the Unistrut connection depend on the in-service conditions and the choice of the channel shape, the nut, and the bolt torque.

- The 2 mm high serrations on the standard nut are found to cause considerable material damage when the bolt is tightened so that full indentation is achieved. Such PFRP damage might be detrimental to the long-term durability and shear properties of the connection.

- To minimise the PFRP damage zone the serrations were removed from the standard nut and the load-slip characteristics of the smooth nut connection gave lower strength and stiffness.

- The structural performance of both the standard and smooth connections are found to be limited by the bearing strength of the PFRP material, as this material property limits the bolt torque that can be applied to them.

- For the connection combination of the General Strut 2 (GS2) channel and standard (serrated) nut the following four design parameters have been established:

  - The initial bolt torque for the M10 bolting is 20 Nm.

  - The mean shear force per connection at ULS is 3.6 kN.

  - The mean short-term connection stiffness (or modulus) at SLS is 1.8 kN/mm.

  - The estimated long-term connection stiffness (or modulus) at SLS is 1.3 kN/mm.

- The long-term stiffness is a rough estimation for an 'in-service' aging and constant load period of two years and the SLS stiffnesses and ULS strength are determined from the mean measured values.

- The four connection design parameters will enable the design engineer to calculate the structural performance of a PFRP modular system beam where composite action is made through the application of Unistrut GS2/standard nut connections.

- Many more load-slip test results are required to apply reliability analysis and statistical evaluation to determine characteristic values and partial safety factors for the strength and stiffness of the Unistrut connection method with PFRP shapes.

- The development of strains in excess of 5000 $\mu\varepsilon$ in the bolt tension investigation, have shown this would have undoubtedly lead to significant damage to the connecting plate especially if the material were as proposed in the Startlink modular system, a foam core with two outer faces of structural PFRP.

- The level of uncontrolled material damage caused to the internal lips by the indentation of the serrations and combined with the bearing of the connector on the lips as shown in Fig. 3.15, is unacceptable for such connections.

- Although the Unistrut connection method provides a unique blind fixing method that is suitable for the proposed Startlink modular system and has been shown to provide purchase and connection between PFRP components, it is by no means an ideal and appropriate method of connection for such a brittle and anisotropic material.

3.9 Figures & Tables
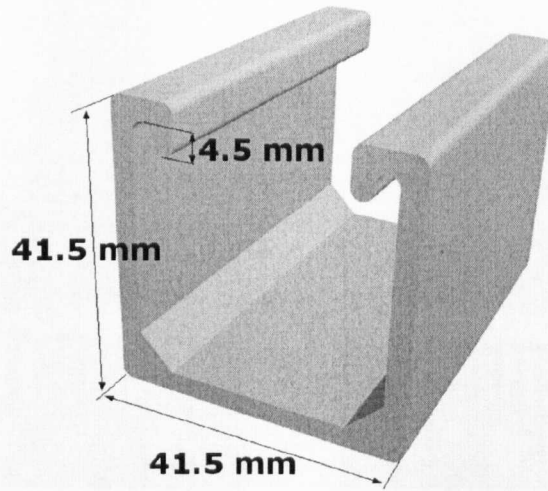
(a)
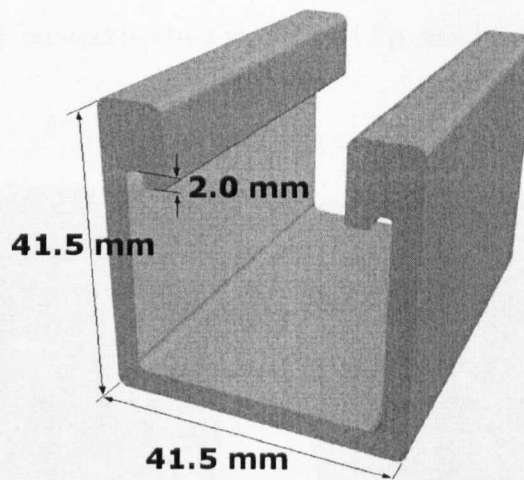
(b)

Figure 3.1: Channel shape dimensions(a) GS1 (b) GS2

(a)   (b)
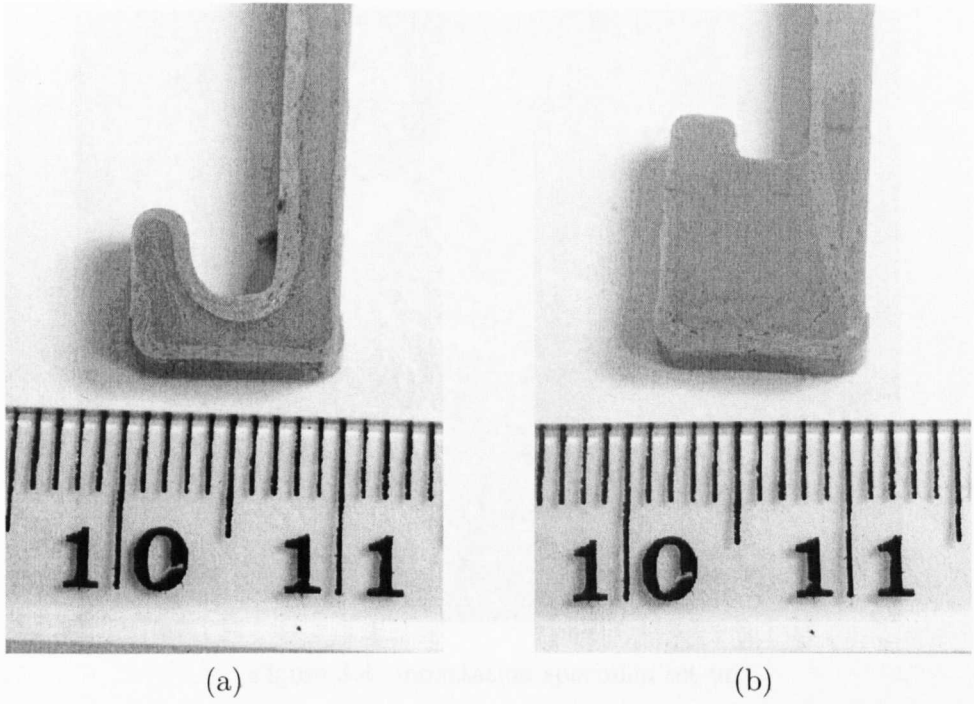
Figure 3.2: Fibre architecture for (a) GS1 lip detail (b)GS2 lip detail

(a)   (b)
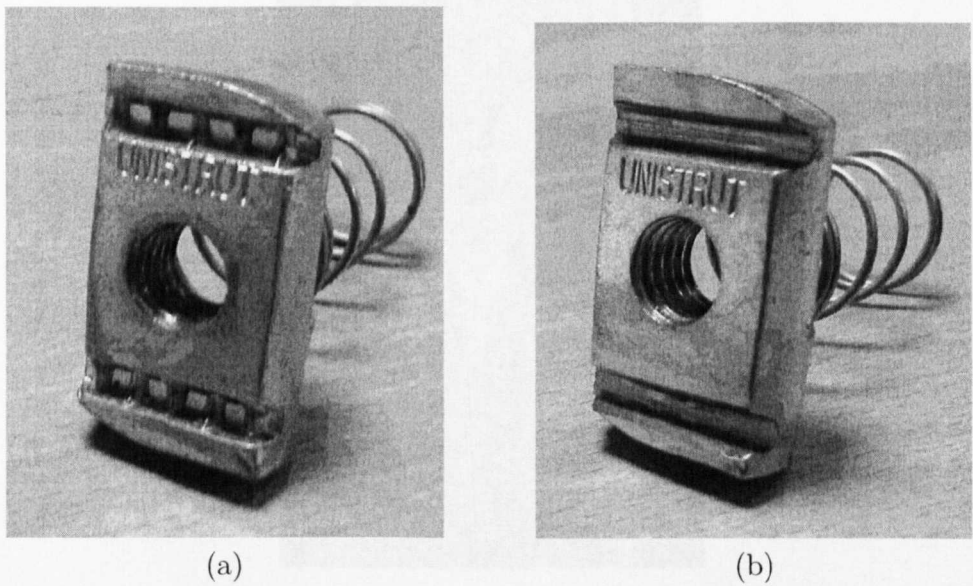
Figure 3.3: M10 Unistrut connectors (a) standard nut (b) smooth nut
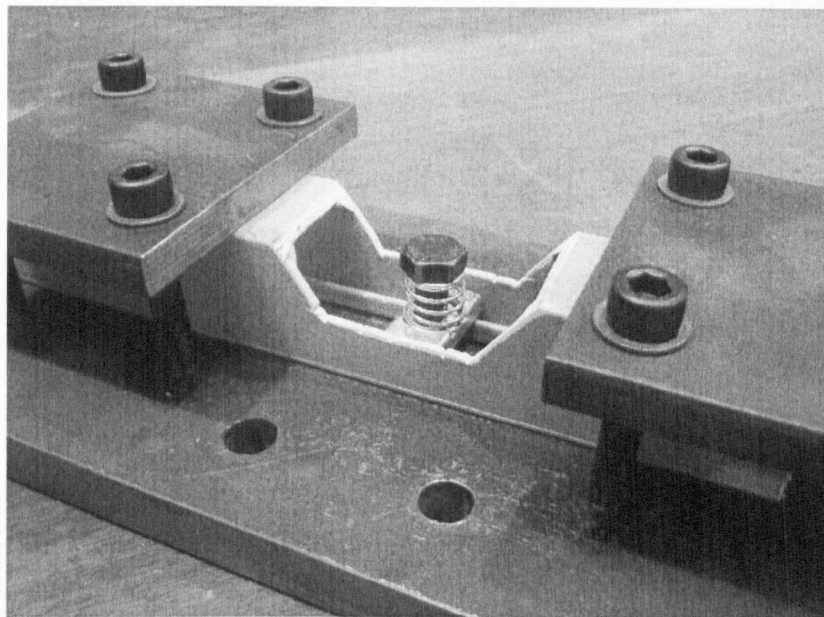
Figure 3.4: Indentation specimen set-up

Figure 3.5: Instrumented torque tube
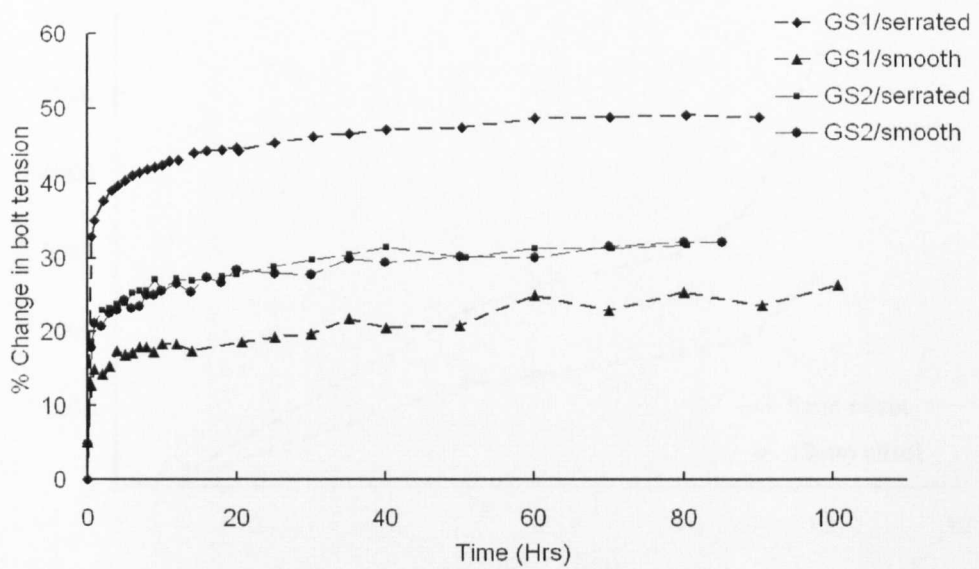
Figure 3.6: Variation in bolt tension relaxation for various connection arrangements
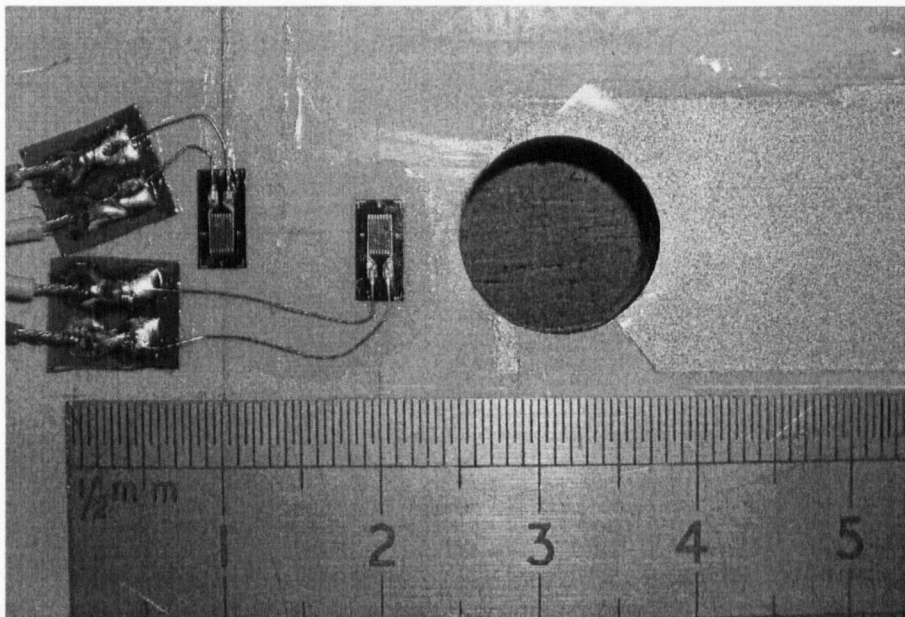
Figure 3.7: Strain gauges and photoelastic surface on underside of bolted Unistrut connection
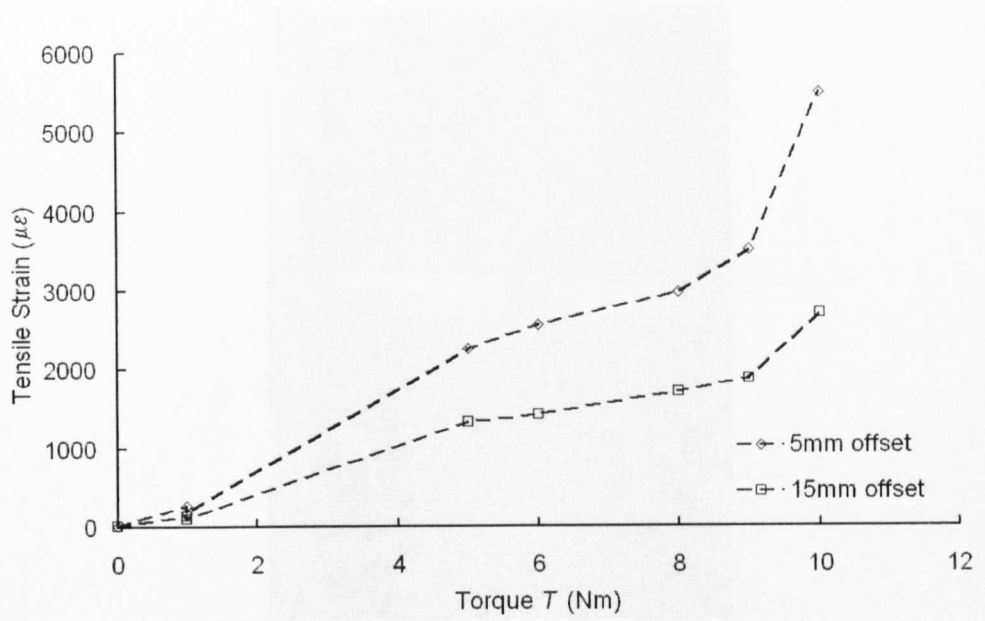
Figure 3.8: Plot of tensile strain - applied torque
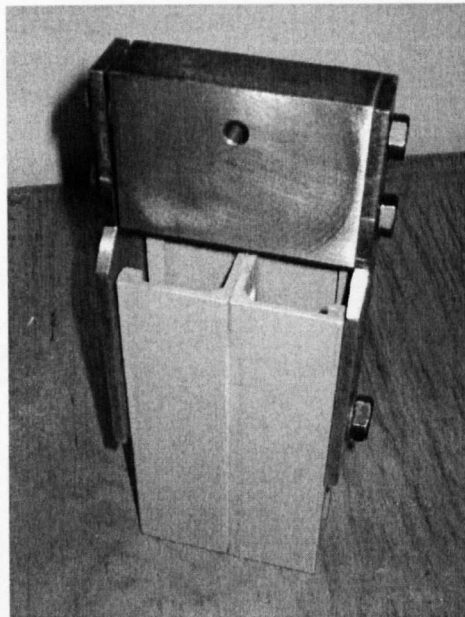
Figure 3.9: Load - slip specimen and steel loading yoke
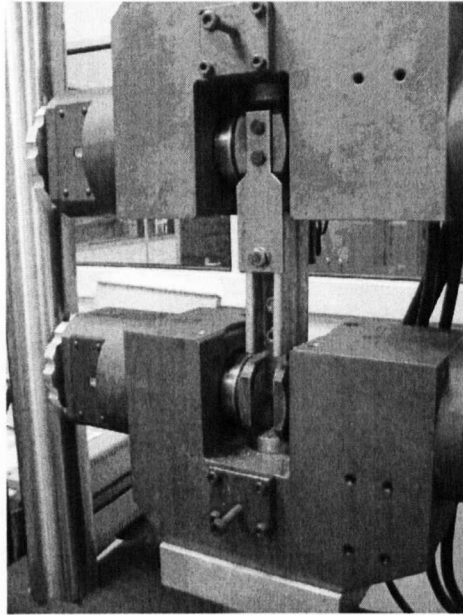
Figure 3.10: Load - slip specimen in Dartec 9500 testing machine
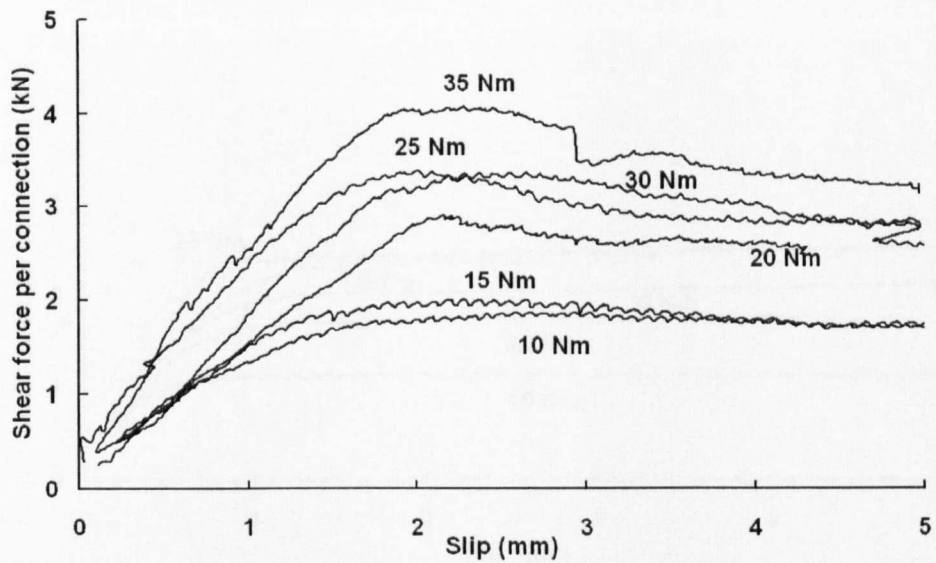
Figure 3.11: Plot of GS1 batch mean load - slip characteristics for the standard nut with increasing bolt torque
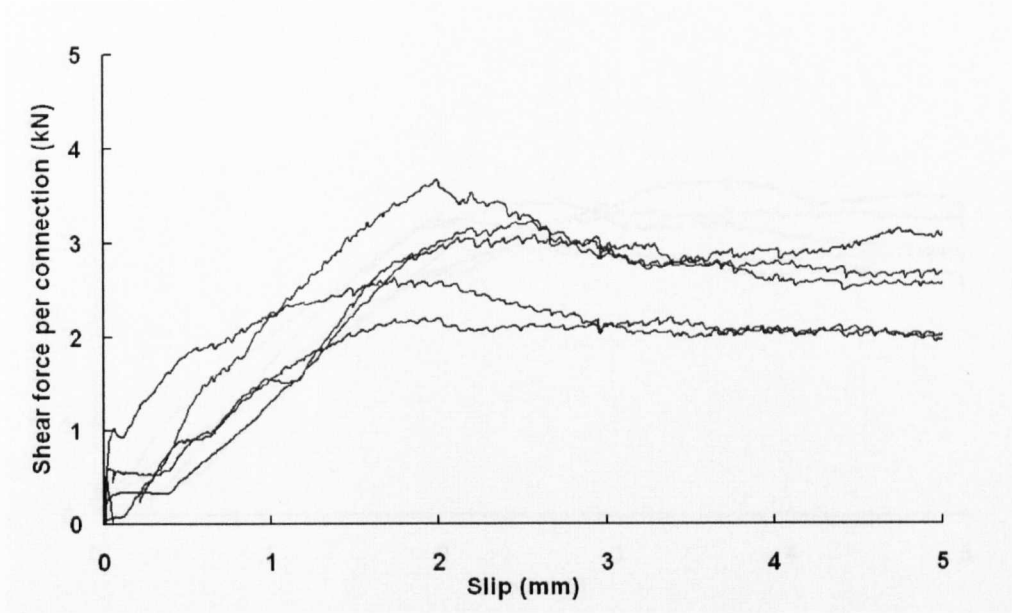
Figure 3.12: Plot of load - slip curves for GS1 samples with the standard nut and bolt torque of 20 Nm
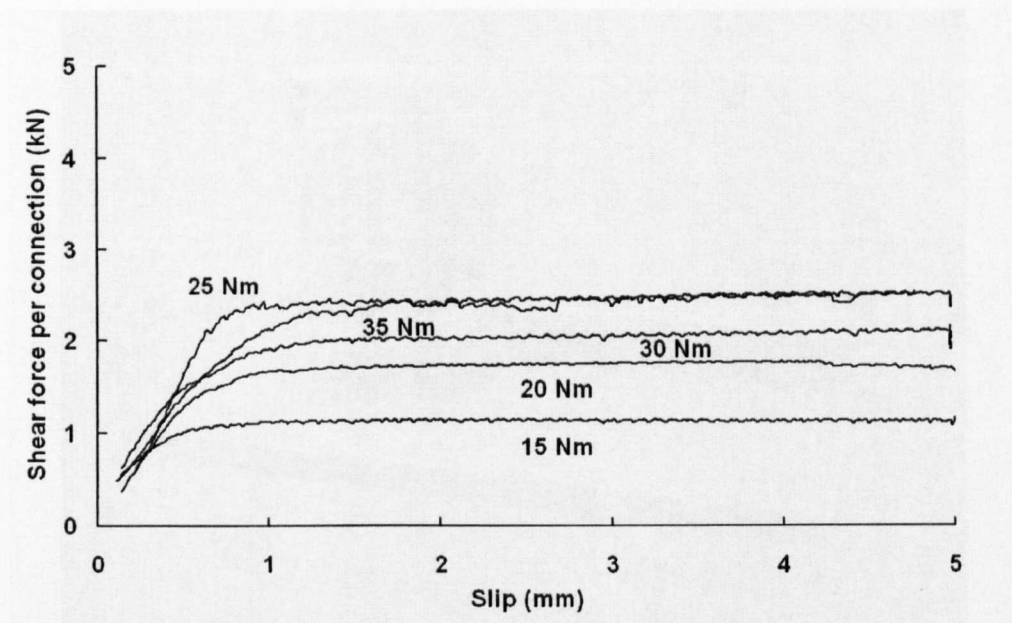
Figure 3.13: Plot of GS1 batch mean load - slip characteristics for the smooth nut with increasing bolt torque
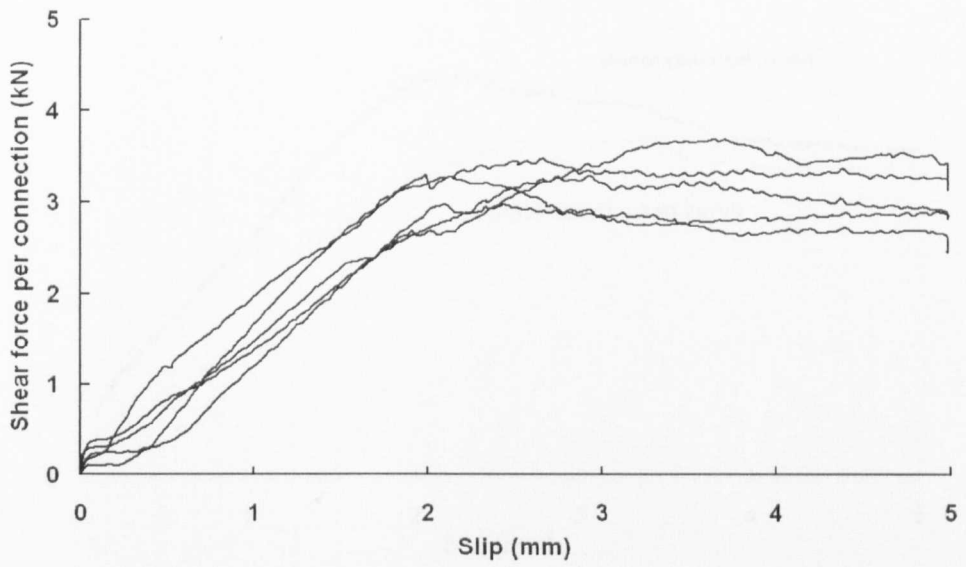
Figure 3.14: Plot of load - slip curves for GS1 conditioned specimens with standard nut and bolt torque of 20 Nm

Figure 3.15: Material damage to GS1 shape after 5 mm slip with standard nut and bolt $\geq$ 15 Nm
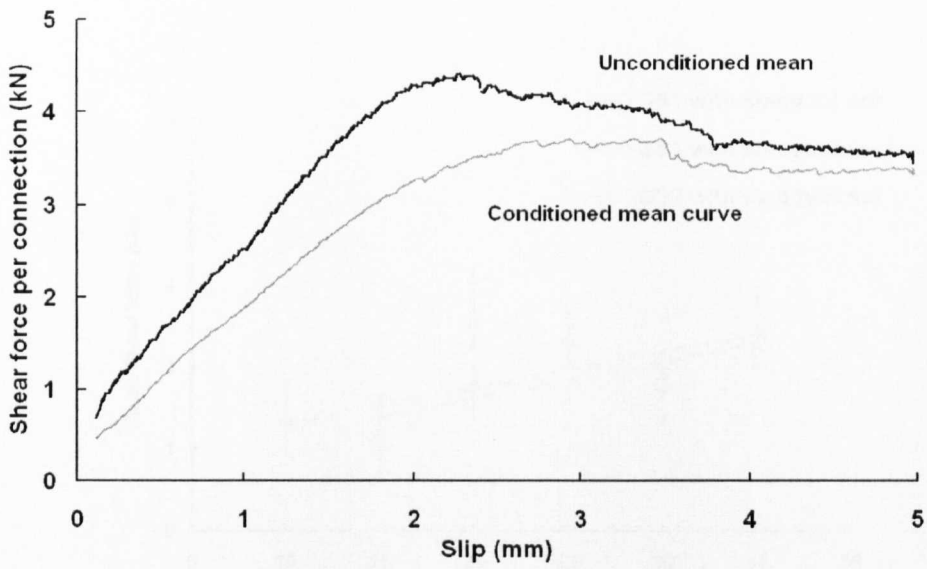
Figure 3.16: Plot of conditioned and unconditioned GS2 batch mean load-slip curves for standard nut with bolt torque of 20 Nm
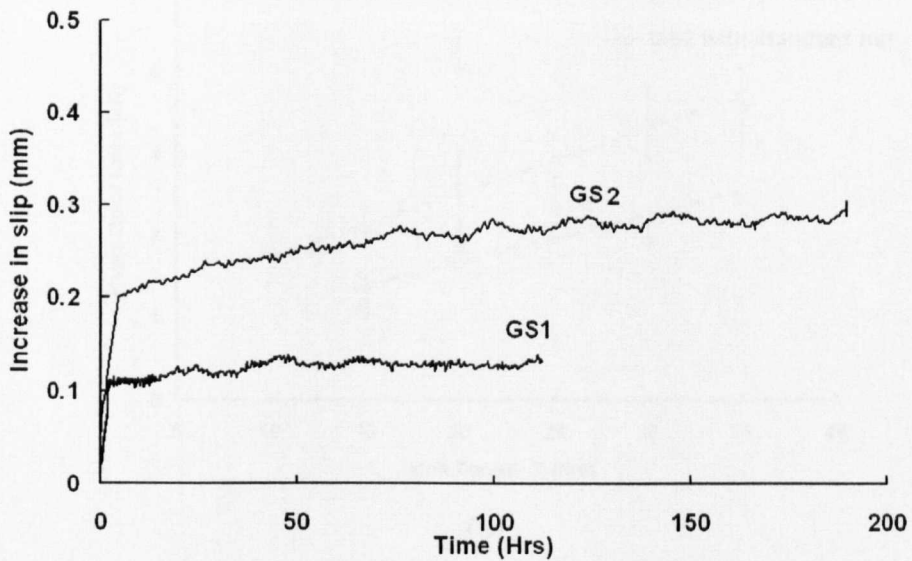
Figure 3.17: Plot showing increase in slip under sustained shear loading for GS1 and GS2 channels with standard nut and bolt torque of 20 Nm
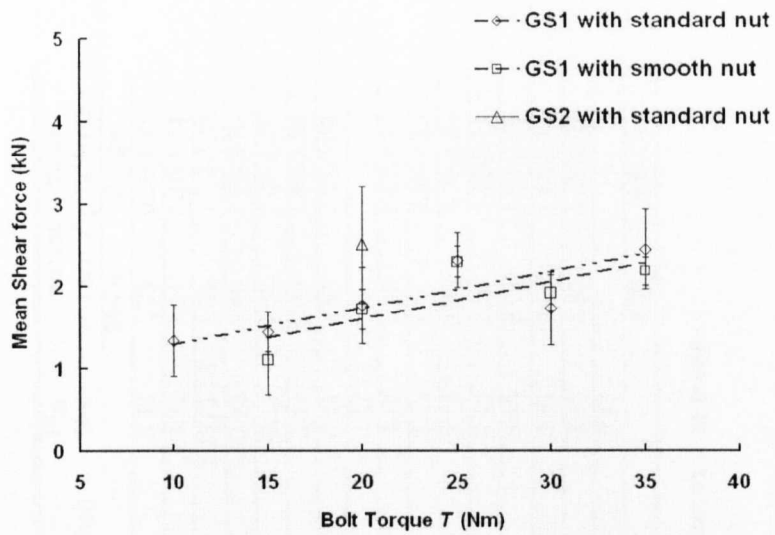
(a)
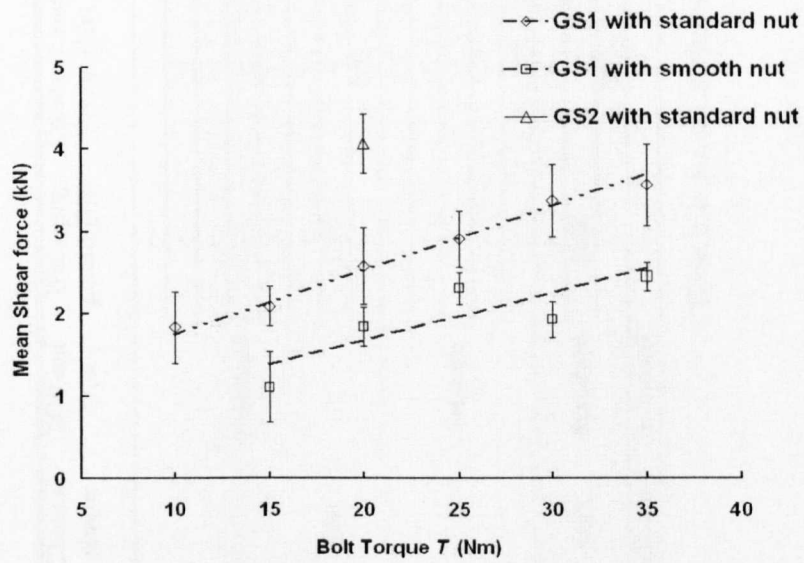
(b)

Figure 3.18: Plots of mean shear force per connection (a) 1 mm slip (b) 3 mm slip

Channel shape	M10 nut type	Wet aging period (Hr)	Constant load period (Hr)	Bolt torque (Nm)	Fig. No.	Secant stiffness at 1mm slip (kN/mm)	
						Mean	Range
	Standard	-	-	10	3.11	1.33	0.96-1.83
		-	-	15	3.11	1.51	1.10-1.74
		-	-	20	3.11/3.12	1.56	1.29-2.20
		-	-	25	3.11	2.40	1.80-2.70
		-	-	30	3.11	1.85	1.27-2.35
		-	-	35	3.11	2.50	1.94-2.80
GS1		1000	-	20	3.14	1.55	1.20-2.00
		-	200	20	3.17	-	-
	Smooth	-	-	15	3.13	1.12	0.67-1.76
		-	-	20	3.13	1.66	1.38-2.20
		-	-	25	3.13	2.00	1.72-2.20
		-	-	30	3.13	1.92	1.75-2.16
		-	-	35	3.13	2.12	1.97-2.40
GS2	Standard	-	-	20	3.16	2.52	1.65-3.43
		1000	-	20	3.16	1.89	1.20-2.59
		-	200	20	3.17	-	-
GS1 Steel	Standard	-	-	20	-	2.90	2.6-3.0

Table 3.1: Secant stiffness of connection at 1 mm slip

Channel shape	M10 nut type	Wet aging period (Hr)	Constant load period (Hr)	Bolt torque (Nm)	Peak force (kN)		Shear force at slip of 3 mm (kN)	
					Mean	Range	Mean	Range
	Standard	-	-	10	1.8	1.3-2.6	1.8	1.4-2.5
		-	-	15	1.9	1.4-2.9	1.9	1.3-2.8
		-	-	20	2.8	2.1-3.6	2.6	2.1-3.0
		-	-	25	3.3	2.4-4.5	3.0	1.7-4.3
		-	-	30	3.3	3.1-4.2	3.2	3.0-4.2
		-	-	35	4.0	3.6-4.4	3.6	3.0-4.2
GS1		1000	-	20	3.1	3.0-3.6	3.1	3.0-3.4
		-	200	20	-	-	-	-
	Smooth	-	-	15	1.0	0.7-1.8	1.0	0.7-1.8
		-	-	20	1.7	1.3-2.0	1.7	1.5-2.9
		-	-	25	2.0	1.7-2.4	2.0	1.8-2.4
		-	-	30	2.3	2.2-2.5	2.5	2.3-2.5
		-	-	35	2.3	2.2-2.9	2.5	2.1-3.0
GS2	Standard	-	-	20	4.4	3.5-5.0	4.0	3.5-4.5
		1000	-	20	3.7	3.4-4.5	3.7	3.3-4.3
		-	200	20	-	-	-	-
GS1 Steel	Standard	-	-	20	3.8	3.3-4.3	3.7	3.0-4.1

Table 3.2: Peak shear force and shear force in connection at continuous slip of 3 mm

CHAPTER 4

Modular beam prototype and its analysis for flexure

The objective of this chapter is to introduce the concepts of modularity and component interaction, into the design of a PFRP structural member. A prototype beam assembly based on the Startlink beam system (Fig. 2.11) and the Unistrut connection method characterised in Chapter 3 is introduced. The response of the assembly is predicted based on the performance of the Unistrut connection (Fig 1.3). The upper load limit on a state of full-interaction is determined for the prototype assembly assuming an infinitely rigid connection and appropriate minimum connection spacing. The response of the assembly when the degree of interaction is reduced is discussed and a possible mode of ultimate failure identified.

4.1   Standard and optimised PFRP shapes

Standard Pultruded Fibre Reinforced Polymer (PFRP) shapes consist of thin-walled composite profiles having overall dimensions typically 400 mm or less and wall thicknesses typically up to 13 mm. They have prismatic section and for

beam members the first-generation shapes are I and H (the latter are known as wide flange shapes, WF), various first generation shapes are shown in Fig. 4.1. Standard reinforcement is E-glass fibre, in the two forms of unidirectional (UD) rovings and continuous filament (or strand) mats (CFM). The UD material has longitudinal glass fibres at typically 60% volume fraction (Mottram, 2004b), while the CFM material has random fibres at about 23 to 28% volume fraction (Mottram, 2004b). The matrix is a thermoset resin such as polyester or vinylester, which often contains filler and other additives. To protect the surface of the shape there is a thin outer layer of a veil, often of nylon. This outer layer can be considered to be resin rich. For standard pultruded shapes, the Young's modulus in flexure is 20 to 25 GPa (Clarke, 1996), the in-plane shear modulus is 3.5 to 4.5 GPa (Mottram, 2004b), and the material tensile/compressive strengths are >200 MPa along the length, and about half this stress in the perpendicular directions. Under short-term loading the material is linear elastic to failure. Standard shapes mimic their steel counterparts although the largest available off-the-shelf beam members are typically less than 400 mm deep (Creative Pultrusions Inc., 2006). The third column in Table 4.1 details the dimensions of the currently largest available off-the-shelf standard PFRP sections from the leading manufacturers.

Standard I and Wide Flange shapes, Fig. 4.1(a) are found to be less efficient in flexure than their steel counterparts due to a lower modulus of elasticity; approximately $1/10^{th}$ that of steel. Moreover, the beam deformation due to shear deformation has to be accounted for in design when the Span - Depth ratio is ≤ 25. This further reduces the maximum span for a given load and deflection limited situation (for SLS design).

Laboratory evidence suggests these first generation shapes do not exploit the full potential of the material, limiting their use in the field (Mottram, 1991; Bank, 1989; Barbero & GangaRao, 1991). The dominant failure mode of pultruded

shapes is elastic buckling due to a high Strength - Modulus ratio resulting in open section shapes being highly susceptible to elastic buckling. The use of closed section shapes greatly reduces the risk of buckling instabilities, by restraining the elastic PFRP material.

Pultruding hollow sections of a useable size significantly increases the complexity and overall costs of the manufacturing process. Strongwell (2004) undertook a research and development project in the 90's to optimize, and pultrude, a second-generation shape for use as a simply supported beam in heavily loaded structures such as vehicular bridges and offshore drilling platforms. Their program, included the development of manufacturing processes and equipment to produce this new product. The result of Strongwell's efforts is a double web beam (DWB)(Fig. 4.1(b)) of overall dimensions 914×457 mm.Carbon fibre rovings are incorporated into the 26 mm thick top and bottom flanges for increased stiffness, as well as stitched glass fabric in the two 17.5 mm thick webs, (Strongwell, 2006). By having hybrid carbon-glass fibre reinforcement the Strongwell DWB has a Young's modulus in flexure of 40 GPa and a shear modulus above 5 GPa.

The 914 mm deep Strongwell DWB is, however, not going to be the preferred choice of member size and mechanical properties in many beam applications. To help the structural engineer choose the right PFRP member there are a number of smaller non-stocked PFRP shapes with depths between 305 and 610 mm (Strongwell, 2006; Creative Pultrusions Inc., 2006; Fiberline Ltd., 2006). Although the range may suit the expected requirements of the industry, the manufacturing costs of such glass fibre based shapes are 50% greater than a steel section and for a carbon fibre based shape, three times the equivalent steel section (Head, 1996). These higher costs are primarily due to tooling costs incurred in producing complex sections. In the case of the Strongwell DWB a significant initial investment of 10M$ was required for full production (NCE, 1992; Barbero

& GangaRao, 1991; Leonard, 1990).

In 1995 it was recognized by Head that complex optimized and modular systems of FRP shapes could be produced without high labour costs using automated production techniques such as pultrusion. Through the application of modularization, in the detailing of such optimised shapes (and systems), a significant reduction in manufacturing costs can be made by reducing the complexity and size of individual pultruded shapes. In order to make relatively large ($\geq$400 mm depth) closed shapes, one can join together smaller plate-like shapes to construct the desired larger complex member, this concept is introduced in Section 2.4.3 and shown in Fig 1.2. Such modular systems have the following potential advantages over large-scale single component PFRP profiles:

- significant reduction in tooling costs, especially if open sectioned profiles are used in the assembly

- large pultrusion machines are not required which are likely to be problematic to operate and requiring a greater number of creels and larger floor plan

- simple modifications to individual dies can produce a range of components

- flat pack nature of loose shapes and the possibility of easy on-site assembly reduce storage and transportation costs

- reduction in minimum economic order due to component repetition.

  - Often the use of PFRP shapes is not economically viable, as the total required length of profile is less than the minimum production run, set by the manufacturer. By making use of component repetition, the modularisation of large and complex components can significantly reduce the minimum production order of the finished product.

The Startlink beam system illustrated in Fig. 1.2, utilises these concepts of modularity and component repetition, as suggested by Head (1995) to produce a family of structural box beams ranging between 300 and 600 mm in depth, providing a clear advantage over the presently largest commercially available off-the-shelf PFRP shapes, presented in Table 4.1.

4.2   The PFRP box beam assembly

The work contained in the following subsections to Section 4.2, discusses the concept of fabricating a box beam shape from two flange and two web panel-type shapes which are fastened at the web-flange junction with mechanical connectors carrying the longitudinal shear, which exists between the shapes when the assembly is in flexure.

The advantages of composite-construction and achieving a state of composite-action have been exploited in composite concrete and steel design, since Caughey & Scott (1929) presented a design theory for concrete slabs atop steel sections, indicating the need for some form of shear connection. This concept of composite-construction has been used with many different traditional and advanced materials to produce structural memebers. The assembly illustrated in Fig. 1.2 applies these concepts of composite-construction and modularity to a family of PFRP beams. The assemblies illustrated in Fig. 1.2 represent part of the Startlink construction system, proposed by (Byers & Singleton, 1999), and discussed previously in Chapter 2. By pultruding a common flange shape and web panels in a variety of depths, it is possible to produce a family of structural beams of varying size at a reduced cost. It is proposed to use the Unistrut connection method characterised in Chapter 3, to provide the necessary composite action between the PFRP web and flange shapes.

4.2.1   The use of composite-action with FRP products

Composite-action between traditional materials has been comprehensively characterised (Newmark *et al.*, 1952), to give proven design guidance in international codes of practice (BSI., 1995b; BSI., 1995c).

At present the use of composite-action with FRP shapes is not considered in the available design guidance (Clarke, 1996), although applications of its use are numerous (Bakis *et al.*, 2002). Recent technological advancements in the manufacture of FRP products and in particular PFRP, have expanded the range of products suitable for construction boosting their use in industry. New applications of FRP products requiring an understanding of interaction between individual components include the strengthening of existing structures with FRP plates, and, the use of PFRP modular bridge deck systems (Keller *et al.*, 2001). Both these applications have received considerable research interest and are faster growing applications than the use of FRP in new build structures.

Models predicting the bond strength and the degree of interaction developed between adhesively bonded FRP and reinforced structures, have been developed (Taljesten, 1997; Karbhari *et al.*, 2000; Smith & Teng, 2001) and (Aurich & Beber, 2002). The use, and effectiveness of mechanical powder actuated fasteners to supply the necessary degree of composite-action between FRP strips and reinforced concrete beams has been investigated by Quattlebaum *et al.* (2005) and Ray *et al.* (2001) as a rapid means of strengthening existing bridges.

A number of PFRP modular bridge decking systems have been developed over the past decade, which, in general utilise a stiff adhesive bond to supply the shear continuity between the individual transversely spanning deck components (Keller *et al.*, 2001). The PFRP decking developed by Strongwell consist of transversely spanning adhesively bonded 153 mm PFRP box beams sandwiched between 10

mm outer flat plates (Strongwell, 2006). the majority of other deck systems utilise complex and modular hollow profiles (Keller *et al.*, 2001). For both systems the cost of on-site adhesive bonding is a disadvantage.

The volume of research into the use of adhesive bonding or mechanical fastening, to produce large scale flexural member for general construction from smaller PFRP shapes is limited by the tighter restrictions on such a general product and the market competition from equivalent steel sections and large single component PFRP shapes.

In 1993 Mottram evaluated the performance of a 90 mm deep adhesively bonded PFRP panelised deck section, fabricated from two I-beams sandwiched between outer flat sheet plates. Beams of 700 mm span were load tested in three point-bending. Although a toughened epoxy resin was employed to bond the assembly where its components mate, the short-term stiffness of the assembly was reduced by 7% from that calculated assuming a linear elastic beam theory and a rigid adhesive bond. This finding shows a state of below full-interaction was present in the bonded assembly.

Sotiropoulos *et al.* (1996) and Turvey (2001) evaluated the structural performance of various beam assemblies built-up of mechanically fastened PFRP profiles. Sotiropoulos *et al.* (1996), evaluated the structural performance of assemblies constructed from commercially available PFRP shapes, producing multi-cell bridge box beams of overall size 2400×890 mm. Details of the shear connection, including stiffness and spacing of the discrete bolted connections are not given, although joint efficiencies are determined from the degree of moment transfer between the components in the system. Strain differences of up to 40% were recorded across the longitudinal joints, indicating that the system had a 60% composite-action between the separate shapes. This is attributed to the inability of the connection detail to carry the shear loading. However, without considera-

tion of the precise connection details, and, the associated joint shear rigidity the results by Sotiropoulos *et al.* (1996) cannot be used to evaluate the effectiveness of the connection and the degree of interaction achieved for the degree of shear connection supplied.

Turvey (2001) has, via a series of three-point flexural tests with a custom produced prototype beam of the Startlink modular beam system (similar to the beam concept shown in Fig. 1.2), highlighted the potential of the Unistrut connection method (Fig. 1.3) as a form of shear connection, and, indicated a need for the characterization of the PFRP/Unistrut nut connection given in Chapter 2, and consideration of the joint shear rigidity on the overall stiffness of the assembly.

4.3 PFRP prototype box beam

The rest of this thesis, concentrates on the theoretical and experimental evaluation and analysis of a prototype box modular PFRP beam assembly, shown in Fig. 4.4, and detailed in Table 4.1 and based on the concept of the Startlink beam system. The proposed theoretical analysis will take account of the finite stiffness of the Unistrut connection, characterised in Chapter 3, and provide comparison for the experimental work which will build upon the initial proof of concept testing completed by Turvey (2001).

The depth of the prototype beam was fixed at 400 mm, to represent the mid-sized Startlink beam illustrated second from the right in Fig. 1.2, a comparison of geometric and flexural properties of the prototype beam assembly and similar commercially available sections is provided in Table 4.1.

4.3.1 Defining the degree of interaction, X

In order to design a suitable connection detail capable of providing the prototype beam with a state of near full-interaction, the concept of *non, full* and *partial-*interaction must be understood in terms of the flexural stiffness of the modular assembly.

Consider the application of composite-construction, to the two rectangular elements a and b in flexure, shown in Fig. 4.2. The total flexural rigidity of such a group of unconnected non-interacting profiles, I_{non}, flexing around their own neutral axis is given by the sum of the flexural rigidities, ΣI_{xx}.

$$I_{non} = I_a + I_b \tag{4.1}$$

Where I_a and I_b are the element second moments of area. By introducing full-interaction between the separate profiles such that no slip occurs ($s = 0$) and assuming a linear elastic strain distribution is present through the total depth of the assembly (Fig. 4.2), the new and higher flexural rigidity of the system, I_{full}, now includes the terms, Ay^2, accounting for each profile bending around a common and parallel neutral axis.

$$I_{full} = (I_a + I_b) + ((A_a y_a^2) + (A_b y_b^2)) \tag{4.2}$$

Where A_a and A_b are the element areas, and, y_a and y_b are the radii of gyration of the elements about the common and parallel neutral axis. For a system of two elements where partial shear connection exists the flexural rigidity of the system can be written as

$$I_{partial} = (I_a + I_a) + X((A_a y_a^2) + (A_b y_b^2)) \tag{4.3}$$

X, is a scalar function of the Λy^2 terms, with the range $(0 \leq X \leq 1)$. Termed as the degree of interaction present in the assembly it is dependent upon the joint shear rigidity, γ, supplied to the assembly and the applied load, P.

A state of full-interaction $(X = 1)$ will provide the assembly of elements with a flexural rigidity of EI_{full}, whilst a state of non-interaction will provide a flexural rigidity of EI_{non}.

For the prototype beam assembly illustrated in Fig. 4.4 and fabricated from the components with properties given in Table 4.1, a state of full-interaction represents an increase in the stiffness of the assembly of over 500% compared to a state of non-interaction.

The value of interfacial slip s, that will occur between elements in flexure in a state of non-interaction is derived in the following section.

4.3.2 Defining the measured slip, s

In a state of non-interaction, there exists no horizontal force at the interface between the two elements, shown in Fig. 4.2. By assuming vertical separation of the two elements is restrained, both elements share the same radius of curvature, k. The moment-curvature relation of the total system is given as

$$M = k(E_a I_a + E_b I_b) \tag{4.4}$$

The effect of flexural loading on the assembly evolves compressive strains on the upper face of element a and tensile strains on the lower face of element b, the difference in magnitude of these interfacial strains is known as the strain difference, e (see Fig. 4.2), and is given by

$$e = k \left(\frac{D}{2} + \frac{d}{2} \right) = \frac{M(D+d)}{2(E_a I_a + E_b I_b)} \tag{4.5}$$

Where D and d are the depth of the elements shown in Fig. 4.3.

Slip is defined as the displacement in the *x-direction* (right to left in Figs. 4.2 and 4.3), of a point on the lower face of element b, relative to the upper face of element a. At mid-span the interfacial slip is zero, due to symmetry and increases in the *x-direction* illustrated in Fig. 4.3, as a result of the interfacial strain difference, e. The relation between strain difference, e, and slip, s, is given by

$$e = \frac{\mathrm{d}s}{\mathrm{d}x} \tag{4.6}$$

The slip developed at the end of the assembly can be found by integration of the strain difference, from mid-span to the free end of the assembly. For an assembly with full-interaction, the interfacial strain difference e and slippage s are both equal to zero.

4.3.3 Design for composite action

For the Startlink modular beam system, presented in Section 2.4.3 (Fig. 1.2) and the prototype modular PFRP beam assembly, shown in Fig. 4.4, the necessary interaction is developed by the purchase provided between the M10 Unistrut connector and the channel section of the PFRP flange shape.

Ideally, the connection detail needs to be of adequate stiffness and strength, to provide a state of near full-interaction between the individual web and flange shapes equivalent to that if the assembly were a single pultruded PFRP shape with full continuity. A state of full-interaction is only obtained when a linear stress distribution is present through the depth of the assembly whilst in flexure. For this to occur there must be longitudinal shear stresses present along the boundaries of the web and flange shapes, where the Unistrut connectors are located. The connectors can be seen in Fig. 4.4 and Fig. 4.5. To restrain the

web and flange shapes from deforming independently, by relative slip, the shear force acting along the interface has to be transferred between the shapes by the rows of discrete individual Unistrut connectors.

The longitudinal shear force per unit length along the line of connections can be identified as the shear flow f_y with units N/mm, and is given by

$$f_y = \frac{V_x Q_{sub}}{I_{full}} \tag{4.7}$$

where V_x is the vertical shear, I_{full} is the second moment of area about the horizontal axis through the beam's centroid. The first moment Q_{sub} is a function of the cross-sectional area of the chosen sub-element. With respect to the beam shown in Fig. 4.4, it is calculated at the level of the flange from which the shear stresses are transferred into the vertical web panels, via the two rows of Unistrut connectors.

Figure 4.5 can be used to define the connection spacing, Sp_x. Given the safe working resistance to shear, R_s, of the individual connectors that is carried before the connection resistance is exceeded, the maximum allowable shear flow, f_{ymax}, is calculated from.

$$f_{ymax} \le \frac{2R_s}{Sp_x} \tag{4.8}$$

From the experimental results in Chapter 3, the safe working resistance to shear of a M10 connector is taken as 2.5 kN. The minimum connector spacing is designated to be 50 mm. This choice was made for economy of construction, and to provide a bolt centre-to-centre spacing greater than four times the bolt diameter of 10 mm, thereby avoiding the possibility of local material shear/tear-out failure between the individual pin-bearing bolts, (Mottram & Turvey, 2003). From Equation 4.8 the maximum allowable shear flow is calculated as, $f_{ymax} = 100$ N/mm.

Substituting for f_{ymax}, Q_{sub} and I_{full} for the beam assembly (see Table 4.1) into Equation 4.7, a maximum allowable vertical shear force V_x, of 44 kN is determined for the beam assembly, assuming the highest possible connection density, i.e. for $Sp_x=$ 50 mm.

For the 2848 mm long prototype beam assembly, shown in Fig. 4.4 under four-point loading with load points at approximately 1/3 spans, this maximum allowable shear force translates to a deflection limit of L/285, under such a load arrangement, shear connections are only required on the shear loaded outer spans. In total 160 connections are required at 50 mm spacing over the outer-spans, to achieve a deflection limit of L/285. For the same load conditions an assembly in a state of non-interaction would theoretically exhibit a deflection equal to L/55 developing an end slippage s, in excess of 12 mm over the half span length. The development of longitudinal axial strains in excess of 13,000 $\mu\varepsilon$ in the web panel would cripple the member.

Ideally a SLS deflection limit of L/250 would be required for design, for the prototype assembly the connection resistance limits the deflection of the asssembly. For connection spacings of 50, 100, 200 and 400 mm the maximum allowable shear force and minimum length required to achieve a deflection limit of L/250 under an equal spaced four-point loading are given in Table 4.3, the fourth column shows that the 400 mm deep prototype beam can achieve a deflection limit of L/250 over a span range of 3300 - 10500 mm by varying the spacing of the connections. This proposed method of calculation is based on the individual Unistrut connectors being infinitely stiff for a shear force up to their specified capacity, R_s, thereby providing full-interaction, as shown in Fig. 4.6(a). Slippage will occur when the loading creates a longitudinal shear force exceeding the total connection resistance in the joint. The load for the onset of slip is referred to as, P_{slip}. Figure 4.6(a) illustrates the increase in P_{slip} with the increase in number

of connections.

However the degree of shear connection, supplied to the assemblies will not directly translate to the degree of interaction that can be expected between elements (Oehlers & Bradford, 1995). The degree of shear connection is governed by the strength, R_s, and number of the connections, whereas the degree of interaction, X, will be governed by the stiffness, K_s, of the connections. The theoretical response of the beam assembly, accounting for the finite stiffness of the total connection is shown in Fig. 4.6(b).

The short-term finite stiffness K_s, of the standard M10 Unistrut connection in a GS2 channel under a 20 Nm applied torque is taken to be equal to 2.5 kN/mm. This was experimentally determined in Chapter 3. The stiffness of the individual flange web connections is given by the joint shear rigidity γ, with units of force per unit length per unit slip, N/mm/mm. It should be noted that for a connection spacing of 50 mm, the corresponding joint shear rigidity is 50 N/mm/mm.

4.3.4   Connection design for a Uniformly Distributed Loading

The fabrication and installation cost included in supplying a full degree of interaction using the Unistrut connection method, may represent a considerable percentage of the total manufacturing costs of the beam assembly, and, it is therefore important to optimise the connection design. Ideally the design of the connection detail will be matched to the intended service load arrangement in the structure. The present use of the Strongwell DWB (Fig. 4.1(b)) and similar size PFRP memebers are limited to primary load supporting members in mid-span girder bridges, carrying a Uniformly Distributed Loading (UDL) between simple supports.

For the case of a UDL the vertical shear force V_x and hence the shear flow, f_y,

are linearly varying along the length of the assembly. For a UDL acting on the assembly the maximum allowable shear force calculated in the previous section, translates to a deflection limit of L/430.

To provide sufficient shear connection in such a situation, the density of the shear connectors must be linearly varying with length. The resulting exponential spacing of individual connections represents the most economical, and the possibly the least practical arrangement of connections. The provision of blocks of uniformly spaced connections, similar to that specified for composite concrete-steel structures (BSI., 1995b), represents a more viable method of supplying the necessary joint shear rigidity.

4.3.5   Consideration of possible failure mode

As illustrated in Fig. 4.6(a) under the assumption of an infinitely rigid shear connection this decrease in flexural rigidity from $5.8 \times 10^8 \text{N/mm}^2$ for full-interaction to $1.1 \times 10^8 \text{N/mm}^2$ for non-interaction, is rapid as indicated in Fig. 4.6(a). Assuming a finite stiffness as shown in Fig. 4.6(b) of connection the flexural stiffness will decrease non-linearly with applied load. For both assumptions the occurrence of slippage significantly reduces the flexural rigidity of the system, and will alter the relative stiffness's of each shape in flexure.

As the shapes in the assembly follow the same radius of curvature k, the occurrence of interfacial slippage will tend to increase the relative stiffness of the deeper web shapes, increasing the axial strain in these shapes, whilst reducing the axial strain in the outer-most flange shapes. Although connection slippage may be considered a progressive and desirable mode of failure, depending on the design of the web panel shapes it may be a precursor to a more catastrophic failure of the webs, the most probable failure modes would arise either as a result of buckling of the web panel in compression between restraining connections, or

from a tension failure of the discountinuous fibres local to the bolt hole.

4.4 Conclusions

- An appropriate minimum connection spacing for the M10 Unistrut connectors has been set at 50 mm, and the maximum allowable shear flow through the Unistrut connection has been calculated.

- It is understood that the prototype beam presented in this chapter will not achieve a SLS state of $L/250$ under four-point load due the limited resistance of the Unistrut connection method.

- Two basic proposals for the behaviour of multiple connections are developed and their implications on the performance of an assembly have been presented and discussed.

- Based on the assumption of a finitely rigid connection the maximum service conditions capable for the prototype assembly are given as $L/270$ for three-point loading and $L/430$ under UDL.

- Buckling of the web panel has been identified as a possible mode of failure following a progressive failure through the occurrence of slippage

4.5 Figures & Tables
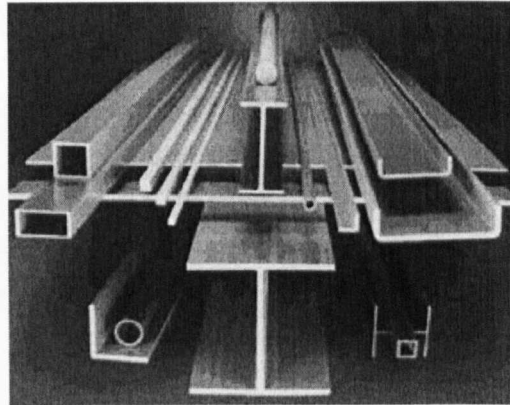
(a)
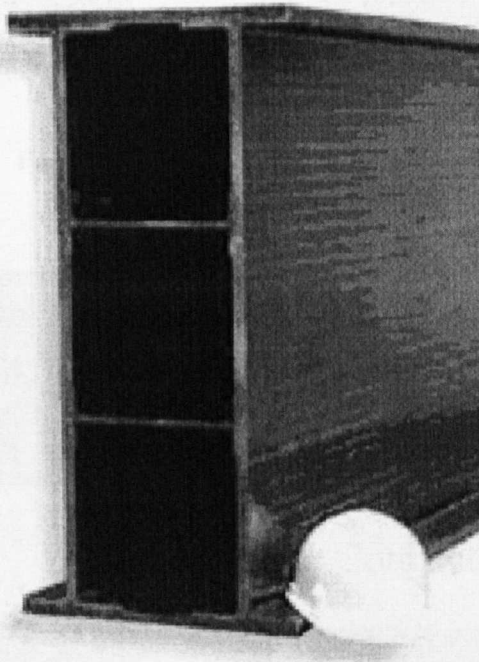
(b)

Figure 4.1: Currently available PFRP sections (a) Standard WF and I sections (b)Strongwell DWB
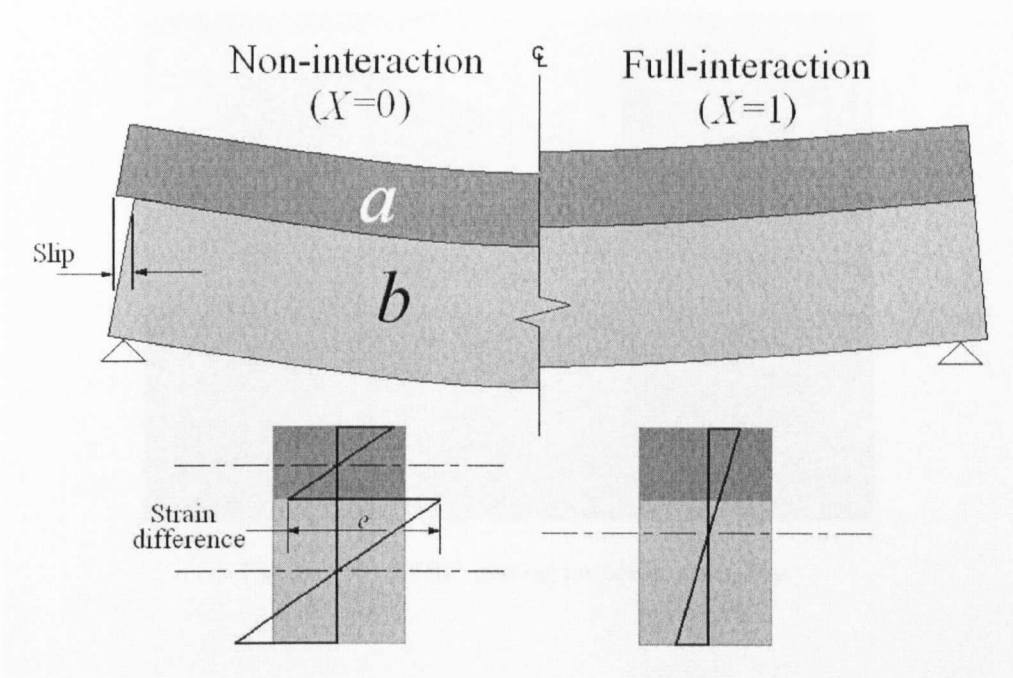
Figure 4.2: Plate elements in flexure
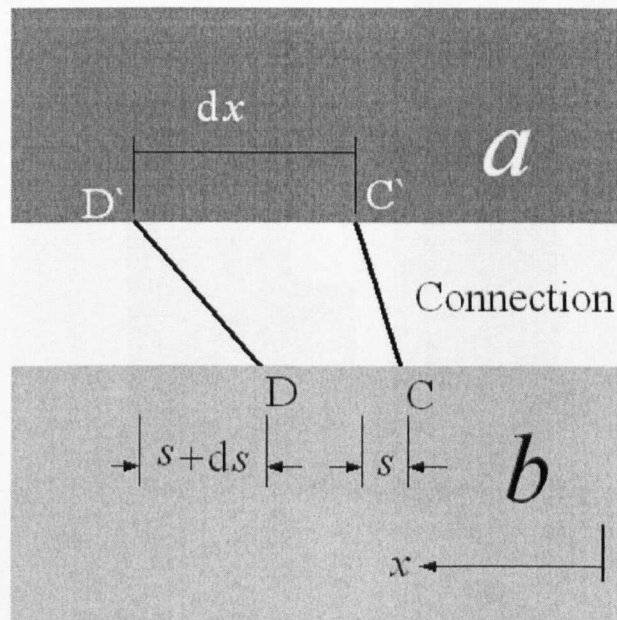
Figure 4.3: Detail of interfacial slip
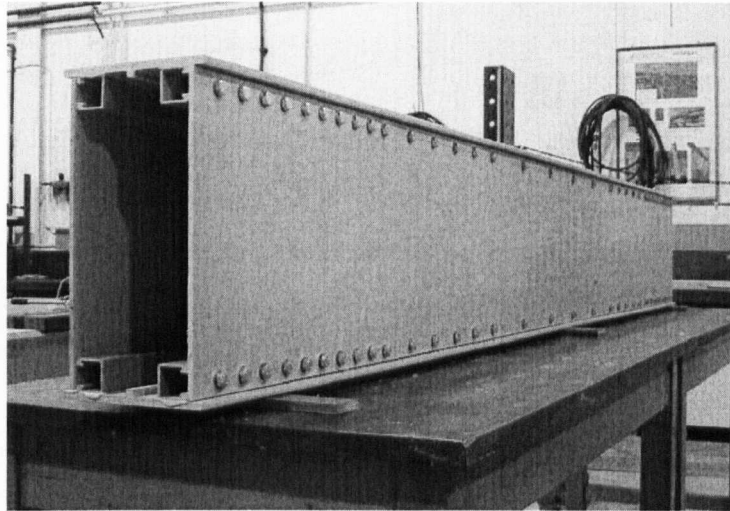
Figure 4.4: PFRP prototype beam assembly
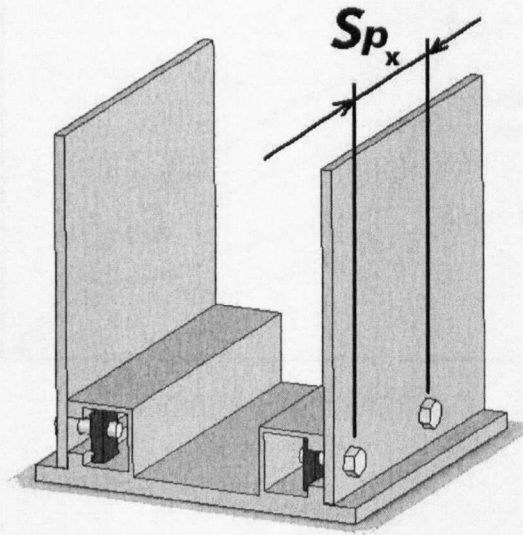
Figure 4.5: Connection spacing definition
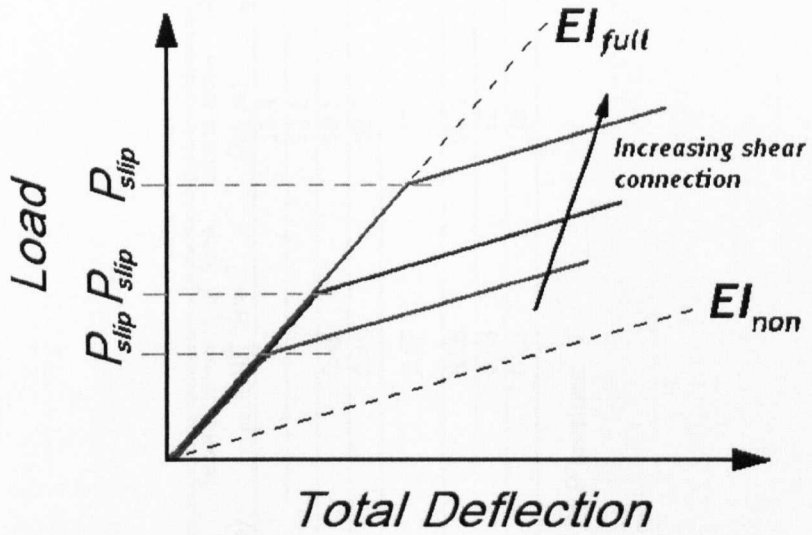
(a)
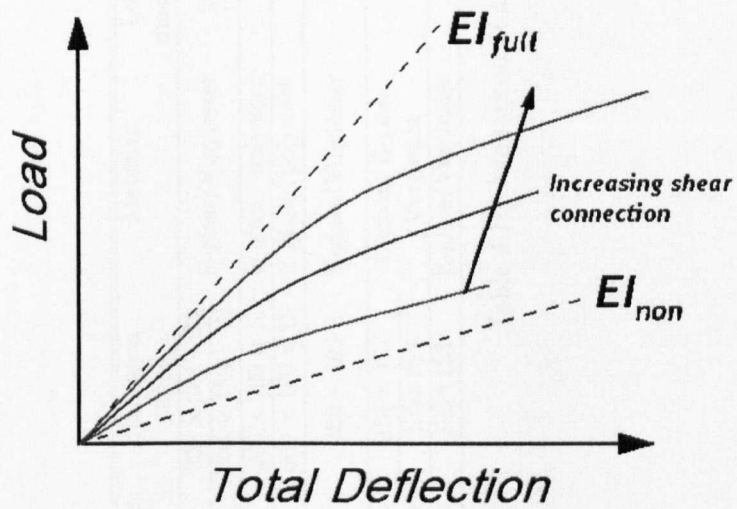
(b)

Figure 4.6: Theoretical load deflection response (a) Infinitely rigid connection (b) Finitely rigid connection

Manufacturer	Shape	Dimension (mm)	Material	Longitudinal modulus (MPa)	Second moment of Area, $I_{xx} \times 10^8$ Nmm²	Linear mass (kg/m)	Normalised I_{xx}/(kg/m)
Creative Pultrusion	WF	305 × 305 × 12	E-glass/Vinylester	26.8 - 27.6		19.8	0.69
	I	305 × 153 × 12				13.1	0.61
Fibreforce	WF	200 × 200 × 10	E-glass/ polyester	13.8	0.42	10.1	0.28
Fiberline	I	360 × 180 × 18	E-glass/ polyester	28	2.48	22.7	0.78
Startlink prototype beam assembly	Box	400 × 203	E-glass/Vinylester	24	2.37	17	1.00
Strongwell	DWB	914 × 457	Carbon, E-glass /Vinylester	40	63.6	95.4	4.70
		203×153	/Vinylester		0.53	15	0.25
		203×153	E-glass/Vinylester	28	0.53	15	0.25

Table 4.1: Comparison of available PFRP sections

Beam Element	Standard component	E_L (GPa)	Connection properties
Flange	Flange WF 203 × 203 × 9.53 mm	24	-
	GS2 Channel		-
Web	6.35 mm thick, Extren©	18	-
	Extern 625 flat sheet		
Connection	M10 Unistrut	-	Stiffness, K_s= 2.5kN/mm
	Connector		Resistance, R_s= 2.5kN

Table 4.2: Properties of the parts to the modular beam shown in Fig. 4.4

Connection Spacing Sp_x (mm)	Maximum shear force V_x (kN)	Required length L_{req}(mm)	Span-Depth ratio	Total No. of M10 Unistrut connections
50	44	3300	8.3	176
100	22	5000	12.5	133
200	11	7300	18.3	97
400	5.5	10500	26.3	70

Table 4.3: Required Span-Depths ratios for SLS deflection L/250

CHAPTER 5

Experimental method and theoretical analysis

The primary objective of the work reported in this, and, the following chapter is to characterize, through full-sized experimental testing, the performance of a modular beam assembly based on the concepts proposed by Byers & Singleton (1999). The completion of two secondary objectives is required to meet this primary objective, and they are:

1. Design of a suitable connection detail, which can provide the condition of full-interaction between the individual components in the assembly using the off-the-shelf M10 steel bolts and specific Unistrut steel channel nuts.

2. Determine the flexural rigidity of the beam assembly with varying degrees of shear interaction.

The remainder of this chapter is subdivided into sections on materials and component specification, experimental test method and theoretical analysis of partial-interaction.

5.1 Materials and component specification

The web and flange shapes for the beam shown in Fig. 4.4, are defined in Table 4.1. The webs are of an off-the-shelf Strongwell Extren© 625 series flat sheet, of nominal 6.4 mm thickness. Each web panel is formed from two flat sheet lengths of 1425×380 mm, joined with a mechanically fastened and adhesively bonded splice joint (see Fig. 5.2). The direction of pultrusion in the webs is along the beam's length. The webs are 170 mm apart (centre-to-centre) and are predrilled at 50 mm centre-to-centre spacing with clearance holes to accept different numbers and arrangements of the M10 Unistrut connectors where connections are to be made. The M10 bolting is tightened to a torque of 20 Nm. In order to increase the buckling resistance of the web panels in the vicinity of the load points, stiffeners consisting of 320×30×5 mm L-shape PFRP sections were attached to the outerfaces of each web panel. Each beam flange shape is constructed by bonding two PFRP GS2 channels (Fig. 3.1(b)), from Mita Ltd., UK, to the flange cut from a Creative Pultrusions Inc. 203×203×9.53 mm WF-shape. This bonding uses a toughened epoxy adhesive of type Araldite-2015, which was selected to provide a shear continuity that would be expected if the built-up flange had been a single pultruded shape. To achieve a uniform bond line thickness of 0.5 mm a number of pieces of copper wire of that diameter are added to the adhesive when the bond is prepared. This flange shape for the prototype modular beam assembly is illustrated in Fig. 5.3. Note that this illustration gives dimensions.

By varying the spacing of the connectors along the web-flange junction, the shear rigidity of the connection γ, is altered and hence the stiffness of the assembly will be influenced. Under the proposed four-point bending arrangement, the outer spans of the beam assembly will be subject to a constant vertical shear force V_x, as illustrated in Fig. 5.1. Connections in this region will be known as

active connections. The mid-span region experiences constant moment Pa, and zero shear force as indicated in Fig. 5.1. Connections made in this region are designated as passive connections.

Table 5.1 provides details of the connections arrangements studied, and provides, in its fourth column, the beam configuration's identify. The fifth to seventh columns indicate the total number, the number of active and the number of passive connections made in the beam assembly. Configuration BA-A50-A is for the beam assembly BA, tested in arrangement A, with a connection spacing of 50 mm, with only active connections A, present in the assembly. When both active and passive connections are present in the assembly the final term of the configuration is given as AP.

The connector spacing ranges from 50 mm (BA-A50-A, BA-A50-AP and BA-B50-A, BA-A50-AP) for near full-interaction to 400 mm (BA-A400-A, BA-A400-AP and BA-B400-A, BA-A400-AP) when the level of interaction is expected to be low. Different degrees of shear connection can now be characterised by a comparison of the theoretical deflections derived in the Chapter 4, the loads at which slip occurs, P_{slip}, and theoretical flexural rigidities, EI_{full} and EI_{non}, are given in Table 5.1. For each of the connection arrangement spacing's tested a joint shear rigidity, γ, has been calculated, these values are provided for both the outer and mid-span region in third and fourth columns of Table 5.2.

5.2 Experimental test method

A prototype modular beam assembly, with varying degrees of joint shear rigidity γ, is tested in a variety of four-point bending arrangements. The basic test arrangement is illustrated in Fig. 5.1, a photograph of the beam assembly in the four-point test rig is shown in Fig. 5.2. As indicated in Fig. 5.1 the outer-spans

of length a, are regions of constant vertical shear force V_x, equal to the applied point load P, and a linearly increasing moment. The mid-span region of length b, is a region of zero vertical shear force V_x, and constant moment Pa.

A variety of methods are used to determine the degree of interaction X, achieved for the degree of joint shear rigidity γ, supplied to the beam assembly. The beam assemblies are tested in two four-point bending loading arrangements, A and B, such that the flexural rigidity EI, and shear stiffness $k_s G_{xy} A_v$, of the assemblies may be simultaneously determined using the graphical method (Bank, 1989). The relative proportions of the two loading arrangements A and B, are given in Table 5.3.

To determine the effect of passive connections in the mid-span region on the overall stiffness, each beam assembly is tested with both active only, and, active and passive connections. Connections with a 0 Nm applied torque (providing minimal resistance to the longitudinal shear force) are supplied to the mid-span region of all 'active only' assemblies, in order to restrain the web panel from local buckling. All other connections are made using the M10 Unistrut Connectors torqued to 20 Nm at the designated connector spacing given in Table 5.1.

Internal supports consist of two simple supports allowing full in-plane rotation creating the mid-span region of length b. Suitable bearing surfaces are provided on the underside of the Lower flange by 200×70×10 mm steel plates. The Southern internal support as indicated in Fig. 5.2(shown on the right hand side), allows longitudinal translation by the means of a roller bearing surface.

Vertical load is applied under stroke control, via a U-section steel hanger system, a ball bearing and bearing plate at the North and South ends of the assembly. The two jacks are independent of each other to improve control of the loading. The four-point flexural load is increased in increments of 1 to 3 kN, until appreciable interfacial slip at the connections is observed. In the following

work, the term applied load P, is the mean of the two end loads; which can differ by up to 10%. The total load on the assemblies is given by $2P$. Prior to all recorded tests a bedding in procedure is followed, in which a load of 50% of the expected capacity of assembly is applied for a duration of 20 minutes. The maximum applied load is limited by the capacity of the U-section loading yokes to 30.5 kN.

Interfacial slip was measured using 100 mm Demec gauges with reference points adhesively bonded to the flange and web shapes. Figure 5.3 details the location of the instrumentation used to monitor the structural performance of the beam assemblies. Deflections of the Upper and Lower flanges were measured at the mid-span section and under the North and South load points. Axial strains were measured using 6 mm TML strain gauges (type FLA-6-120-11) on the Upper and Lower flanges at mid-span and at a distance of 550 mm from the South load point. Axial strains of the East facing web were also taken at this location. Shear strain was measured using TML ±45° (type PFR-10-11) strain gauges on the outer face of the East web panel. All instrumentation required for the monitoring of the structure with the exception of the 100 mm Demec gauges was recorded in real time using an Orion Solartron 3531 data acquisition system.

It was originally proposed to trial an innovative photo-elastic stress analysis technique, to determine the stress field and magnitude of bearing stresses around the individual discrete connections along the length of a web-flange connection.

Following the results of a preliminary evaluation of the technique and an investigation into the short-term time dependent response of a suitable epoxy based photo-elastic coating, it was decided that the technique could not be reliably used to determine with confidence and accuracy the stress distribution in the webs caused by the bolted connections. A full account of the author's preliminary investigation is given in Appendix A.

5.3 Theoretical analysis of the PFRP prototype assembly

5.3.1 Theoretical bounds on deflection

To provide a comparison and define upper and lower bounds to the structural performance of the assemblies the experimentally determined deflections will be compared to a pair of theoretical assemblies with flexural rigidities of EI_{full} and EI_{non}. These flexural rigidities represent the states of full interaction ($X = 1$) and zero interaction ($X = 0$). The deflection response of the theoretical beams is generated using Timoshenko's Beam Theory, (Timoshenko, 1955), the general form of which is

$$\delta = \frac{C_1 P L^3}{E I_{xx}} + \frac{C_2 P L}{k_s G_{xy} A_v}$$

(5.1)

Where the central and maximum deflection δ depends upon the applied load P, the span length L, the section modulus E, the second moment of area I_{xx}, the shear correction factor k_s, the shear area A_v and the section shear modulus G_{xy}. The constants C_1 and C_2 depend upon the load case and the particular location along the span length that the deflection is desired. Table 5.3 gives the values of the constants C_1 and C_2 for the case of total deflection at the mid-span, for the two four-point load arrangements, A and B. They are given in terms of the outer span a and the beam span L as

$$C_1 = \frac{1}{24} \left(\frac{3a}{4L} - \left(\frac{a}{L} \right)^3 \right), \qquad C_2 = \frac{a}{L}$$

5.4 Theoretical analysis of partial-interaction

Whilst a state of full-interaction is desirable, it is rarely achievable in reality owing to the finite stiffness of the shear connection. Under a state of partial-interaction, the strain difference e, and associated slip s, must be taken in to account in

determining the service load deflections (Oehlers & Bradford, 1995), and the strain profile cannot be determined from the bending moment (Yam, 1981).

On the subject of composite action in composite steel and concrete T-beams consisting of a steel I-beam and concrete slab above, the first numerical analysis of partial-interaction was made by Newmark *et al.* (1952), using simplifying linear elastic assumptions. Numerical models incorporating the non-linear material characteristic, and the time dependent effects of material creep (Ansourian & Roderick, 1978) have been developed to further the analysis proposed by Newmark *et al.* (1952).

Presented in the following section is a basic numerical analysis of a three layer beam system in flexure, shown in Fig. 5.4, for the condition of partial-interaction, based on the two layer system developed by Newmark *et al.* (1952) and presented by both Knowles (1971) and Yam (1981). The results of this modified Newmark analysis will be compared to a model offered by Kuenzi & Wilkinson (1971) for the theoretical determination of deflection in timber box beam assemblies accounting for fastener rigidity, based on the numerical analysis of stressed skin sandwich constructions with highly shear flexible cores presented by Norris *et al.* (1952).

5.4.1 Modified 3-layer Newmark analysis

It is convenient to consider the bending moments on the beam assembly to be the resultant of sectional forces acting on the individual beam shapes. These sectional forces will consist of couples and axial forces F_f and F_w acting on the flange and web shapes. The resultant axial forces are defined in Fig. 5.4. By making the following assumptions, the form of the solution may be simplified:

- Discrete shear connection may be replaced by an equivalent uniform con-

tinuous linearly elastic medium over the whole length of the assembly

- Initially plane sections remain plane after bending

- There is no vertical separation of the web and flange shapes

Figure 5.4 represents the strain distribution over the depth of the beam assembly for a state of partial-interaction. This can be assumed equal to the strain distribution arising from a state of non-interaction and uniform strain distributions in the beam shapes arising from sectional forces (F_f and F_w). The couple resulting from these resultant sectional forces is sufficient to impose a state of partial-interaction upon the beam assembly in a state of non-interaction.

Without vertical separation of the shapes in the beam's assembly, their curvature k for small deflections, can be assumed to be equal at any given depth, resulting in the slope of the strain distribution (M/EI) remaining constant throughout the depth of the assembly.

The effect of incomplete interaction is the presence of a strain difference e, as shown in Fig. 5.4, at the boundary of the web and flange shapes.

From Fig. 5.4 the forces F_f and F_w, bending moment M, and strain difference e can be written as

$$F_f = kE_fA_f\left(n_1 - \frac{d}{2}\right) \tag{5.2}$$

It can be assumed that n_2 is equal to $D/2$ due to the symmetry of the assembly

$$\therefore F_w = kE_w\frac{A_wD}{8} \tag{5.3}$$

The resisting moment can be calculated by resolving the forces shown in Fig. 5.4.

$$M = k\Sigma EI + F_f(D+d) - F_w(\frac{D}{2}) \tag{5.4}$$

The strain difference at the interface is given by

$$c = k \left(d + \frac{D}{2} - n_1 \right) \tag{5.5}$$

Rearranging Equation 5.2 for n_1

$$n_1 = \left(\frac{F_f}{k E_f A_f} + \frac{d}{2} \right) \tag{5.6}$$

And substitute into Equation 5.5 and rearrange for k

$$k = 2 \left(\frac{e + \frac{F_f}{E_f A_f}}{D + d} \right) \tag{5.7}$$

Substituting into Equation 5.4

$$M = 2 \left(\frac{e + \frac{F_f}{E_f A_f}}{D + d} \right) \left(\Sigma EI - \frac{E A_w D^2}{16} \right) + F_f (D + d) \tag{5.8}$$

Rearranging

$$M = \left(\frac{2 \Sigma EI}{E A_f (D + d)} - \frac{E A_w D^2}{8 E A_f (D + d)} + (D + d) \right) F_f + \left(\frac{2 \Sigma EI}{(D + d)} - \frac{E A_w D^2}{8(D + d)} \right) e \tag{5.9}$$

Now consider an element of the flange section, (Fig. 5.5). Equating the forces on the element dx.

$$q \, dx + dF_f = 0 \tag{5.10}$$

Therefore

$$q = -\frac{dF_f}{dx} \tag{5.11}$$

To provide a link to the stiffness of the connection detail, the elastic stiffness of the individual connection K_s, (determined in Chapter 3) is introduced and

defined as the load to cause unit slip given that Sp_x, is the continuous connection spacing and the relative slip s at the level of the connection.

$$K_s = \frac{qSp_x}{s} \tag{5.12}$$

Using the relationship between slip s, and strain difference e, defined in Equation 4.1 and described in Fig. 4.3.

$$e = \frac{ds}{dx} = \frac{Sp_x dq}{K_s dx} = \frac{Sp_x}{K_s} \left(-\frac{d^2 F_f}{dx^2} \right) \tag{5.13}$$

Substituting Equation 5.13 into Equation 5.9, the following second order differential equation is obtained, for the analysis of the partial-interaction of an elastic three layer composite beam assembly with uniform connector spacing.

$$
\begin{aligned}
M &= \left(\frac{2\Sigma EI}{EA_f(D+d)} - \frac{EA_w D^2}{8EA_f(D+d)} + (D+d) \right) F_f.. \\
&\quad - \frac{Sp_x}{K_s} \left(\frac{2\Sigma EI}{(D+d)} - \frac{EA_w D^2}{8(D+d)} \right) \frac{d^2 F_f}{dx^2}
\end{aligned}
\tag{5.14}
$$

The bending moment M can be replaced by Px, and the differential equation can be simplified by introducing the three constants (λ, β, ψ).

$$
\begin{aligned}
0 &= \frac{Sp_x}{K_s} \left(\frac{2\Sigma EI}{(D+d)} - \frac{EA_w D^2}{8(D+d)} \right) \frac{d^2 F_f}{dx^2}.. \\
&\quad - \left(\frac{2\Sigma EI}{EA_f(D+d)} - \frac{EA_w D^2}{8EA_f(D+d)} + (D+d) \right) F_f + Px
\end{aligned}
\tag{5.15}
$$

Simplifies to

$$0 = \frac{d^2 F_F}{dx^2} - \frac{\beta}{\lambda} F_f + \frac{Px}{\lambda} \tag{5.16}$$

$$0 = \frac{d^2 F_F}{dx^2} - \psi^2 F_f + \psi^2 \phi x \tag{5.17}$$

Where

$$\lambda = \frac{Sp_x}{K_s}\left(\frac{2\Sigma EI}{(D+d)} - \frac{EA_w D^2}{8(D+d)}\right) \tag{5.18}$$

$$\beta = \frac{2\Sigma EI}{EA_f(D+d)} - \frac{EA_w D^2}{8EA_f(D+d)} + (D+d) \tag{5.19}$$

$$\psi^2 = \frac{\beta}{\lambda} \tag{5.20}$$

$$\phi = \frac{P}{\beta} \tag{5.21}$$

The solution satisfying the boundary conditions, $F_f = 0$ at the support and $\frac{\mathrm{d}F_f}{\mathrm{d}x} = 0$ at $x = \frac{L}{2}$ is.

$$F_f = \phi\left(x - \frac{\sinh\psi x}{\psi\cosh\psi\frac{L}{2}}\right) \tag{5.22}$$

Full derivation of Equation 5.22 is given in Appendix B. Substituting Equation 5.22 into Equation 5.4 a solution for the distribution of curvature k, is given

$$\Sigma EIk = Px - \phi\left(x - \frac{\sinh\psi x}{\psi\cosh\psi\frac{L}{2}}\right)(D+d) + \frac{kEA_w D^2}{16} \tag{5.23}$$

The relationship between curvature k and vertical deflection v, is given as.

$$k = \frac{\frac{\mathrm{d}^2 v}{\mathrm{d}x^2}}{\left(1 + \left(\frac{\mathrm{d}v}{\mathrm{d}x}\right)^2\right)^{\frac{3}{2}}} \tag{5.24}$$

For small slopes, $\frac{\mathrm{d}v}{\mathrm{d}x} \leq 0.174$ rad, the equation may be simplified to.

$$k = \frac{\mathrm{d}^2 v}{\mathrm{d}x^2} \tag{5.25}$$

Substituting for k, into Equation 5.23 yields the following equation relating vertical deflection v, to the state of partial-interaction. Note vertical deflection

is given as v and not δ as to avoid confusion with the differential terms.

$$\left(\Sigma EI - \frac{EA_w D^2}{16}\right) \frac{\mathrm{d}^2 v}{\mathrm{d}x^2} = Px - \phi\left(x - \frac{\sinh\psi x}{\psi\cosh\psi\frac{L}{2}}\right)(D + d) \qquad (5.26)$$

Expanding Equation 5.26 and integrating once with respect to x gives

$$\left(\Sigma EI - \frac{EA_w D^2}{16}\right) \frac{\mathrm{d}v}{\mathrm{d}x} = \frac{Px^2}{2} - \phi\left(\frac{x^2}{2} - \frac{\cosh\psi x}{\psi^2\sinh\psi\frac{L}{2}}\right)(D + d) + C \qquad (5.27)$$

Integrating Equation 5.26 for the second time gives

$$\left(\Sigma EI - \frac{EA_w D^2}{16}\right) v = \frac{Px^3}{6} - \phi\left(\frac{x^3}{6} - \frac{\sinh\psi x}{\psi^3\cosh\psi\frac{L}{2}}\right)(D + d) + Cx + E \qquad (5.28)$$

The solution for the constants C and E satisfying are given by enforcing the following boundary conditions.

For $\frac{\mathrm{d}v}{\mathrm{d}x} = 0$ at $x = \frac{L}{2}$

$$C = \phi(D + d)\left(\frac{L^2}{8} - \frac{\cosh\psi\frac{L}{2}}{\psi^2\sinh\frac{L}{2}}\right) - \frac{PL^2}{8} \qquad (5.29)$$

For $v = 0$ at $x = 0$

$$E = 0 \qquad (5.30)$$

Substitution of these constants into Equation 5.28 allows the vertical deflection at any position along the beam in outer-span range of $0 \leq x \leq a$ to be calculated. In the mid-span region, where $a \leq x \leq \frac{L}{2}$, there exists a region of constant moment Pa, and zero shear force V_x, hence full composite action is developed independent of the degree of shear connection supplied the vertical deflection of the mid-span region is determined from.

$$v_{mid} = \frac{Pab^2}{2EI_{full}} \qquad (5.31)$$

Total deflection at mid-span v_{total} including the effect of shear deformation is given by

$$v_{total} = \frac{1}{\Sigma EI - \frac{EA_w D^2}{16}}\left(P\left(\frac{a^3}{6} - \frac{L^2 a}{8}\right)\right.$$
$$\left.+\phi(D+d)\left(\frac{L^2 a}{8} - \frac{a^3}{6} + \frac{\sinh \psi a}{\psi^3 \cosh \psi \frac{L}{2}} - \frac{a \cosh \psi \frac{L}{2}}{\psi^2 \sinh \psi \frac{L}{2}}\right)\right)$$
$$+\frac{Pab^2}{2EI_{full}}$$
$$+\frac{Pa}{k_s G_{xy} A_v} \tag{5.32}$$

For the beam assembly detailed in Fig. 4.4 and Tables 4.1 and 4.2 the following values can be ascribed to the constants β and λ.

- $\beta = 385$ mm for connections spacing's 50, 100, 200 and 400 mm respectively

- $\lambda = 39.7 \times 10^6$, 79.5×10^6, 159.0×10^6 mm^3, 318.1×10^6 mm^3 for connections spacing's 50, 100, 200 and 400 mm respectively

- $\psi^2 = \frac{\beta}{\lambda} = 9.69 \times 10^{-6}$, 4.85×10^{-6}, 2.42×10^{-6}, 1.21×10^{-6} for connections spacing's 50, 100, 200 and 400 mm respectively

The family of curves in Fig. 5.6(a) and (b) show for the two test arrangements A and B respectively, the theoretical total deflections v_{total}, plotted against applied load P, for the prototype beam assembly detailed in Table 4.1 with the varying connections, detailed in Table 5.1. The cases of full-interaction and non-interaction are given by the bold lines.

5.4.2 Kuenzui and Wilkinson partial-interaction analysis

For the analysis of timber box beams by Kuenzi & Wilkinson (1971), the mid-span deflection is given by the following expression derived from the mathematical

analysis.

$$v_{total} = \frac{k(3 - 4k^2)PL^3}{48(EI)} \left(1 + \frac{6}{(3 - 4k^2)} \left(\frac{EI_{full}}{EI_{non}} \right) \cdot \left(\frac{2}{\alpha L} \right)^2 \left(1 - \frac{\sinh \alpha kL}{\alpha k \cosh \frac{\alpha L}{2}} \right) \right) + \frac{Pa}{k_s G_{xy} A_v} \tag{5.33}$$

Where:

- v_{total} is the total deflection

- P is the applied load

- L is the span length

- k defines the load position as shown in Fig. 5.3

- EI_{full} is the flexural rigidity for a state of full-interaction ($X = 1$)

- EI_{non} is the flexural rigidity for) a state of non-interaction ($X = 0$)

$$\alpha^2 = \frac{h^2 S}{EI_{full} - EI_{non}} \left(\frac{EI_{full}}{EI_{non}} \right) \tag{5.34}$$

Where:

- h is the distance between the centroids of the principal moment carrying members

- S is the shear load per unit length to cause unit slip between the principal moment carrying members

- S is given by $S = \frac{n}{m}y$, where n is the number of shear planes across the width of the composite beam, and m is the number of shear planes through the depth of the beam.

For the Startlink beam assembly shown in Fig. 4.4 and defined in Tables (4.1 and 5.1) both n and m are equal to two. Figure 5.7 presents the theoretical load-deflection response calculated using Equation 5.34, assuming the load arrangements defined in Table 5.2, and the range of joint shear rigidities γ, given in Table 5.1.

5.4.3 Comparison of theoretical models

As shown in Figs. 5.6 and 5.7, both the Newmark and Kuenzui and Wilkinson models predict almost linear responses, which will significantly limit their correlation with the expected non-linear deflection response as hypothesised in Chapter 4. It is expected that the initial stiffness of the assemblies will exceed the flexural rigidities predicted by the numerical analyses. For both the Modified Newmark analysis and Kuenzui and Wilkinson model, the determined mean values of flexural rigidity EI_{xx} are given in Table 5.4 for each proposed test specimen and load arrangement, defined in Table 5.1 and Table 5.3.

Comparison of Figs. 5.7(a) and 5.6(a) indicates the Modified Newmark analysis predicts a slightly higher degree of non linearity in the initial load phase compared to the Kuenzui and Wilkinson model, and provides a greater and more realistic spread of flexural rigidities for the range of connection spacings. At present the mathematical derivation of the Kuenzui and Wilkinson model is not available for comparison and valid conclusions cannot be made about its appropriateness.

5.5 Conclusions

- An appropriate experimental method has been determined for the analysis of the prototype PFRP beam assembly.

- The use of an innovative photo-elastic stress analysis tool to determine the bearing stress associated with individual connection has been ruled out.

- The Newmark model for partial interaction has been modified to predict the deflection for a three layer assembly system with connections of finite stiffness.

- Theoretical deflections for the prototype PFRP assembly with varying degrees of connection, have been calculated using both the modified Newmark model originally based on composite steel-concrete interaction, and, the model presented by Kuenzui and Wilkinson for the analysis of partial interaction in timber beams.

- For the prototype assembly the Modified Newmark analysis is expected to show better correlation than the Kuenzi and Wilkinson model with the predicted non-linear response.

5.6 Figures & Tables
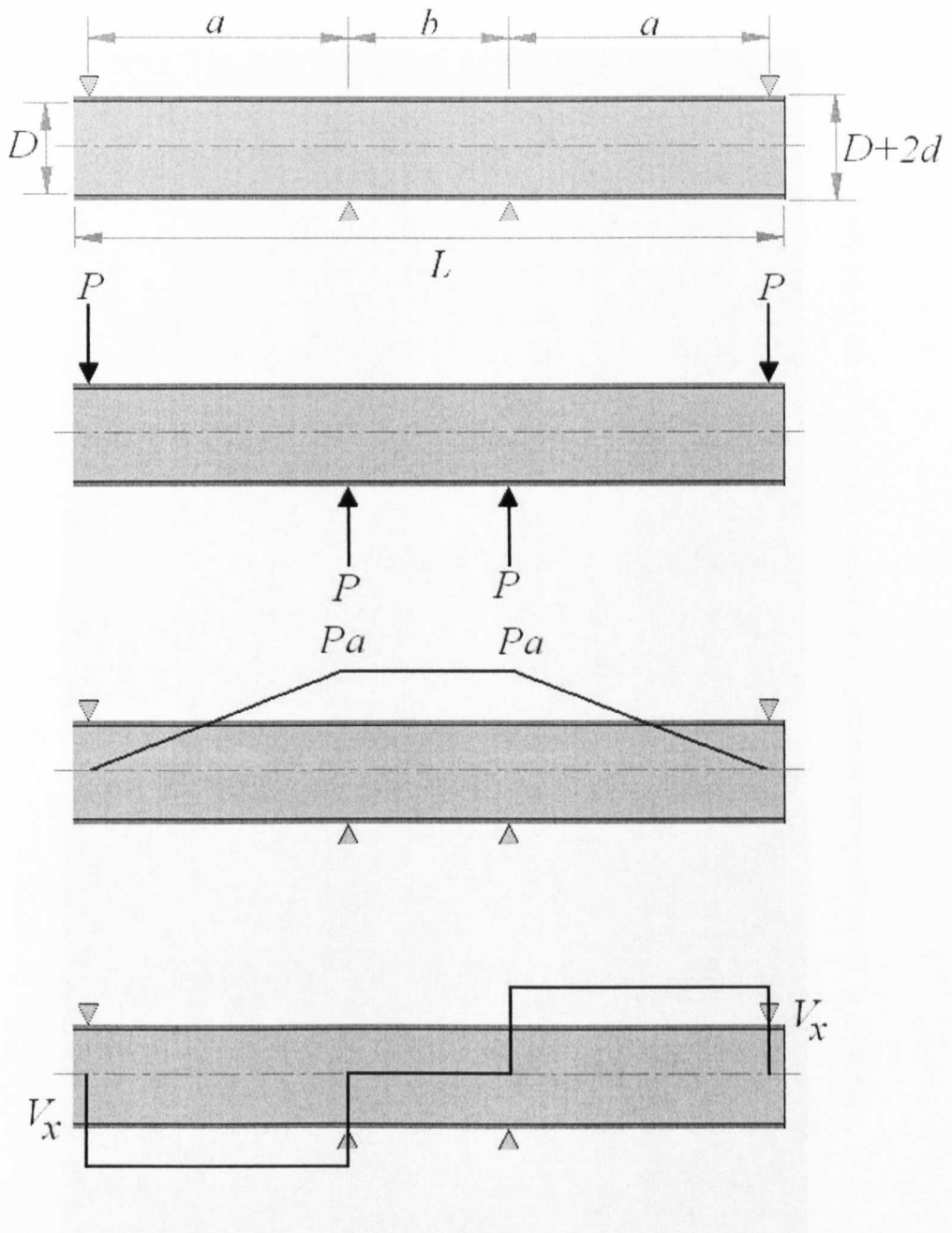
Figure 5.1: Load arrangement, bending moment and vertical shear force distribution
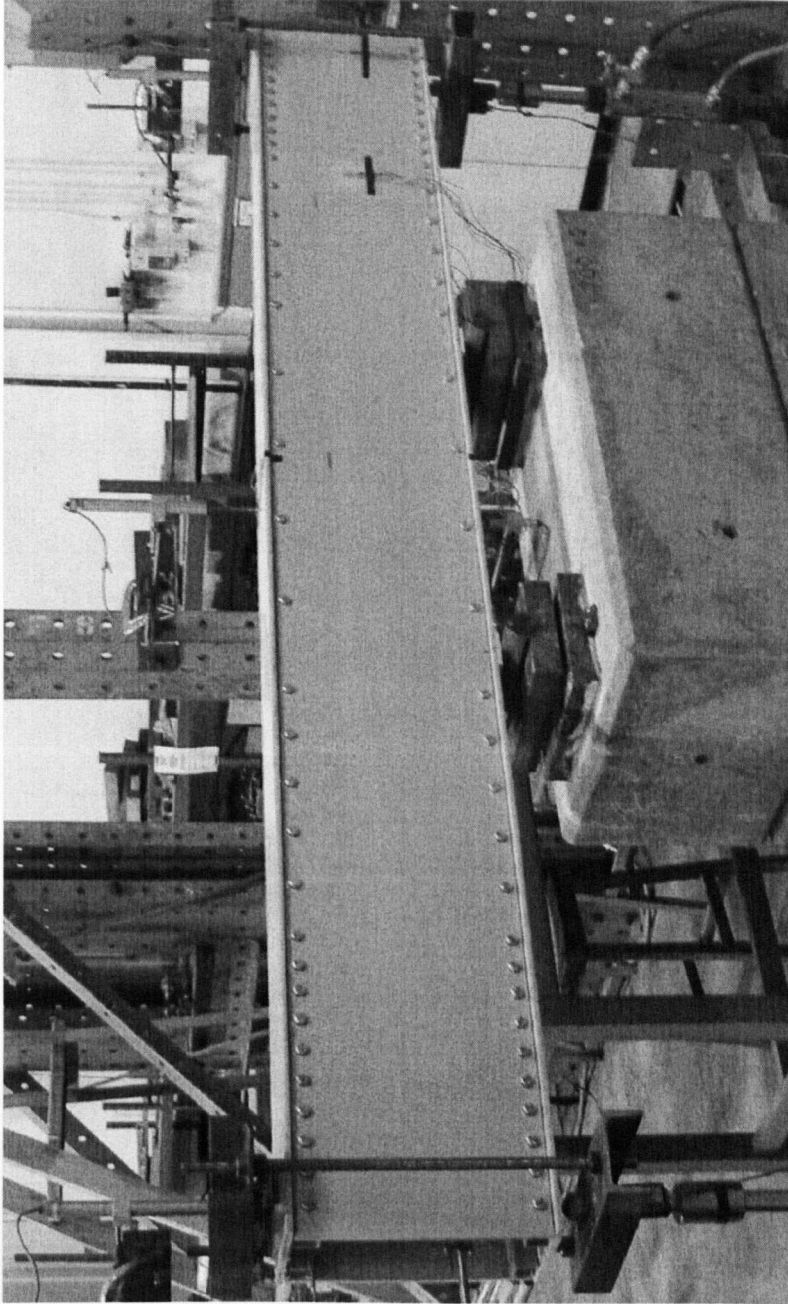
Figure 5.2: Prototype beam assembly in four-point bending test rig (West face)

(a) Upper flange South end deflection
(b) Upper flange Mid-span deflection
(c) Upper flange North end deflection
(d) Lower flange South end deflection
(e) Lower flange Mid-span deflection
(f) Lower flange North end deflection

(g) Upper flange Mid-span longitudinal strain (2 gauges)
(h) Lower flange Mid-span longitudinal strain (2 gauges)
(i) Upper flange longitudinal strain (2 gauges)
(j) Lower flange longitudinal strain (2 gauges, topside + underside)
(k) East web longitudinal strain (2 gauges, topside + underside)
(l) East web shear strain
(m) Upper connection interfacial strain (De-mech gauge)
(n) Lower connection interfacial strain (De-mech gauge)

Figure 5.3: Experimental setup of Prototype Beam assembly with instrumentation positions (Dimensions in mm)
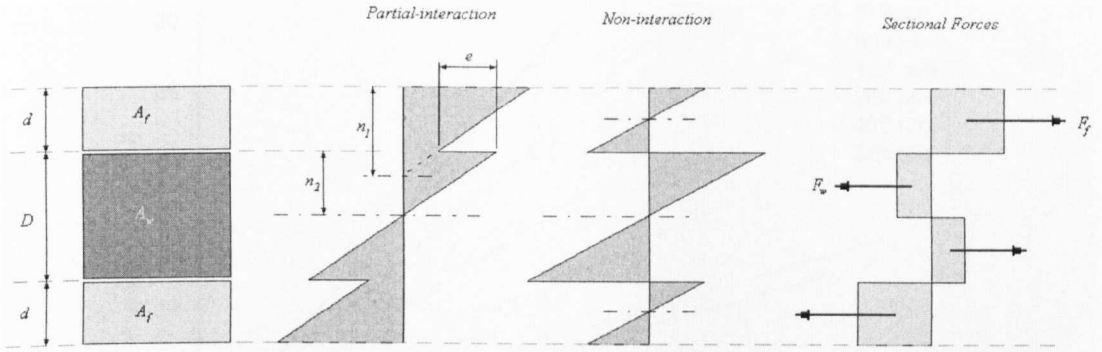
Figure 5.4: Assumed strain distribution in 3 layer system with partial-interaction

Figure 5.5: Flange section element of width dx

(a)
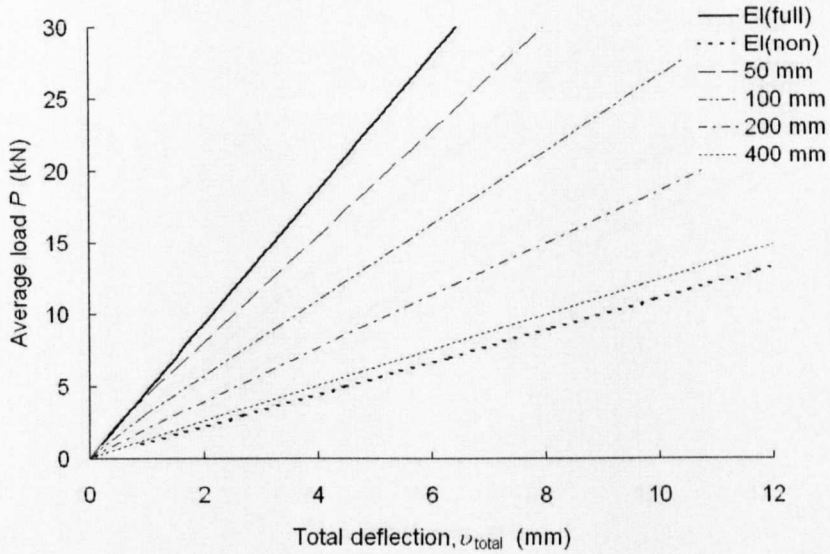
(b)

Figure 5.6: Plots of Modified Newmark model predictions for deflection responses of beam assembly in (a) load arrangement A (b) load arrangement B
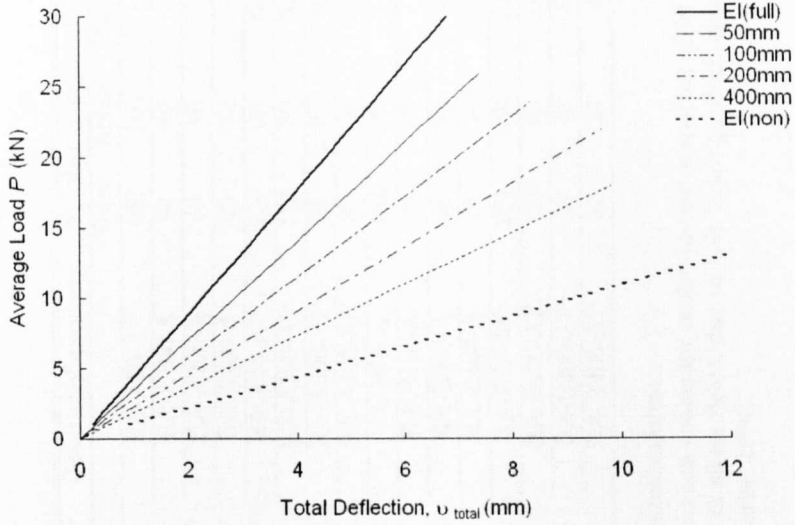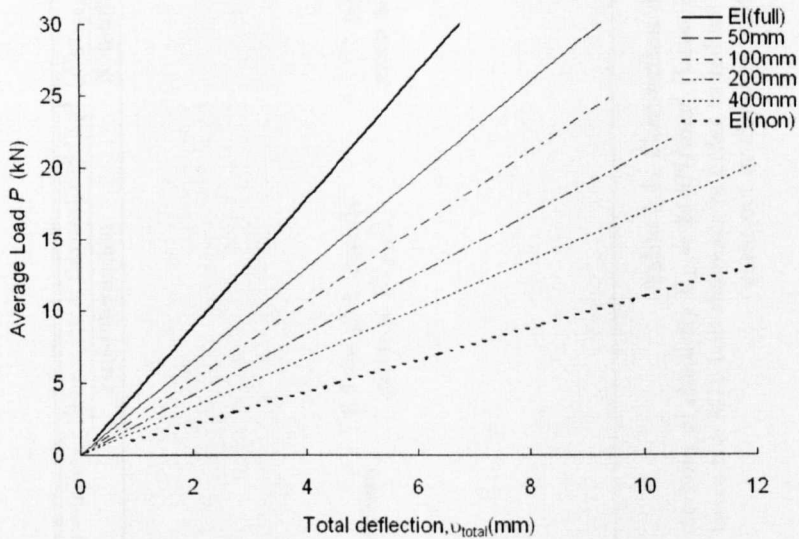
Figure 5.7: Plots of Kuenzui and Wilkinson model prediction for deflection responses of beam assembly in (a) load arrangement A (b) load arrangement B

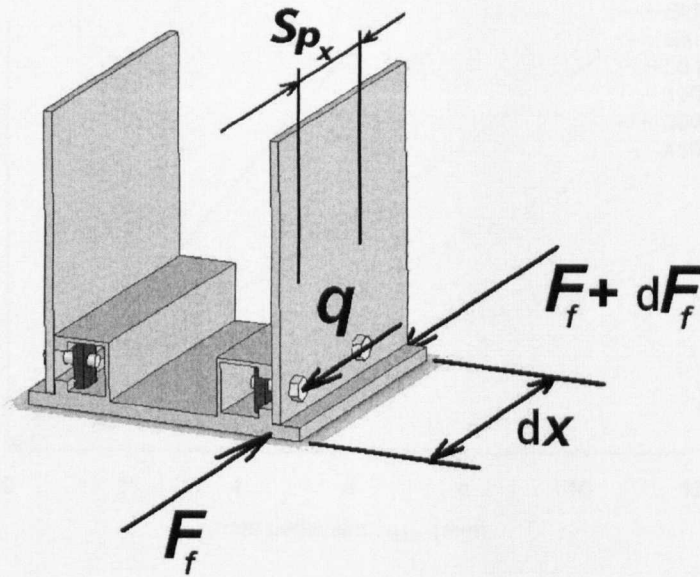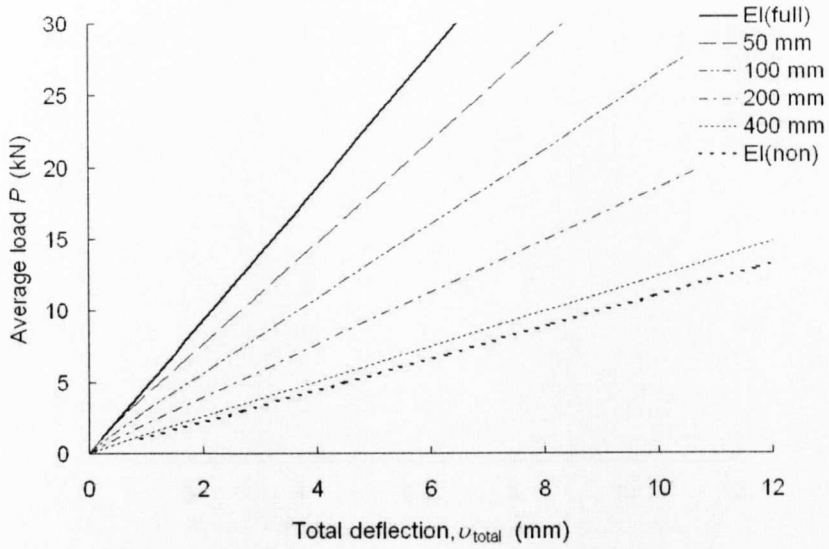| Beam overall dimensions (mm)	Theoretical flexural rigidity[1] $(E_L I_{maj}) \times 10^{12}$ Nmm²		Beam configuration	Number of connections		
	Full-interaction	Non-interaction		Total	Active	Passive
$400 \times 203 \times 3000$mm	5.7 (in plot legends given as EI_{full})	1.1 (in plot legends given as EI_{nom})	BA-A50-A [2]	160	160	-
			BA-A100-A	80	80	-
			BA-A200-A	40	40	-
			BA-A400-A	20	20	-
			BA-A50-AP	224	160	64
			BA-A100-AP	112	80	32
			BA-A200-AP	56	40	16
			BA-A400-AP	32	20	12
			BA-B50-A	192	192	-
			BA-B100-A	96	96	-
			BA-B200-A	48	48	-
			BA-B400-A	24	24	-
			BA-B50-AP	224	192	32
			BA-B100-AP	112	96	16
			BA-B200-AP	56	48	8
			BA-B400-AP	32	24	4

Table 5.1: Connection details of beam assemblies

Notes: 1. Based on a modulus of elasticity $E_L = 24$ kN/mm² (Lane, 2002). 2. A minimum connector centre-to-centre spacing of 50 mm was designated as being ≥ 4 times the M10 bolt diameter in order to reduce the interaction of stress fields, due to bolt bearing, which may result in a shear-out or cleavage mode of failure (Clarke, 1996).

Beam configuration	P_{slip} (kN)	Joint shear rigidity, γ (N/mm/mm) External span, a	Mid-span, b
BA-A50-A	44	50	-
BA-A100-A	22	25	-
BA-A200-A	11	12.5	-
BA-A400-A	5.5	6.25	-
BA-A50-AP	44	50	50
BA-A100-AP	22	25	25
BA-A200-AP	11	12.5	12.5
BA-A400-AP	5.5	6.25	6.25

Table 5.2: Theoretical joint properties

Bending	Load arrangement designation	Dimensions of loading arrangement (mm) Total span, L	External span, a	Internal span, b	Constants C_1	C_2
Four -point	A	2848	1022	800	0.223	2.786
	B	2848	1222	400	0.243	2.330

Table 5.3: Load arrangement details

Beam configuration	Load arrangement designation	Mean Flexural rigidity $EI_{xx} \times 10^{12}$ N/mm^2 Modified Newmark	Kuenzui and Wilkinson
BA-A50-AP		3.87	3.80
BA-A100-AP	A	2.65	2.90
BA-A200-AP		1.71	2.20
BA-A400-AP		1.14	1.17
BA-B50-AP		4.60	3.78
BA-B100-AP	B	3.00	2.95
BA-B200-AP		1.89	2.25
BA-B400-AP		1.17	1.18

Table 5.4: Flexural rigidities determined from the Modified Newmark analysis and the Kuenzui and Wilkinson model

CHAPTER 6

Results and Analysis

Reported in the following chapter are the results of a series of full-sized experimental tests to determine the performance of a modular beam assembly based on the concepts proposed by Byers & Singleton (1999) and presented in the two previous chapters.

The prototype beam assembly illustrated in Fig. 4.4 and defined in Table 4.1 has been supplied with eight different connection details, as specified in Table 5.1, and tested in two four-point load arrangements. This test matrix yields a total of 16 flexural tests completed on the prototype beam assembly. In the following analysis, only the results of the beam assemblies in loading arrangement A are discussed.

The primary objective of the work reported herein is to characterize, through full-sized experimental testing, the performance of the modular beam assembly and determine the efficiency of the Unistrut connection method for use in modular assemblies. The experimental analysis covered in this chapter is subdivided into sections covering, analysis of deflection and displacement response, analysis of the strain response and conclusions.

6.1   Analysis of deflection and displacement response

A full and in-depth analysis of the experimentally determined vertical deflections and longitudinal interfacial displacements, is presented in the following subsections. The flexural rigidity EI_{ASSEM}, and effective joint shear rigidity γ_e, are determined for the range of assemblies tested. Comparisons are made with the two theories detailed in Section 5.4, and a new method for the simultaneous graphical determination of the flexural rigidity EI_{ASSEM}, and shear stiffness $k_s G_{xy} A_v$, is presented.

6.1.1   Experimental deflections

The total deflection δ_{total}, of the assembly in four-point bending is given below in Equation 6.1. And can be defined, as the vertical deflection of the mid-span section with respect to the location at which the two external loads are applied, as illustrated in Fig. 6.1.

$$\delta_{total} = \delta_{end} + \delta_{mid} \tag{6.1}$$

As described in the previous chapter and detailed in Fig. 5.3, measured vertical deflections were taken at three locations (North load point, Mid-span and South load point) along the Upper and Lower flanges. These experimentally measured deflections, are not solely subject to the longitudinal flexure of the assembly which can be defined as the classical effects of loading in this case. Non-classical and secondary effects of loading, such as out-of-plane deformations resulting from buckling, or sway mechanisms, as well as in-plane mechanisms such as vertical joint compression will also influence the measured deflections. The following analysis provides a suitable treatment of the measured deflections.

The measured vertical deflection response for the Upper and Lower flanges in test BA-A50-A (Table 5.1) at the South load point and at mid-span are shown

in Fig. 6.2. The vertical displacement of the Upper and Lower flange under the South load point and at mid-span are shown as dashed lines in Fig. 6.2 and are representative of the behaviour observed throughout the test series. The solid lines in Fig. 6.2 indicate the expected theoretical response of the assembly assuming a state of full-interaction ($X = 1$), calculated using Equation 5.1 and the value EI_{full} given in Table 5.1.

As shown in Fig. 6.2(a) the stiffness of the assembly as measured from both the Upper and Lower flanges appear less than that of the theoretical model for full-interaction. Both measurements from the Upper and Lower flange exhibit a slight non-linearity, and, differ in magnitude by approximately 25%, with the Upper flange being the least stiff.

The experimental readings taken at the mid-span location as shown in Fig. 6.2(b) exhibit a greater variation and non-linearity. Both sets of experimental data are opposite in magnitude to the theoretical prediction, indicting a general downward movement of the assembly at mid-span.

These abnormal deflections are a direct result of the low tolerances used in the hand manufacture of this prototype structure. The measured variation in the depth of the web panels has been found to be ± 3mm, leading to localised compression of the assembly, at the level of the web-flange connection in the area of the internal and external supports. Figure 6.3(a) indicates the presence of local compression under the Northern load point of test BA-A50-AP, it is possible to identify a slight buckle in the free edge of the web panel by comparison to the displacement transducer on the inside of the specimen. Close examination of the top flange directly under the load point, as shown in Fig. 6.3(a), indicates a compression of the uppermost connection row. The compression of two pairs of connection beneath the load plate, shown in Fig. 6.3(b), further increases the displacement measured in the Upper flange, producing the significant difference

(20 - 40%) in the displacement measured in the two flanges throughout the test series.

Settlement of the structure over the internal support, has the effect of increasing the measured displacements of both the Upper and Lower flanges, Fig. 6.3(b) clearly shows the local bending of the Lower flange and compression of the lowermost connection row, directly above the Northern internal support for test BA-A50-AP. The magnitude of the compressive movement of the assembly over the internal support, shown in Fig. 6.3(b) and illustrated as, $\Delta_{support}$ in Fig. 6.4, dominates over the expected upward deflection of the mid-span region, producing the apparent negative deflection shown in Fig. 6.2(b).

A suitable measurement technique accounting for the local compression of single component PFRP members in flexure has been developed by Roberts & Marsi (2003). By comparing the deflection at mid-span taken on the underside of the member, to the deflection of the neutral axis at mid-span, the effects of local compression can be determined. For the multi-shape assembly and set-up shown in Fig. 5.2 it is not possible use the technique.

To provide a realistic value of the total deflection due to bending for the set-up shown in Fig. 5.2, the non-classical effects of localised compression need to be taken into account in calculating the actual deflection. The measured displacements from the Lower flange provides a more accurate depiction of the actual end deflection of the assembly, as they are unaffected by the compression of the uppermost connection row. The deflection measured from the Upper flange will be influenced by the compression of both the Upper and Lower connection rows.

The deflection of the Lower flange relative to its original position as illustrated in Fig. 6.4, is given by the subtraction of the settlement over the internal supports (which may be taken as the measured displacement of the Lower flange at mid-

span), from the end deflection measured at the Lower flange location.

The theoretical upward deflection, δ_{mid} at the mid-span, Fig. 5.1, can be calculated using

$$\delta_{mid} = \frac{Pa^2}{8EI} \tag{6.2}$$

Equation 6.3 gives the relative proportion of the theoretical mid-span deflection (Equation 6.2), to the theoretical end deflection, assuming a constant flexural rigidity along the assembly's length.

$$D_f = \frac{\left(\frac{PL^3}{6EI}\left(\frac{3a}{4L} - \left(\frac{a}{L}\right)^3\right)\right) - \left(\frac{Pab^3}{8EI}\right)}{\frac{Pab^2}{8EI}} \tag{6.3}$$

Using Equation 6.3 it can be shown that for load arrangements A and B, given in Table 5.2, the mid-span deflection, δ_{mid}, is only 10.5% and 2.7% of the theoretical end deflection, δ_{end}. By factoring the end deflection δ_{end}, of the Lower flange relative to its original position by 1.105 for load arrangement A, and, by 1.027 for arrangement B, an appropriate total deflection δ_{total}, may be be determined from the experimental measurements.

6.1.2 Total deflection response

Figure 6.5 shows the total deflection response δ_{total}, plotted against the applied load P, calculated in the manner described earlier for the 8 beam assemblies tested in load arrangement A, allowing comparison of their relative stiffness, given by the gradient of the curves. Figure 6.5(a) details the response of the four assemblies with only active connections, whilst Fig. 6.5(b) details the response of the four assemblies (see legend) with both active and passive connections. Taken from Table 5.1 the upper bound EI_{full} and lower bound EI_{non} on the theoretical flexural rigidity, are used to give the limits on the deflection-load response, as described in Chapter 4.

The general trend found in both Figs. 6.5(a) and (b), of an increase in stiffness with joint shear rigidity is as expected. The nature of the individual load deflection curves shown in Fig. 6.5, appears to be dependent on the joint shear rigidity. For assemblies with high joint shear rigidity ($50 \geq \gamma \geq 25$ N/mm/mm), the experimental load-defection may be approximated to a linear response, while at low joint shear rigidities ($12.5 \geq \gamma \geq 6.25$ N/mm/mm), the experimental load-defection may be approximated to a bi-linear response. Numerical values for the flexural stiffness of the assembly EI_{ASSEM}, based on the measured total deflections are determined in Section 6.1.5.

The occurrence of local buckling in the web shapes in the mid-span region, shown for test BA-B400-A in Fig. 6.6, may account for the significant non-linearity in the behaviour of assemblies with the lowest degree of connection. Similar local buckling effects were noted in all four specimens with such a low number of discrete connections ($200 \leq Sp_x \leq 400$ mm).

Comparison of Figs. 6.5(a) and (b) indicates a minimal increase in stiffness with the inclusion of passive connections in the mid-span region, when tested in load arrangement A. As indicated in Section 5.1, the inclusion of connections in this mid-span region of zero shear, is likely to have little influence on the overall stiffness of the assembly.

6.1.3   Comparison of theoretical and experimental defections

Figures 6.7(a) and (b) provide a comparison between the experimentally determined and theoretically calculated total deflection δ_{total}, plotted against the applied load P, for the assemblies tested in load arrangement A.

The predictions from the modified Newmark analysis in Chapter 5 are shown in Fig. 6.7(a) whilst the predictions from the Kuenzui and Wilkinson analysis are shown in Fig. 6.7(b). The results from assemblies with only active connections

are not compared to the theoretical analysis, as these cannot be assumed to have a constant joint rigidity over the entire length of the assembly as assumed in both theoretical models. The dashed lines without symbols in Fig. 6.7(a) and (b), indicate the theoretical stiffness of the beam assembly with various connection spacing's, for which the joint shear rigidities are given in Table 5.2.

As indicated earlier the load-deflection response of the assemblies may be interpreted as approximately bi-linear, exhibiting an initial high stiffness followed by a region of lower stiffness. Although the modified Newmark analysis provides a slight non linear response during the intial loading phase the bi-linear experimental behaviour provides poor correlation with the two nominally linear theoretical models.

In nominally general the linear predictions of the two theoretical models provide an underestimate of the initial stiffness of the assemblies. At higher loads the Kuenzui and Wilkinson model overestimates the stiffness of those assemblies with lowest effective joint shear rigidity, whilst the modified Newmark model underestimates the stiffness of all assemblies, providing a poor correlation.

Sotiropoulos *et al.* (1996) successfully applied a modified form of the Newmark analysis in order to determine the theoretical load-deflection behaviour of mechanically fastened PFRP floor and bridge beam assemblies. They used experimentally measured slip strains, recorded from the assemblies in bending, as opposed to the author's method of calculating a theoretical joint stiffness based on experimental individual connection tests, to find a good correlation between the experimental and theoretical behaviours.

The use of such an evaluation methodology as adopted by Sotiropoulos *et al.* (1996) may be considered inappropriate in the determination of a purely theoretical model. By using the effective joint shear rigidity (taken from the experimentally measured slip strains) they are measuring the behaviour of multiple

discrete connectors and not individual discrete connections, the presence of any secondary effects or errors in the measurement technique will not be visible in the comparison of the theoretical and experimental responses, providing a poor reference for a measure of performance.

Also the validity of the slip measurements must be considered, the value of slip strain recorded will be dependent on the location of the measurement, a single point measurement may not provide an accurate representation of the degree of interaction between the shapes in the assembly. Consider a linear element of the assembly containing an active connection; it is reasonable to assume that the axial strains present in the flange shape of the assembly will be influenced to some extent by the locality of the discrete mechanical fastening, which will transfer bearing and shear stresses into the flange and web shapes. The effect of such connection stresses in the web and flange shapes will decrease in a near exponential type form, with distance from the discrete connection.

The use of a bi-linear model would potentially provide a better correlation with the experimental evidence shown in Fig. 6.5. However, on accounting for the significant and unknown differences between the behaviour of discrete connections in shear (see Chapter 3) and that of multiple discrete connections in the modular beam assembly, establishing the transitional load for the change in stiffness could prove difficult.

In order to define the transitional load for such a bi-linear model certain assumptions have to be made concerning the behaviour of the multiple discrete connections, and these can be summarised to be the following.

If the discrete connections are assumed to be infinitely rigid up until their ultimate resistance, taken as 2.5 kN (see Chapter 3), the transitional load P_{slip}, for which the onset of slip is expected may be easily calculated as shown in Chapter 5. Such values of P_{slip}, are given in Table 5.2. Under such an assumption the

assembly would act in a state of full-interaction ($X = 1$) up to the transitional load P_{slip}, after which the degree of interaction decreases.

Alternatively, by assuming the individual discrete connections, (and any arrangement of multiple discrete connections) have finite rigidity, the interfacial slip, defined as the relative movement between the flanges and the webs at the level of the connection, will evolve from the onset of flexural loading. Under such an assumption an assembly would exhibit a degree of full interaction ($X = 1$) upon initial loading, followed by a linearly decaying degree of interaction ($X \to 0$), providing the assembly with a decaying stiffness, and non-linear deflection response.

In practice it is not possible for any assembly with a non-zero finite joint shear rigidity to exhibit a state of non-interaction ($X = 0$). From observing the individual load-slip plots of the Unistrut connection given in Chapter 3, it can be seen that once the peak resistance is surpassed, the secant stiffness linearly decreases with slip. As the slip tends to infinity the secant stiffness will tend to zero. The effect on the assembly would be a linear decrease in the degree of interaction (an exponential deflection response). This is shown through the load-deflection curves of the prototype modular beam in Fig. 6.5 for the range of connection arrangements tested.

From the experimentally determined deflections in Fig. 6.5, it is not possible to identify which of the above assumptions, for the behaviour of the Unistrut connections and its effect on the response of the assembly, is the most applicable. In order to accurately determine the behaviour of multiple discrete connections, from the flexural response of any assembly, would require an exact measurement of the total deflection during the initial loading phase. As highlighted in Section 6.1.1, the validity of the determined total deflection is questionable, due to the effect of secondary and non-classical effects of bending.

6.1.4 Determination of the translation load P_{slip} and effective joint shear rigidity, γ_c

To provide a comparison to the theoretical transitional load P_{slip}, measurements of the interfacial slip were taken for the Upper and Lower flanges in the North and South spans. Figure 6.8 shows the mean of the North and South and Upper and Lower interfacial slips with applied load for the complete range of assemblies tested in load arrangement A. Figure 6.8(a) shows the mean slip plotted against load for the beam assemblies tested in arrangement A with active connections, whist Fig. 6.8(b) shows the mean slip plotted against load for the beam assemblies tested in arrangement A with both active and passive connections.

The trend of increasing connection stiffness with number of active connections is as expected, as highlighted by the increase in assembly stiffness shown in the load-deflection plots in Fig. 6.5. The involvement of passive connections further increases the stiffness of the assembly. This additional increase in stiffness, above that of increasing the degree of connection, is most apparent in assemblies with high degrees of connection ($50 \leq Sp_x \leq 100$ mm), due to the large numbers of passive connections.

From inspection of the load-mean slip plots in Fig. 6.8 it may be observed that all connection arrangements exhibit a secant connection stiffness in excess of that expected for a state of non-interaction, indicated in Fig. 6.8. A general non-linear trend is visible in all plots, with a high initial stiffness. For the assemblies with low degrees of connection ($200 \leq Sp_x \leq 400$ mm), the gradient of load-mean slip plot approaches that of a case of non-interaction under increasing load.

It may be concluded that the non-linear deflection response, seen in Fig. 6.5, is attributed to slippage, as a result of the required longitudinal shear force exceeding the available shear strength R_s, from the Unistrut connection per unit

length. It may also be observed from the load-mean slip curves that the theoretical loads for slip P_{slip}, given in the second column of Table 5.2, are significant over estimates. This result is expected, as a theoretical P_{slip}, was calculated assuming all connectors were transferring the shear force R_s, simultaneously. In reality this does not occur because of inherent imperfections. The load-deflection plots in Fig. 6.5 are therefore bi-linear/non-linear, with significantly lower transitional loads for the initiation of slip.

From a comparison of the results in Figs. 6.5 and 6.8 it is seen that an interfacial slip in the order of 0.1 mm has a significant effect on the stiffness of the assembly. The most severe example is in test BA-A400-A, where the secant stiffness is reduced by 33% following an interfacial slip of only 0.1 mm.

From the experimental data shown in Fig. 6.8 it is possible to back calculate effective joint shear rigidity, γ_e, for the connection arrangements supplied to the assembly. Figures 6.9(a) and (b) show the response of the back calculated effective joint shear rigidity γ_e, for the assemblies tested in arrangement A with active connections and active and passive connections respectively. A trend of decreasing effective joint shear rigidity is common to all degrees of connection tested. Assemblies with both active and passive connections (Fig. 6.9(b)) exhibit an increased effective joint shear rigidity over assemblies with only active connections (Fig. 6.9(a)). This increase in joint shear rigidity is most noticeable between assemblies BA-A50-A and BA-A50-AP undoubtedly due to the large number of passive connections (64) present in the mid-span region of BA-A50-AP. This change in joint shear rigidity with the inclusion of passive connections, disproves the earlier assumption of an idealised rectilinear shear force distribution (Fig. 5.1). Moreover all connections arrangements shown in Fig. 6.9 exhibit initial effective joint shear rigidities several orders of magnitude in excess of the theoretical joint shear rigidities γ, given in the third and fourth columns of Table

5.2. However in general (with the exclusion of BA-A50-A), the final effective joint shear rigidities are approximately 100% greater than the theoretical joint shear rigidities, shown in Figs. 6.9(a) and (b) by the dashed vertical lines, at 50, 25, 12.5 and 6.25 N/mm/mm, indicating to an individual connection stiffness of approximately 5 kN/mm opposed to the experimentally measured value of 2.5 kN/mm.

The theoretical joint shear rigidities, γ, were based on the value of individual connection stiffness, K_s, experimentally determined in Chapter 3, and defined as the gradient of the batch mean load-slip response, in the initial linear range up to a slip of 1 mm. Considering the low values of interfacial slippage expected in the assembly ($s \leq 1$ mm) as shown in Fig. 6.8, the use of such a comparatively large range, to define the connection stiffness K_s, may have resulted in providing an underestimate of the actual connection stiffness present in the beam assembly. Referring back to Fig. 3.16, for a slip of approximately 0.2 mm the corresponding resistance is almost 1 kN, indicating a much higher initial stiffness of approximately 5 kN/mm over the range of slip likely to be present in the connection detail than initially predicted.

Although the individual characterisation tests, completed in Chapter 3 are supposed to be representative of the multiple connections in the assembly, there exists several significant differences in the load transfer behaviour between the individual and multiple connections. In the individual connection characterisation tests, it is possible to adjust the specimen such that the M10 bolt is bearing on the surrounding material before the onset of load. However in the multiple connection arrangement of the assemblies, it is not practically possible to arrange for every connector to be in bearing with the web material, after the beam has been assembled, owing to the vast number of connections in each row (up to 56 discrete connectors). As a result some connections may be transferring their

shear force either in bearing or through friction generated under the washer upon loading of the assembly.

For connections transferring their shear force through friction, the preload generated under the applied fastening torque of 20 Nm will decay in an exponential form as determined in Section 3.4.3, resulting in a time dependent decreasing frictional resistance.

For the connections with bearing load transfer the web panel and the Unistrut will move relative to the flange. However the flange and Unistrut will move relative to the web panel for transfer through friction over the compressed material surfaces beneath the M10 bolt head and washer. Due to the difference in resistance of the two load transfer processes it is difficult to directly compare the performance, of the connections in the assembly to the individual characterised connections.

6.1.5 Determination of assembly flexural rigidity EI_{ASSEM}

By substituting the measured total deflection δ_{total}, into Equation 5.1, it is possible to back calculate the flexural rigidity (Clarke, 1996; Bank, 1989)of the assembly, which is given the notation EI_{ASSEM}. This back calculated stiffness is the secant value of the flexural rigidity.

In order to apply the Timoshenko beam expression, the shear rigidity of the beam assemblies is assumed to remain constant, to be independent of the effective joint shear rigidity, and to be equal to that assumed had the beam cross-section been the product of a single pultrusion. This shear rigidity, given by the expression $k_s G_{xy} A_v$, therefore has a shear correction factor k_s equal to 1 (Nagaraj & GangaRao, 1997), a shear area A_v equal to the cross-sectional area of the two web shapes (4826 mm^2) and the in-plane shear modulus, G_{xy}, taken to be equal to 4.0 GPa (Mottram, 2004b).

Plots of the back calculated flexural rigidity EI_{ASSEM}, against applied load, P, are given in Fig. 6.10 for the assemblies tested in load arrangement A. Considering each family of curves, a general trend of increasing flexural rigidity EI_{ASSEM}, with increasing degree of shear connection is clearly identified. Other trends found on evaluating the results in Fig. 6.10 are that:

- All assemblies, with the exception of BA-400-A and BA-400-AP develop a peak stiffness of between 8% and 19% higher than the initial stiffness.

- Assemblies, BA-A50-A, BA-A100-A, BA-A200-A, show an increase in peak stiffness of, 13%, 11%, and 20% respectively.

- For the two assemblies with the lowest densities of connection ($Sp_x = 400$ mm), the initial rigidity is the peak value and that upon further loading, EI_{ASSEM} decays away with a non-linear response.

Direct interpretation of the results plotted in Fig. 6.5 and Fig.6.10, may however, be misleading, in that the load-deflection response is not that had the beam been pultruded as a single product. The latter would have full continuity of the PFRP material at the levels in the modular beam where the discrete shear connections of finite stiffness are located

6.1.6   The graphical method for modulus of elasticity

As expressed in the Timoshenko beam theory (Timoshenko, 1955), shown in Equation 5.1 (repeated below for clarity), the deflection of the assembly may be divided into two principal components.

$$\delta = \frac{C_1 P L^3}{EI_{xx}} + \frac{C_2 P L}{k_s G_{xy} A_v}$$

The primary component represents the magnitude of deflection arising from the flexural stiffness of the assembly. The secondary component represents the magnitude of deflection arising from the shear stiffness of the assembly. For the earlier deflection analysis used to determine EI_{ASSEM}, the global shear stiffness $k_s G_{xy} A_v$, of the assembly was taken to be equal to 19304 kN, based on the assumptions given in the previous subsection.

Due to the discrete and intermittent nature of the connections present, and, the material and geometric properties, it is reasonable to assume the section shear stiffness and shear flow are not constant along the length of the assembly. Hence the results of coupon testing cannot be used to determine the global section shear stiffness of the assembly.

The global shear stiffness and the flexural rigidity of the assembly may be simultaneously determined, from the experimental deflection response of the assembly over a range of different spans or load arrangements (Bank, 1989). The experimental procedure is based on Timoshenko beam expression (Timoshenko, 1955) and has been used by Sims & Johnson (1987), Bank (1989) and Mottram (1991), in order to simultaneously determine both the section flexural modulus and section shear modulus of pultruded I-beams and box beams. The term section is used to show that the moduli are specific to the test method and data reduction method used to obtain the two moduli.

Each set of data results (δ_{total} and P), from the bending tests completed with the different length of beam L, produces a Timoshenko expression for four-point bending with two unknowns EI_{ASSEM} and $k_s G_{xy} A_v$. The Timoshenko expression can be interpreted as being a line of the form $y = m(x) + c$, by dividing through by PL, such that the independent variable L^2, is plotted on the abscissa and

δ/PL, plotted on the ordinate, as shown below.

$$\frac{\delta}{PL} = \frac{C_1 L^2}{EI_{ASSEM}} + \frac{C_2}{k_s G_{xy} A_v} \qquad (6.4)$$

The slope of the fitted line will be proportional to the flexural rigidity term EI_{ASSEM} whilst the intercept is proportional to the Timoshenko shear stiffness term $k_s G_{xy} A_v$.

Owing to the initially low Span-Depth ratio of 7.5 it was inadvisable to further reduce the span L, increasing the effect of shear on the assemblies. For this reason the relative proportions of the internal and external spans are altered between loading arrangements A and B, such that the length of the external span, a, becomes the primary variable.

Although it may have been possible to test the assemblies in a third arrangement, with an external span ($a \leq \frac{L}{3} \approx 1\text{m}$), such an arrangement would have greatly increased the shear force carried by the reduced number of active connections. The effect of this would be to cause an early onset of slip producing a non-linear deflection response for which it would have difficult to define the deflection quantity δ/Pa, for analysis. The geometric properties of load arrangements A and B, were chosen in order to ensure a measurable difference in the response of the assembly, whilst keeping external span in the range ($\frac{L}{3} < a < \frac{L}{2}$). A third load arrangement with an external span between that of load arrangements A and B, would not provide sufficient difference in the deflection response to be accurately determined.

Substituting the expanded form of constants C_1 and C_2 into Equation 5.1, gives

$$\delta = \frac{Pa}{24EI_{ASSEM}}(3L^2 - 4a^2) + \frac{Pa}{k_s G_{xy} A_v} \qquad (6.5)$$

Which can be rearranged into the form $y = m(x) + c$, by dividing through by

Pa, such that the independent variable a^2, is plotted on the abscissa and δ/Pa, plotted on the ordinate. This can be expressed as

$$\frac{\delta}{Pa} = \frac{-4a^2}{24EI_{ASSEM}} + \left(\frac{1}{k_s G_{xy} A_v} + \frac{3L^2}{24EI_{ASSEM}} \right) \qquad (6.6)$$

In this way the deflection quantity δ/Pa can be plotted against a^2, for the test completed with constant span L, but differing external span length a. The slope of the fitted line will be proportional to EI_{ASSEM} whilst the intercept is proportional to both EI_{ASSEM}, and $k_s G_{xy} A_v$.

Linear fits using the method of least squares were performed on the linear initial portions of the load deflection curves in Fig. 6.5. Values of the deflection quantity δ/Pa, for the beam assemblies are given in the third and fourth column of Table 6.1 for load arrangements A and B, respectively. The assemblies used in each test are identified in the seventh column, whilst a description of the connection detail and connection spacing are given in the first and second column.

The graphical plots of the deflection quantity δ/Pa, against a^2, for the assemblies with only active connections are shown in Fig. 6.11(a), and, Fig 6.11(b) for the assemblies with passive connection.

The fifth and sixth columns of Table 6.1 provide the flexural rigidity EI_{ASSEM}, and shear stiffness $k_s G_{xy} A_v$ of the assemblies, values given in *italics* are theoretical values, whilst those in normal font have been calculated using the graphical method as described earlier.

Both sets of data for EI_{ASSEM} and $k_s G_{xy} A_v$, show significant variation with no trend observed as the number of connections is increased. The values of flexural rigidity EI_{ASSEM}, and shear stiffness $k_s G_{xy} A_v$, given in Table 6.1 are nonsensical in value and magnitude and show very poor correlation, with the expected theoretical values and the experimentally determined values of EI_{ASSEM},

given in the previous section (Fig 6.10).

There exists a number of possible sources of error in the experimental method, which may significantly affect the application of the graphical method, and, the calculation of the flexural rigidity EI_{ASSEM}, and the shear stiffness $k_sG_{xy}A_v$. These possible sources of error are investigated as follows:

- The validity of the calculated flexural rigidity EI_{ASSEM}, and the shear stiffness $k_sG_{xy}A_v$ are questionable owing to the lack of a third data set.

- Due to the limited length of the assemblies only limited changes in the external span were possible limiting the possible difference in the deflection responses. From a purely theoretical approach a beam assembly with full-interaction ($X = 1$) provides only a 7% difference in the deflection quantities δ/Pa, for the two load arrangements owing to the small change in the external span length a, from 1022 mm in load arrangement A to 1222 mm in load arrangement B.

- The presence of non-classical and secondary effects of bending as discussed in Section 6.1, significantly limit the accuracy to which the true magnitude of the deflection can be determined. Although a suitable method has be developed to minimise these significant secondary effects, the presence of ± 3 mm tolerances on the depth of the web panel, allowing significant vertical compression of the assembly, may still affect the calculated deflection. A vertical compression of 1 mm represents only 1/400 of the depth of the assembly, but approximately 1/10 of the SLS deflection L/250. To demonstrate the sensitivity of the graphical method to the accuracy of the calculated total deflection, values of the deflection quantity δ/Pa, based on the theoretical assembly with full-interaction, have been altered by an acceptable 1% error in the total deflection. As the third row of Table 6.1

shows the new theoretical values obtained for the flexural rigidity EI_{ASSEM}, decreased by 29% and the shear stiffness $k_sG_{xy}A_v$ increased by a massive 440%.

- The method used to determine the Timoshenko shear stiffness $k_sG_{xy}A_v$, by the extrapolation to locate the intercept is highly dependent on the accuracy of the measured deflection.

As highlighted above, the solution to the graphical method for the assembly in load arrangements A and B, is highly sensitive to accuracy of the total deflection. It is believed by the author, that the inclusion of a third data set to provide more validity to the solution of the graphical method, would be ineffective in its application. If the external span length for the third arrangement were midway between that of load arrangement A and B, the difference in the deflection quantity would be approximately 3%, however if the deflection is only accurate to ±10% the advantage of a third data point would be lost. The influence of localised compression on the measurement of flexural rigidity and shear stiffness in single component PFRP members, has been investigated (Roberts & Marsi, 2003; Wagner *et al.*, 1982; Bank *et al.*, 1992).

Better results and a more accurate solution to the graphical method from the same measurement set-up, could have been acquired, if the Span-Depth ratio of the assembly were increased. Increasing the span of assembly would have the effect of lessening the stiffness of the system, and greater defections could be measured without over loading the individual connections. Increasing the span would allow the use of three sufficiently differing load arrangements such that the possible error, in the measured total deflection would be minimal compared to the variation in deflection quantity between load arrangements.

6.2   Analysis of longitudinal strain response

The following subsections contain an analysis of the longitudinal strains present in the assembly, the flexural rigidity at mid-span EI_{MID}, is determined and two methods for calculating the degree of interaction X, at the location of the strain gauges are presented.

6.2.1   Determination of mid-span flexural rigidity, EI_{MID}

The flexural rigidity EI_{xx} of a standard beam in four-point bending may be determined from the longitudinal strains measured at mid-span, using engineering beam theory (Clarke, 1996) from

$$EI_{xx} = \frac{My}{\varepsilon} \tag{6.7}$$

Where, M is the moment, taken as Pa, the surface strain given as ε, is taken as the mean of the two measurements on the Upper flange , and, y is the distance from the neutral axis to the point of measurement. As the four-point bending arrangement has an internal span of constant moment Pa, and zero vertical shear V_x, there is a shear flow f_y equal to zero over the mid-span. No shear connectors are therefore required in this region for a state of full-interaction ($X = 1$) to exist. However, connectors are required to prevent separation of the webs and flange shapes.

It can therefore be assumed that the experimentally determined flexural rigidity (at mid-span) EI_{MID}, will be approximately equal to EI_{full}, and independent of the joint shear rigidity supplied to the assembly.

Figure 6.12 shows the flexural rigidity, EI_{MID}, in the constant moment region determined from the mean recorded longitudinal strains at mid-span and the

application of engineering pure bending theory.

Comparison of EI_{MID} to the value determined for the whole assembly EI_{ASSEM}, shown in Fig. 6.10, highlights the lack of equivalence of the two quantities, that would be expected if the assembly were a single pultruded shape, possessing full continuity throughout.

Assemblies with the high degrees of connection ($50 \leq Sp_x \leq 100$ mm), provide an almost constant mid-span flexural rigidity, between 5 - 15% greater than EI_{full}, connection spacings of less than 100 mm provide the assemblies with a generally increasing mid-span flexural rigidity. A general trend of decreasing EI_{MID}, with increasing joint shear rigidity is present in all cases, such a trend appears nonsensical upon initial investigation.

The apparent increase of EI_{MID}, for the lower joint shear rigidities ($Sp_x \geq 200$ mm), is the result of connection slippage. As the assemblies lose composite action, the individual beam shapes begin to act independently of each other, flexing about their own neutral axes with a common radius of curvature. In this state of partial-interaction, the stiffness, and thus the proportion of load and strain generated in the flange shapes, is greatly reduced. This reduction in the axial strains of the outer flanges, influences the strains measured at the mid-span, thereby yielding unrepresentative values for the mid-span flexural rigidity EI_{MID}, as shown in Fig. 6.12. The experimental evidence presented in Fig. 6.12, suggests the assumptions in the theoretical modeling concerning the distribution of vertical shear force V_x over internal supports are invalid.

In practice, for a beam with full continuity loaded in four-point bending, it can be assumed that EI_{MID}, and, EI_{ASSEM} have the same value. The shear stiffness $k_s G_{xy} A_v$, may be back calculated by substituting the flexural rigidity at mid-span EI_{MID}, and the total deflection δ_{total}, into Equation 5.1. Although this procedure provides a quick and simple method to determine shear stiffness, it is

highly dependent on the accuracy of the measurement δ_{total}, and is inaccurate in its determination (Hayes & Lesko, 2004).

As discussed above, and illustrated in Fig. 6.12(a) and (b), assemblies which lack full continuity between web and flange shapes, that is to say there exists a finite joint shear rigidity, the flexural rigidity EI_{MID}, cannot be assumed to exist over the length of the assembly while under four-point bending. This observation means the back calculation approach is not acceptable and for this reason the shear stiffness $k_s G_{xy} A_V$, will not be calculated based on the measured axial strains at mid-span.

6.2.2 Determination of degree of interaction X, from the strain difference e

As indicated in Fig. 5.3 longitudinal strains were measured in both the web and flange shapes, at a distance of 550 mm from the Southern load point. Assuming a linear strain distribution through the individual flange and web shapes, the strain at the extreme fibres can be found through extrapolation. The degree of interaction X, may be determined from this assumed strain distribution, in the flange and web shapes, using a similar method to that described by Sotiropoulos *et al.* (1996). Figure 5.3, details the longitudinal position of the 6 strain gauges attached to the Upper and Lower flanges and East facing web panel. The vertical height of the longitudinal strain measurements from the lowermost surface of the assembly, are given as 0 and 9.6 mm for the gauges attached to the Lower flange, 90 and 310 mm for the gauges attached to the East web, and, 390.4 and 400 mm for the gauges attached to the Upper flange.

Strain distributions plotted against height through the assemblies with increasing applied load P, of two representative assemblies, BA-A50-A and BA-

A400-A are shown in Figs. 6.13 and 6.14.

The strain distribution present in test BA-A50-A, representative of a high degree of interaction ($X \rightarrow 1$), is shown in Fig. 6.13, for the following loads, 8.3, 16.0 and 23.8 kN, proceeding from top to bottom. The strain distribution present in test BA-A400-A, representative of a low degree of interaction ($X \rightarrow 1$), is shown in Fig. 6.14 for the following loads, 5.0, 9.0 and 13.6 kN, proceeding from top to bottom. The assumed strain distribution, present in the flange shapes are identified by the solid lines, whilst the assumed strain distribution present in the web shape are given by the dashed lines.

Comparison of the three plots given in each of Figs. 6.13 and 6.14, indicate significant differences in the development of strain profiles between the two representative assemblies.

The change in the strain distribution within BA-A50-A, as shown in Fig. 6.13 is representative of the change in strain distribution found in all the assemblies with relatively high degrees of connection ($50 \leq Sp_x \leq 100$ mm). At an applied load of 8.3 kN the Upper and Lower flanges carry solely tensile and compressive stresses respectively. The strain distribution in the web appears non-symmetrical and linearly varying with the neutral axis at a height of 244 mm from the underside. The tensile strain at the level of the connection is 36% less, than the strain in the flange at this level, whilst the compressive strain in the web panel is approximately 55% greater than the adjacent flange strain at the level of the Lower connection. The strain differences e, at the level of the Upper and Lower connections are -51 $\mu\varepsilon$ and 50 $\mu\varepsilon$ respectively.

These relationships increase proportionally with further applied load up to 28.3 kN. The relative proportions of the strains in the web and flange at the level of the connection do not change, although the strain difference increases proportionally with load indicating the assembly remains in a state of high interaction.

It is noted that the strain in the web shape remains approximately 35% less than the flange shape for the Upper half of the assembly, indicating a negative strain difference. It is possible that the measured strains in the flange may be influenced to some extent by the local stresses around the connections.

The variation in the strain distribution within BA-A400-A, as shown in Fig. 6.14 is representative of the change in strain distribution found in all the assemblies with a low degree of connection ($Sp_x \geq 200$ mm). Under an applied load of 5.0 kN the Upper and Lower flanges carry purely tensile and compressive stresses respectively. The strain distribution in the web appears non-symmetrical and linearly varying with the neutral axis at a height of approximately 230 mm.

At the level of the Upper connection (a height of 370 mm from the underside of the assembly), there exists a strain difference e, of 84 $\mu\varepsilon$ with strain in the flange being only 19 % of the strain in the web at the same level. For the Lower connection row, the interfacial strain difference e, at the level of the connection is 114$\mu\varepsilon$, with the value of strain in the flange being only 16 % of that in the web at the same level. From the average of strain ratios of the Upper and Lower connection rows, it is possible to determine a degree of interaction X, for the assembly at this load stage. At the 5 kN load stage the degree of interaction X, inferred from the strain diffferences is approximately 0.17. This low degree of interaction and high strain difference shown in Fig. 6.14 are expected. For an applied load of 5.0 kN, a shear flow of 11/N/mm/mm acts on each pair of the 400 mm spaced discrete connectors, which is comparable to the maximum shear flow calculated for the arrangement equal to 12.5 N/mm/mm, based on the individual characterisation tests in Chapter 3.

At an applied load of 9.0 kN, strain differences of 201$\mu\varepsilon$ and 302$\mu\varepsilon$ exist across the Upper and Lower connections, with the strain in the Upper and Lower flanges being only 25% and 16% of the adjacent strain in web. The average degree of

interaction at the 9.0 kN load stage is approximately 0.20. The 80 % increase in applied load, produced a 160% increase in both the maximum tensile and compressive strains of the web, the Upper and Lower flange shapes show only a 117 % and 46 % increase in their maximum strain. It is noted that minimal compressive strains are present on the underside of the Upper flange.

Further increasing the applied load to 13.6 kN, strain differences of $429\mu\varepsilon$ and $629\mu\varepsilon$ exist across the Upper and Lower connections, with strains in the Upper and Lower flanges being only 11% of the adjacent strain in the web. The average degree of interaction at the 13.6 kN load stage is approximately 0.11. This non-proportional increase in the strain difference, is due to the presence of increasing slippage at the level of the connection. This slippage results from the low joint shear rigidity of the connection arrangement, and causes the assembly to lose stiffness as indicated in Fig. 6.5. Figure 6.15 details the variation in average degree of interaction X, determined from the interfacial strain differences e, with applied load P, for the range of assemblies tested.

The general trend of increasing degree of interaction, with joint shear rigidity is visible in both plots, as expected. Assemblies with a high degree of shear connection ($50 \le Sp_x \le 100$ mm) provide an initial near full degree of interaction ($0.8 \le X \le 1.0$). This initial and constant degree of interaction decays at approximately 16 kN for BA-A100-A resulting in a lower final degree of interaction of approximately 0.5. An initial region of near constant degree of interaction followed by a period of decaying degree of interaction is common to all plots.

It is noted that the plots contain significant variation. The determination of the degree of interaction, from the strain difference at the level of the connection, is highly sensitive to the assumed linear strain distribution in the flange shape. For the following reasons the validity of the results shown in Fig. 6.15 is questionable:

- The measured surface strains in the flange shape are likely to be influenced by the locality of the connections.

- The linear strain distribution in the flange shape is solely based on the extrapolation of longitudinal strains on either side of the 9.6 mm thick flange plate, the accuracy of this extrapolation over a greater depth of 30 mm is questionable.

- The assumption of a linear strain distribution through the thickness of the flange shape, may also be in doubt. As the flange shapes consist of several adhesively bonded PFRP profiles there is the possibility for a strain difference to occur over these adhesive bonds.

6.2.3 Determination of degree of interaction X, from the degree of moment transfer

As discussed in Section 4.3.5, the change in relative stiffness of the web and flange shapes as shown in Fig. 6.14, are expected as the degree of interaction decreases due to relative interfacial slip. In a state of full-interaction the couple generated by the two flanges shapes, would account for 85 % of the total applied moment, the remaining 15 % is due to bending of the two web shapes. For a state of non-interaction, this flexure of the web shapes, resists 96 % of the total applied moment.

From the strain distribution through the shapes of the assemblies, as shown in Figs. 6.13 and 6.14, it is possible to calculate the relative proportion of the total moment Px that is carried by each shape, and the degree of moment transfer. The ratio of the theoretical moment $0.85Px$, carried by the flange to the couple M_f generated from the strain distribution in the flange shapes, can be used to determine a measure of the degree of interaction X, achieved for the given joint

shear rigidity γ supplied to the assembly.

As noted in the previous subsection, the validity of the degree of interaction, derived from the measured surface strains, and, the assumed linear distribution in the flange shapes is questionable. Calculation of the couple generated in the flange shapes M_f from the linear strain distribution, in the web shapes, provides a more appropriate method to determine the degree of interaction. Assuming the local stress fields around the individual connections to be negligible the assumption of a linear strain distribution for the single component web shapes remains valid. Owing to the location and vertical separation (220 mm) of the longitudinal strain measurements in the web, the measured longitudinal strains may be assumed to be representative of the total longitudinal strain distribution.

In this way, the degree of interaction X, may be inferred from the longitudinal axial strains present in the web shapes. Plots of the degree of interaction X, against applied load P, of the full range of assemblies tested in load arrangement A are given in Fig. 6.16(a) for assemblies with only active connections, and, Fig. 6.16(b) for those with active and passive connections.

The general trend of increasing initial degree of interaction with increasing joint shear rigidity as shown in both Fig. 6.16(a) and (b) is expected. As shown in Fig. 6.16(a) all assemblies provide an initial high degree of interaction, which increases with joint shear rigidity from 0.7 for test BA-A400-A, to 0.96 for test BA-A50-A. In general, the initial degree of interaction X, remains constant until the applied load P, causes excessive connection slippage, upon this the degree of interaction appears to decrease linearly, with further applied load. As indicated in Fig. 6.13 the strain response of all components in the assemblies with high joint shear rigidities ($50 \leq Sp_x \leq 100$ mm), increases proportionally with load, and thus the assemblies remain in a constant state of near full-interaction ($X = 0.96$) to a load in excess of approximately 20 kN for BA-A50-A.

Both methods of calculation inferred near full degrees of interaction for assemblies with the highest degrees of connection ($50 \leq Sp_x \leq 100$ mm), however the strain difference method (Fig. 6.15), indicates lower degrees of interaction for the assemblies with low degrees of connection ($200 \leq Sp_x \leq 400$ mm), than the moment transfer method (Fig. 6.16).

As discussed in Section 6.1.1 the accuracy of the calculated deflection response of each assembly is questionable, owing to the presence of secondary load effects, for this reason a direct comparison between the deflection and strain responses will not be made. The degrees of interaction determined from the moment transfer method, show greater correlation with the earlier deflection analysis, shown in Figs. 6.5 and 6.10 which indicate an initial high degree of interaction for all assemblies ranging from 0.6 for BA-A400-A, to 0.8 for BA-A50-A.

It is the author's belief that the degree of interaction calculated from the degree of moment transfer, provides a more representative value than that calculated from the strain difference which is sensitive to local stress variations in the flange shape. It should be noted that the values of longitudinal strain in the webs may also be affected by the location of the measurement and the vicinity of connections. For assemblies with closely spaced connections, the measured longitudinal strains are likely to be influenced to some extent by the local stresses around the connections. As the spacing of the connection is increased it is plausible to assume that a lower degree of interaction will exist between the widely spaced connections. For assemblies with connection spacings of 400, 200 and 100 mm the longitudinal strain gauges were 50 mm away from the nearest active connection, at a spacing of 50 mm the location of strain measurement is directly over the active connection. It had originally been proposed to use an innovative photo-elastic stress analysis technique (see Section 5.2) to determine the full-field variation in longitudinal strains between the individual connections, following an

initial study given in Appendix A the technique was deemed to be unsuitable.

It is recognised by the author that the degree of interaction determined from the strain analysis, is a local value, and only representative of the degree of interaction present in the assembly at the location of the measured longitudinal strains, and, not the global degree of interaction that may be in inferred from an accurate deflection analysis.

6.3 Conclusions

The flexural rigidity EI_{ASSEM}, and, degree of interaction X, have been determined for the prototype assembly with varying degrees of shear connection, using the measured deflection and strain responses. The following conclusions can be drawn from the experimental investigation:

- For the prototype beam, and, load arrangements studied it has been shown that to attain a stiffness close to that of an equivalent single pultrusion requires, in excess of 160 connectors are required. The cost of such a number of Unistrut connections may be comparable to that of a suitable structural adhesive bond, but offers the possibility of a demountable and low-skill connection system.

- The linear predictions of the deflection made using both the Modified Newmark analysis and the Kuenzui and Wilkinson model, show poor correlation with the approximately non/bi-linear experimentally determined deflections. Back calculation of the theoretical deflection from the experimentally determined effective joint shear rigidity, γ_e (Fig. 6.9), as used by Sotiropoulos *et al.* (1996) would have provided a non-linear response with improved correlation.

- The method of connection characterisation, does not accurately match the intended use of the Unistrut connection in this particular instance.

  - The connection stiffness determined in Chapter 2, provides an over conservative estimate of the joint shear rigidity. As indicated in Fig. 6.8, the magnitude of the interfacial slip experienced in the assembly does not exceed 0.2 mm.

  - A more accurate characterisation of the connection, in which the stiffness of the connection could be modeled as a function of slip, would provide both the Modified Newmark analysis and the Kuenzui and Wilkinson analyses with greater correlation.

- The shear force resistance of the off-the-shelf M10 Unistrut connection, governs the limit on deflection, while the limit on flexural rigidity is governed by the stiffness of the Unistrut connection.

- The effect of having a finite connection stiffness with the M10 Unistrut connector limits initial degree of interaction that can be attained with the prototype beam of depth 400 mm.

  - Increasing the Span-Depth ratio of the assembly would reduce the longitudinal shear flow acting on each connector, allowing the assembly to retain a high degree of interaction and achieve a SLS deflection of L/250, required for design purposes. As indicated in Table 4.3, the length of 400 mm prototype beam required to achieve full-interaction for a SLS deflection of L/250 is approximately 3300 mm.

  - Further studies are required to identify the range of flexural stiffnesses, that would make the Unistrut method of connection viable for practical modular PFRP beam assemblies.

- The assumption of a rectilinear shear force distribution under a four-point load is invalid for a state of partial-interaction.

- A new procedure for the use of the graphical method, has been developed and applied to the experimental data to determine flexural rigidity EI_{ASSEM} and shear stiffness $k_s G_{xy} A_v$.

- The method of manufacture, and, low Span-Depth ratio of the prototype assembly greatly reduced the accuracy of the measured deflection response.

  - Low tolerances, ± 3 mm used in the hand manufacture of the prototype assembly gave rise to secondary effects from the flexural load.

  - Owing to the low Span-Depth ratio, the displacements arising from secondary effects of loading local to the point of applied load, represents a significant proportion of the measured deflections.

  - The expected 7% variation in deflection response between load arrangements A and B, could not be accurately determined due the inaccuracies in the measurement of the total deflection δ_{total}.

- The accuracy of the measured vertical deflections coould have been improved, through the use of a similar measurement technique to that described by Roberts & Marsi (2003).

6.4 Figures & Tables
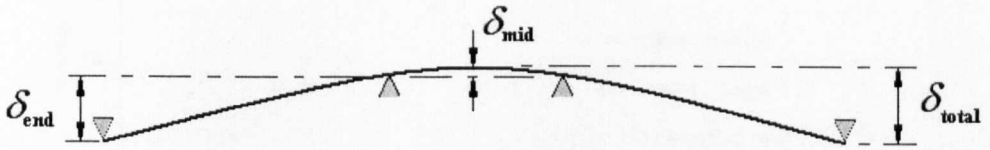
Figure 6.1: Illustration of total deflection, δ_{total}
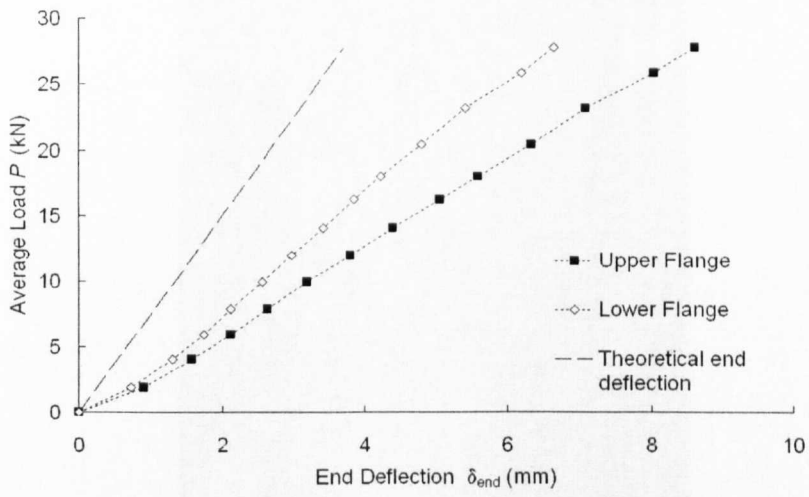
(a)
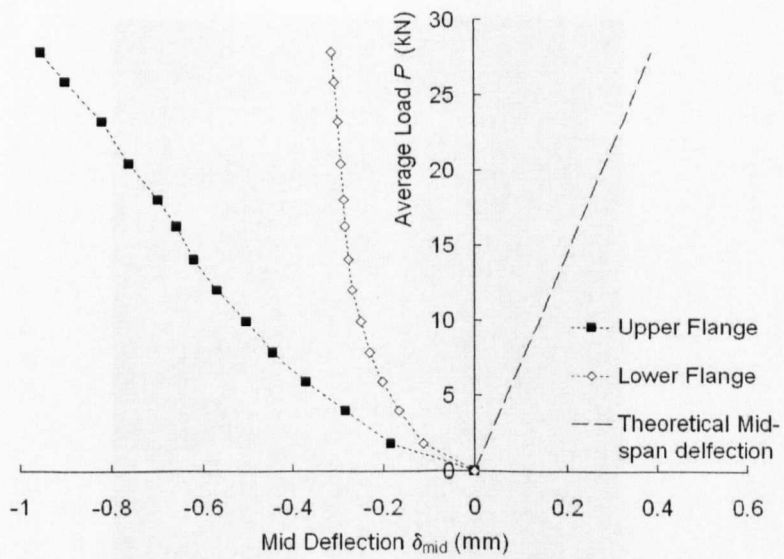
(b)

Figure 6.2: Plots of load P- measured deflections (a) end deflection δ_{end} (b)mid-span deflection δ_{mid}
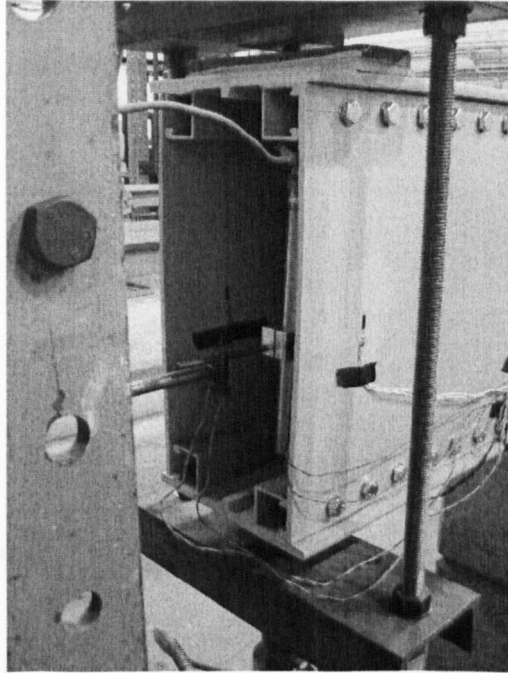
(a)
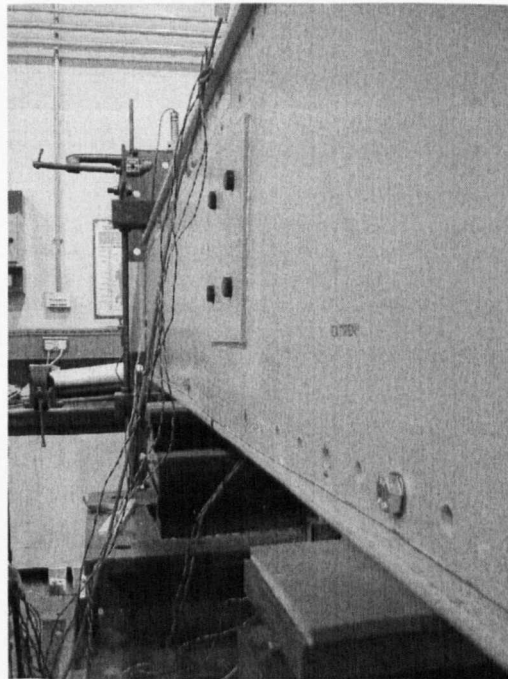
(b)

Figure 6.3: Local effects of loading (a) Beneath load point (b) Above internal support
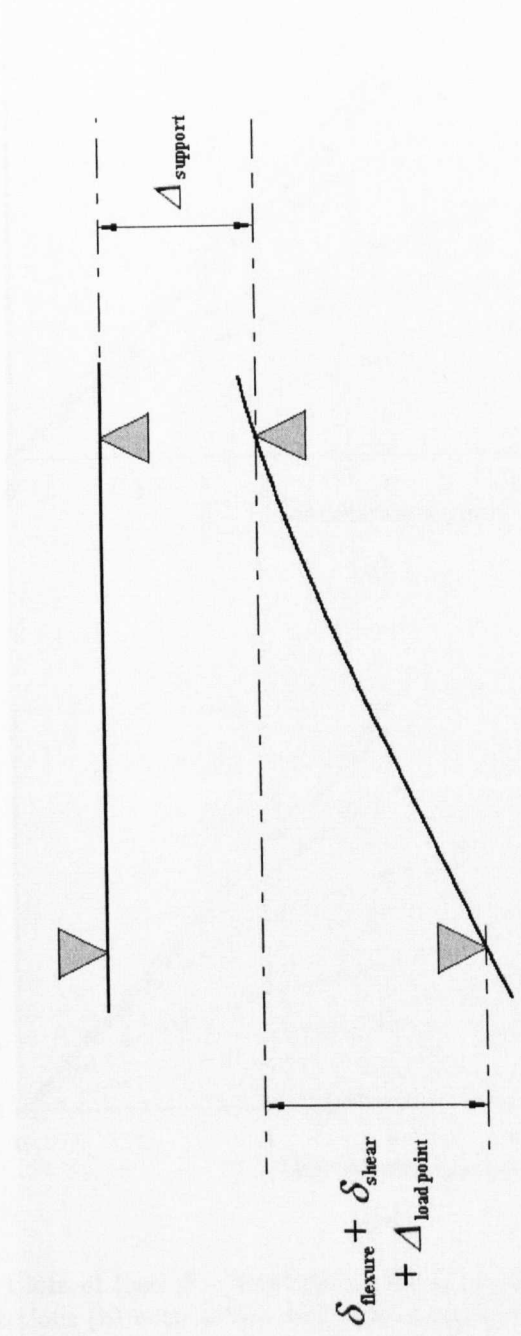
Figure 6.4: Illustration of end deflection δ_{end}
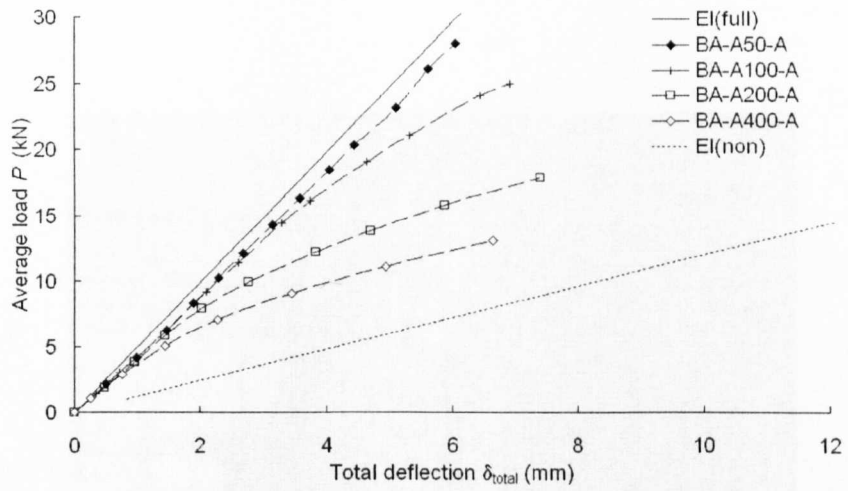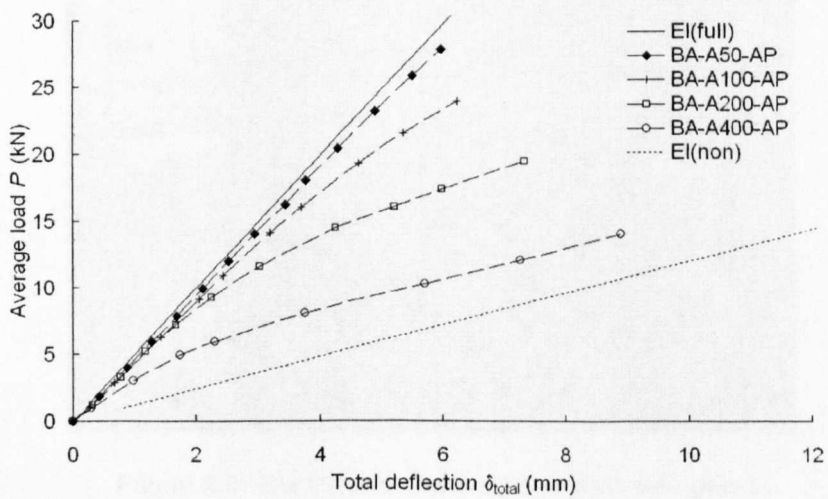
Figure 6.5: Plots of load P - total deflection δ_{total} for load arrangement A (a) with active connections (b) with active and passive connections
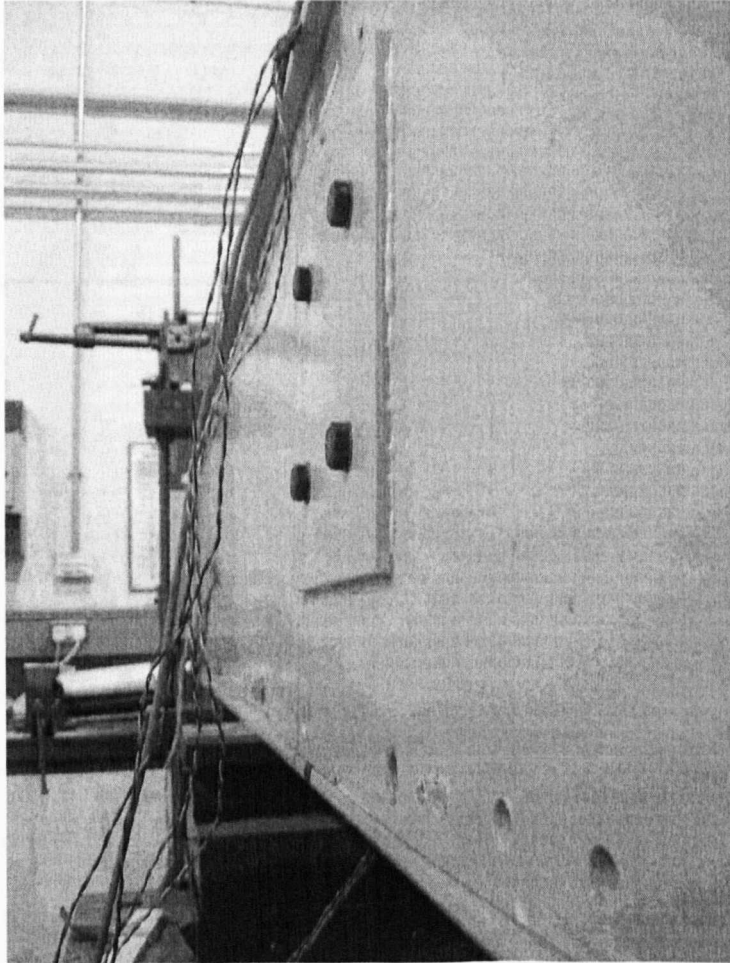
Figure 6.6: Buckling in lower side of East web panel
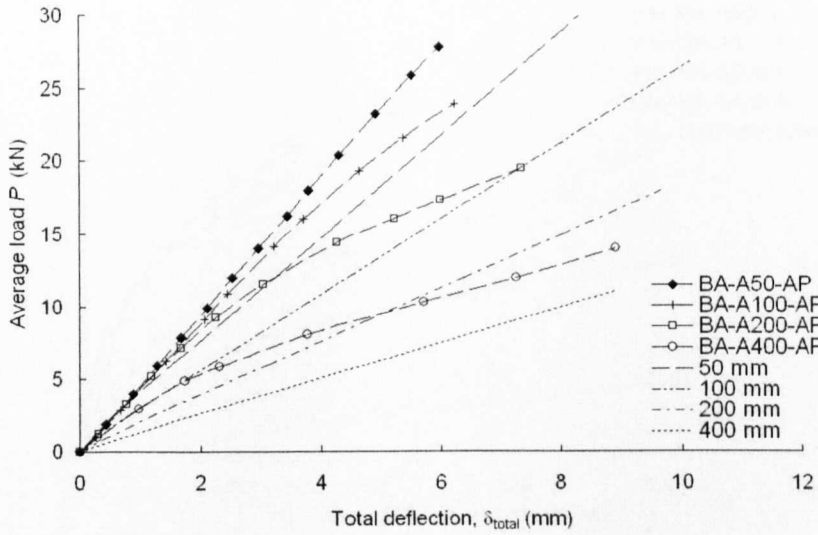
(a)
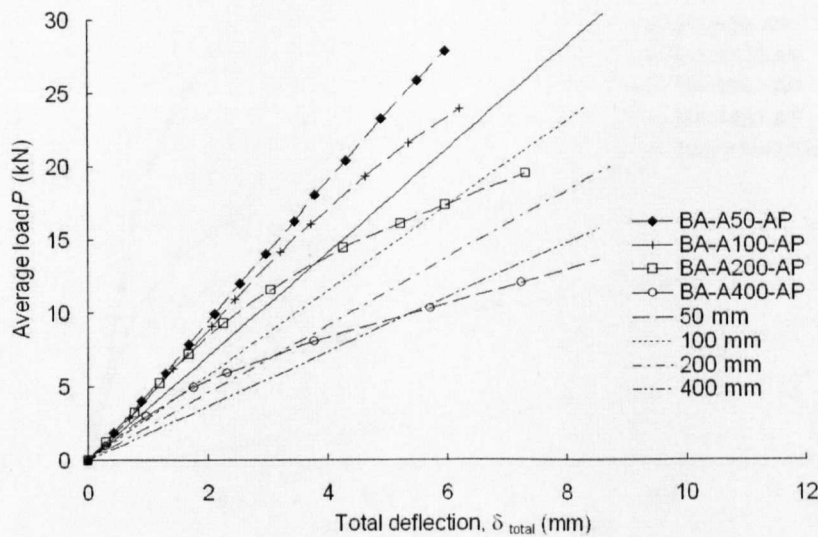
(b)

Figure 6.7: Plots of experimental and theoretical load P - deflection δ_{total} response(a) Modified Newmark analysis (b) Kuenzui and Wilkinson model
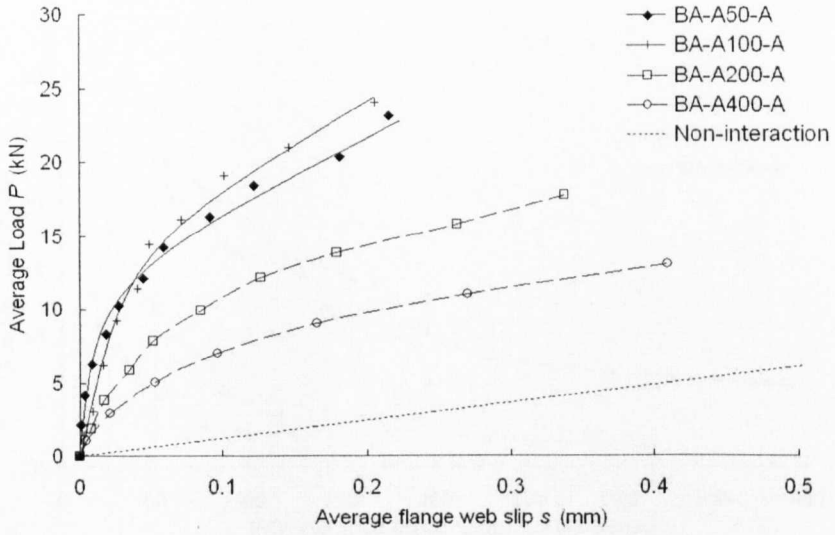
(a)
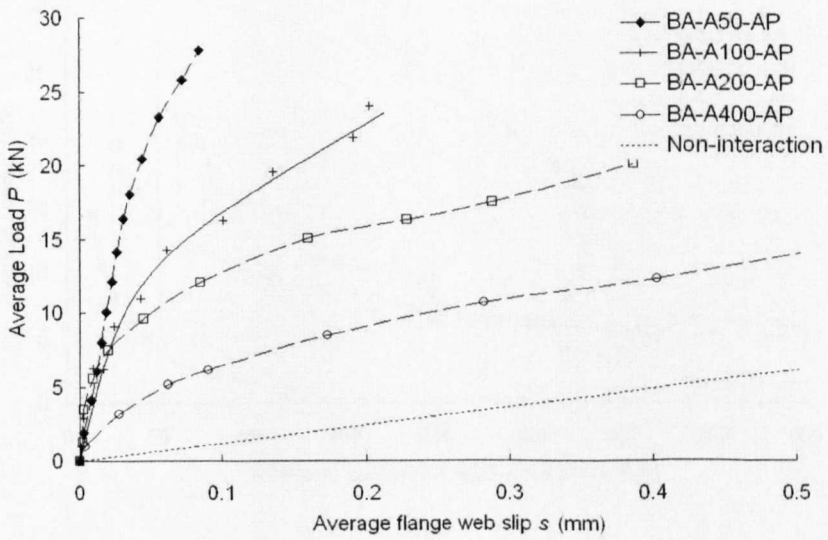
(b)

Figure 6.8: Plots of load P - interfacial slip s for load arrangements A (a) with active connections (b) with active and passive connections
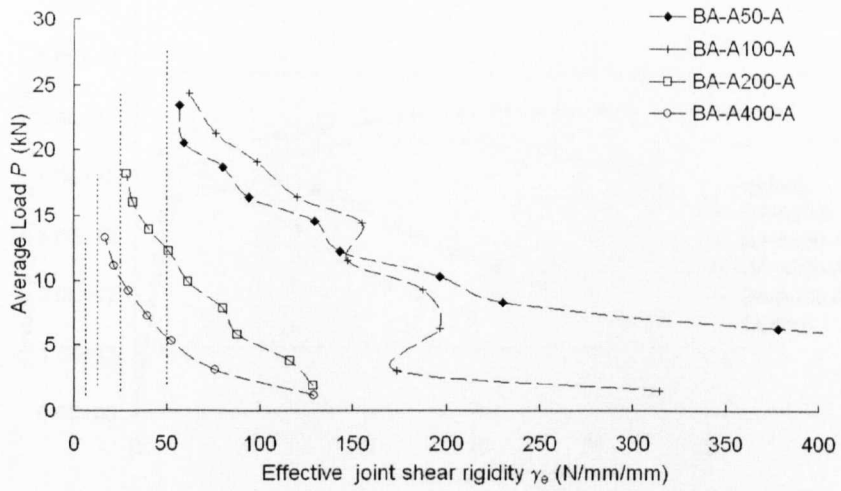
(a)
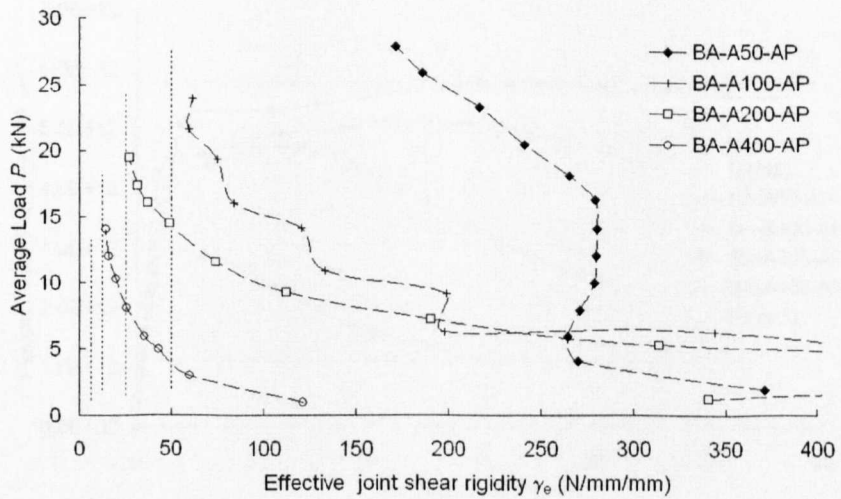
(b)

Figure 6.9: Plot of back calculated effective joint shear rigidity γ_e - load P for load arrangement A (a) with active connections (b) with active and passive connections
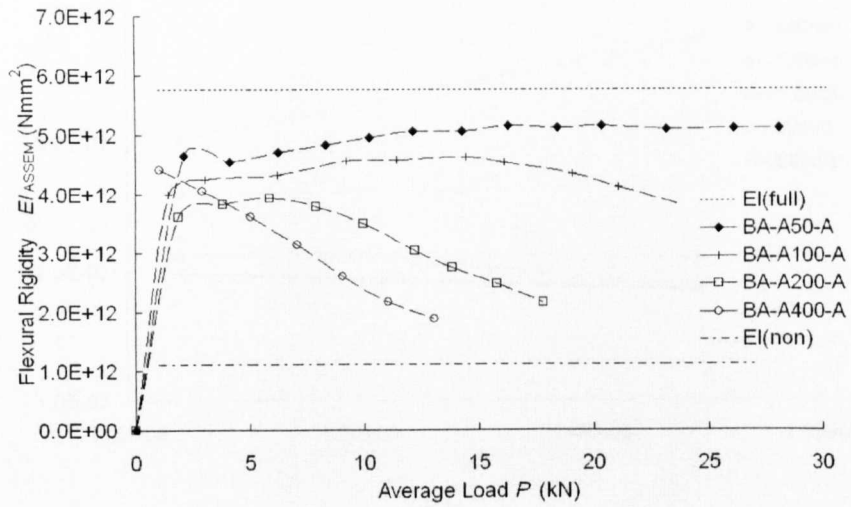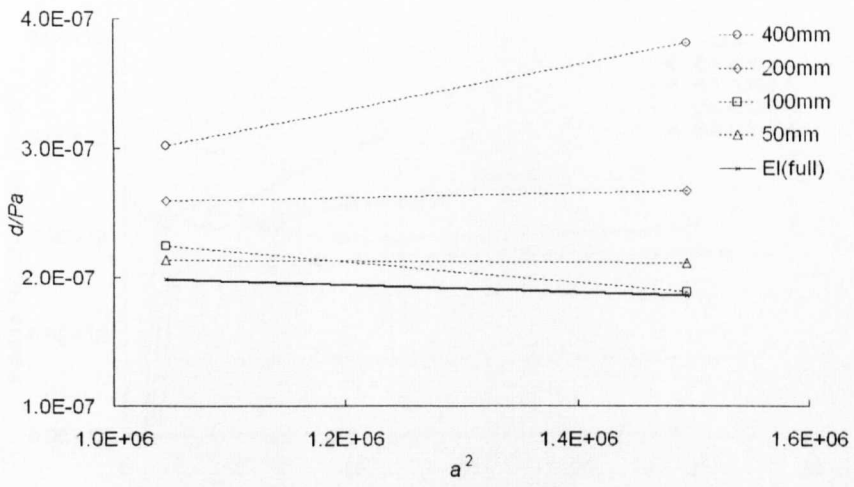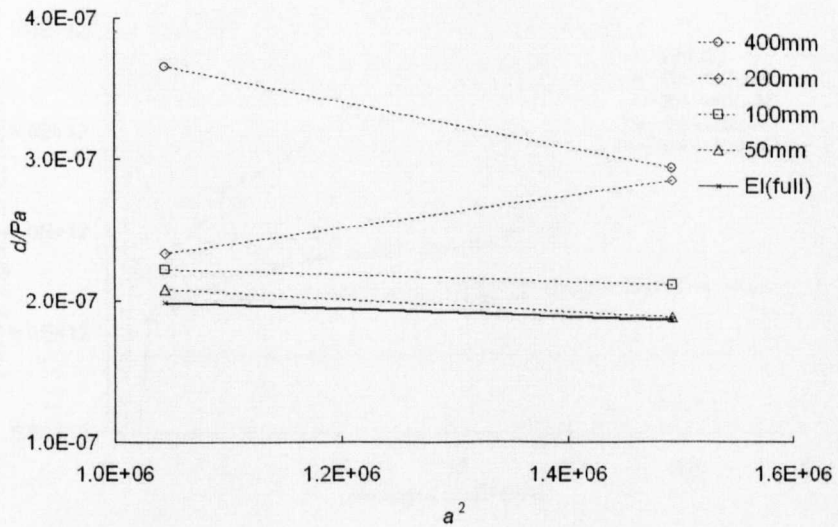
(a)
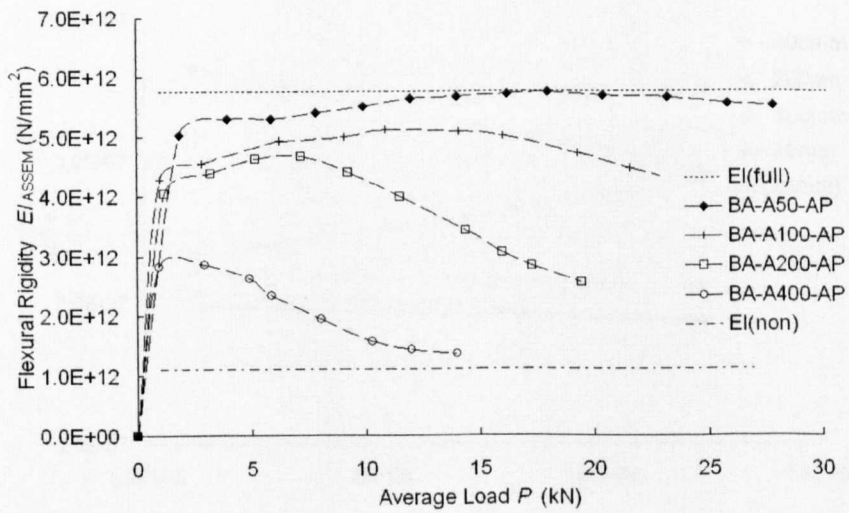
(b)

Figure 6.10: Plots of flexural rigidity EI_{ASSEM} - load P for load arrangement A (a) with active connections (b) with active and passive connections
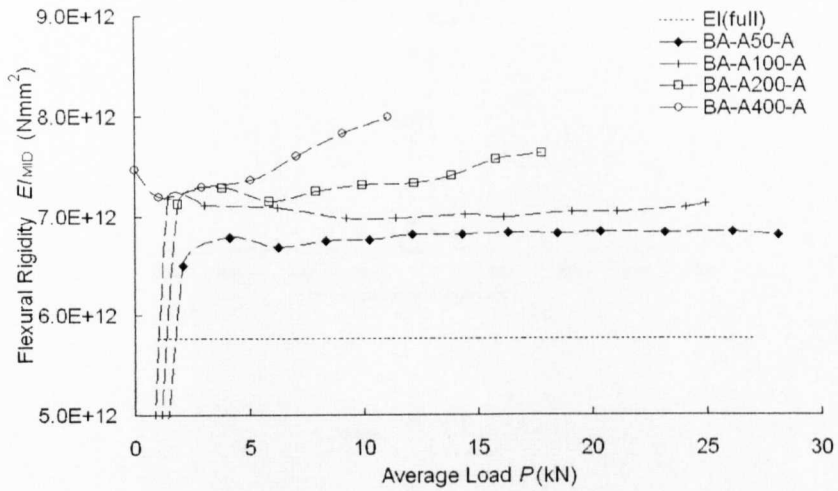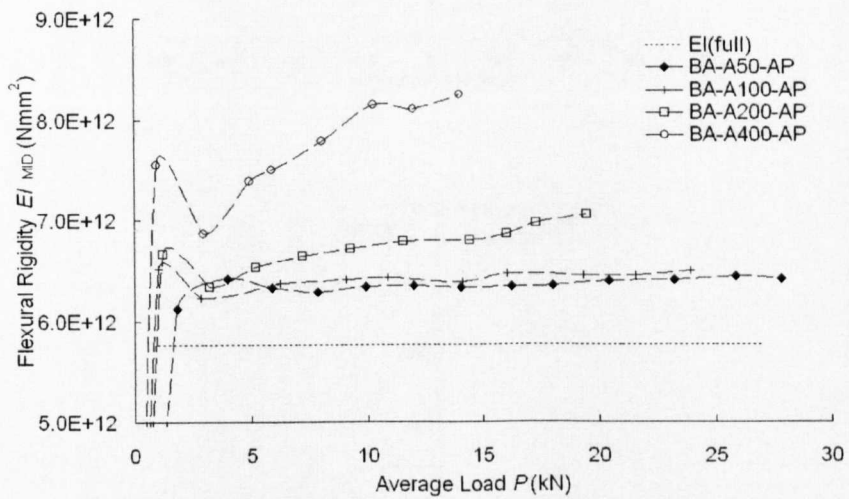
Figure 6.11: Plots of δ/Pa - a^2 for assemblies with (a) active connections only, (b) both active and passive connections

(a)

(b)

Figure 6.12: Plots of flexural rigidity EI_{MID} - load P for load arrangement A (a) with active connections (b) with active and passive connections
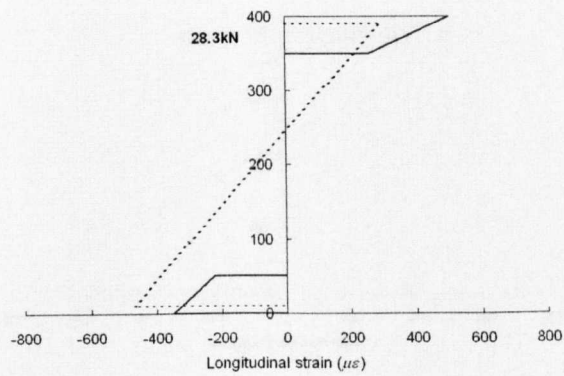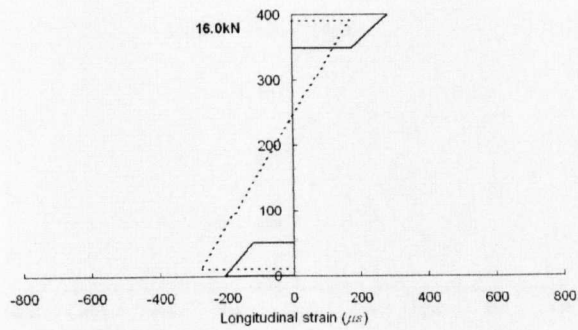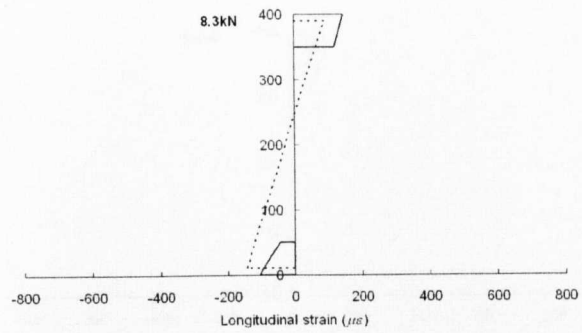
Figure 6.13: Plots of longitudinal strain distribution for various loads for BA-A50-A
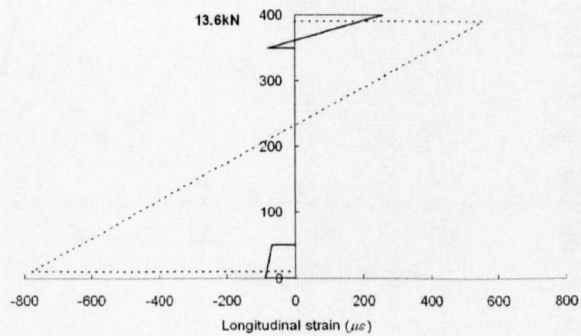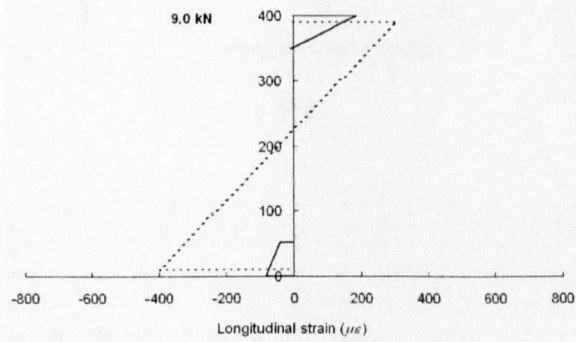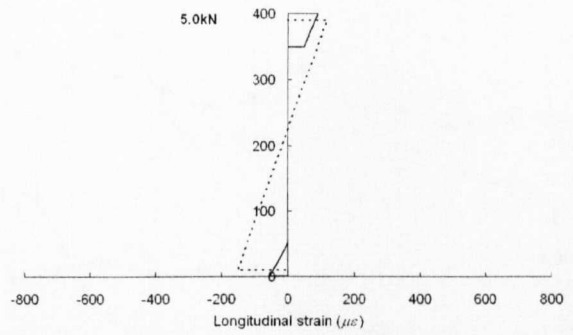
Figure 6.14: Plots of longitudinal strain distribution for various loads for BA-A400-A

(a)
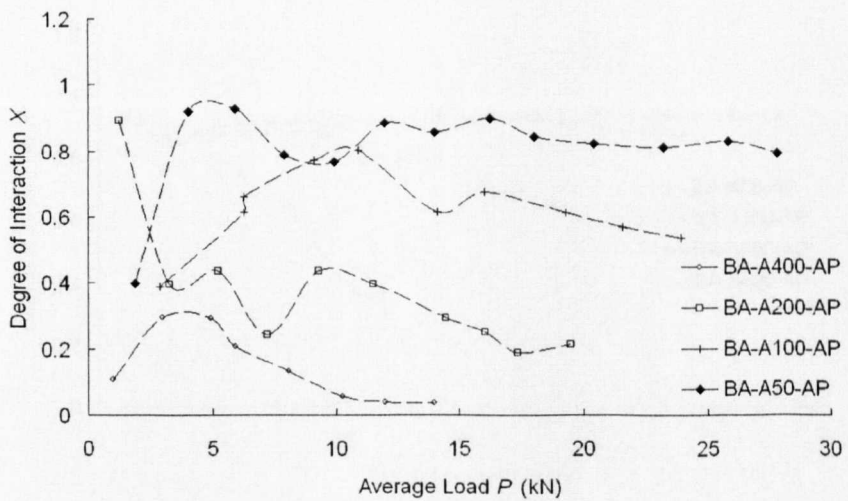
(b)

Figure 6.15: Plots of degree of interaction X - load P for load arrangement A (a) with active connections (b) with active and passive connections
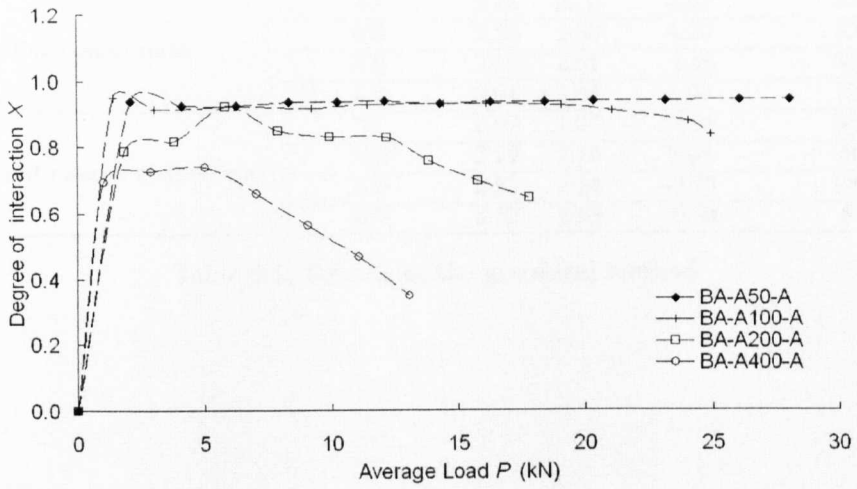
(a)
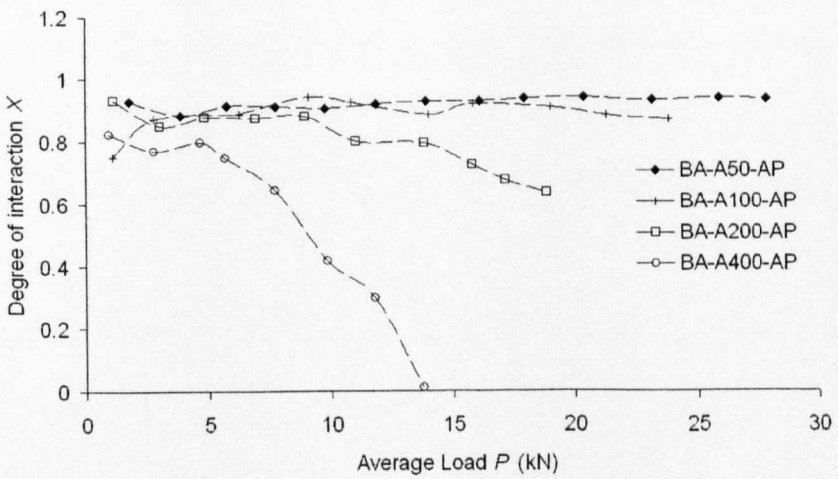
(b)

Figure 6.16: Plots of degree of interaction X - load P for load arrangement A (a) with active connections (b) with active and passive connections

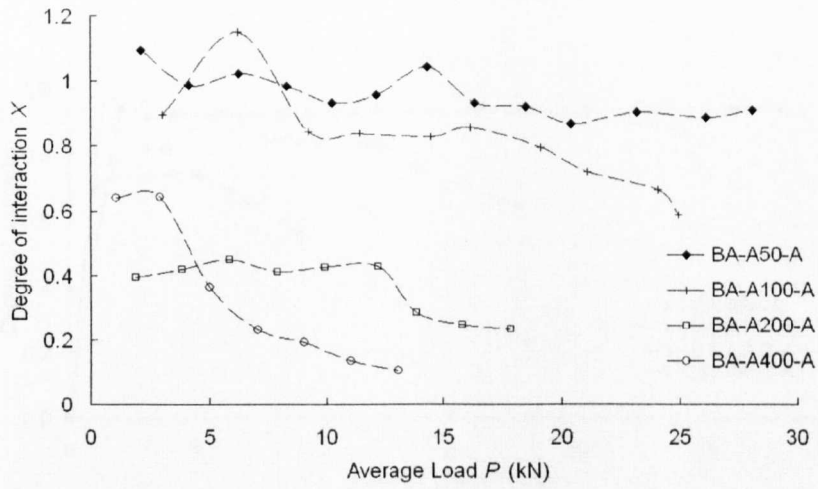| | Spacing, Sp_x (mm) | $\frac{\delta}{Pa}$ | | $EI \times 10^{12}$ Nmm^2 | $k_s G_{xy} A_v \times 10^3$ N |
		A	B		
Ideal Assembly (EI_{full})	-	*1.98*	*1.86*	*5.72*	*19304*
Ideal Assembly +1% deflection error	-	*2.01*	*1.83*	*4.43*	*84787*
Only Active connections	50	2.13	2.10	3.61	3903
	100	2.24	1.88	6.26	3998
	200	2.59	2.67	-1.46	8715
	400	3.01	3.81	1.03	1875
Active and passive connections	50	2.07	1.87	24.98	5549
	100	2.22	2.10	2.08	-5641
	200	2.33	2.84	-9.75	2894
	400	3.65	2.93	-0.93	838

Table 6.1: Results of the graphical method

CHAPTER 7

Conclusions and recommendations for further work

The primary objective of the work presented herein is to provide an evaluation of the Startlink Pultruded Fibre Reinforced Polymer (PFRP) building system, and, in particular, the Startlink beam system illustrated in Fig. 1.2. The fulfilment of this primary objective was dependent on the completion of the following two secondary objectives:

1. The characterisation and provision of design guidance on the Unistrut connection method with PFRP shapes

2. Evaluation of the effectiveness of using the Unistrut connection method as a form of shear connection in a modular PFRP box beam assembly.

The following sections provide a summary of the conclusions to the investigation presented in this thesis and main findings from the work to the primary and secondary objectives of the research. More detailed and direct conclusions can be located at the rear of Chapters 2 to 6.

7.1 Use of the M10 Unistrut connection method with PFRP shapes

The M10 Unistrut connection method has been characterized in Chapter 3 for use with PFRP channels through the use of a new load-slip test method. Four connection design parameters have been identified and determined. This will enable the design engineer to predict the structural performance of a connection made using the Unistrut connection method in the manner proposed in the Startlink building system. A preliminary series of tests were conducted to determine the reduction in properties due to durability phenomena, no serious deterioration in properties was detected. Based on findings of the experimental characterization work, the use of the Unistrut connection method in PFRP building systems is not recommended, without careful consideration of the connection behaviour and the detailing of the shapes being fastened. It is recognised by the author that further characterisation work is required to apply reliability analysis and statistical evaluation to determine characteristic values and partial safety factors to the design parameters for the M10 Unistrut connection method.

7.2 Modular PFRP box beam

A 400 mm deep prototype modular PFRP box beam, based on the Startlink beam system (Fig. 1.2), has been designed, built from off-the -shelf PFRP shapes, and tested under four-point bending. The flexural rigidity and degree of interaction X present in the assembly have been determined from analysis of vertical deflection and longitudinal strain responses as the beam is deformed. Due to experimental errors in the form of secondary effects of the flexural loading, as discussed in Section 6.1, and poor experimental methodology as discussed in Section 6.2,

there exists a poor correlation between the two sets of analysis.

Analysis of the interfacial slippage, present in the assemblies indicates a much higher individual initial M10 Unistrut connection stiffness than originally determined, in the connection characterisation work in Chapter 3. A more accurate characterisation of the Unistrut connection is required for the range of slip likely to be present in the intended use, for the 400 mm deep beam tested, the maximum recorded slippage was less than 0.5 mm. It is understood that further work is required, in order to characterise the performance of linear connections transferring a longitudinal shear flow.

For the prototype box beam tested in Chapter 6, the low Span-Depth ratio (7.5) limits the maximum attainable deflection to between L/470 and L/350. For the highest joint shear rigidity, given by a minimum connection spacing of 50 mm, the assembly remains in a state of near full-interaction ($X \approx 0.9$), to the maximum applied load of 27 kN at each load point. This spacing requires a total of 160 connections (40 per longitudinal connection) and this is likely to make the modular beam too expensive for the market place.

Although the results presented in Chapter 6 suggest that it would be possible, providing the Span-Depth ratio exceeds 8.3 (Table 4.3) to construct a 400 mm deep beam that can achieve a SLS deflection L/250 using the low stiffness M10 fasteners, further work is needed with new beam assemblies giving higher Span-Depth ratios to find out if a SLS deflection of L/250 is achievable with a connection spacing that would make the flat pack modular beam system a commercial possibility.

The long-term performance of the prototype modular beam has not been considered in this thesis. Considering the highly time-dependent nature of PFRP shapes and systems and the approximately 50% increase in short-term slippage of the connection under sustained load, determined in Section 3.6.3, a notable

decrease in flexural rigidity of any beam assembly is expected. Such effects would have to be included in the design process and would further limit the use of the beam system studied.

7.3 Startlink building system

The Startlink construction system has been introduced and classified within the sense of Modern Methods of Construction (MMC), that are being developed to satisfy the growing short-fall in low-cost housing in the UK. The merits of the proposed system are discussed. A critical review by the author suggests that, although the building system offers design flexibility, the proposed Startlink system is limited in its market potential, for the following reasons:

- Significant barriers to entry into the MMC market

    - High initial investment and set-up costs

    - Increasing competition from existing light weight steel and timber building systems for MMC

    - Poor social/industrial acceptance of *plastic* based materials as structural building materials

- Over complex product design

- Reliance on the Unistrut connection method

Changes to the Startlink building system in 2006, have seen the removal of the modular PFRP beam concept from the product range, and a move away from the use of the Unistrut connector as the sole method of providing interaction between the building elements. Instead Singleton (2006) is favouring now to have high-stiffness adhesive bonded connections and a non-demountable building system..

The author's PhD work has contributed to this significant change in product offerings and connection method seen in the latest 2006 Startlink product range.

7.4 Recommendations for further work

The work presented in this thesis represents only a proof of concept investigation, it is understood by the author new work is required before the modular beam concept can be utilised in practice. The following is a list of prioritized recommendations for further study:

1. Connection characterisation: A full physical characterisation of low-cost mechanical and adhesive fasteners, including total cost of fabricating each connection is required to assess their suitability for use in a PFRP assembly. The suitability of structural adhesive tapes should also be considered as a form of supplying a low-cost low-skill adhesive bond, for longitudinal shear force transfer.

2. PFRP Modular beams: Research is required to develop knowledge and understanding of the relationship between the degree of shear connection and the degree of interaction developed in a box beam assembly, and to identify the actual 'cost' saving of this form of beam compared to an equivalent section from a single pultruded shape.

   - At present research is being carried out at the University of Warwick, to determine the performance of a PFRP box beam fabricated from commercially available channel shapes fastened using standard M16 bolts as a low-cost solution to the pultrusion of deep shapes($\geq$ 400mm).

Medium-term photoelastic response of Devcon 2-Tonn epoxy resin

Objectives

The primary objective of this study is to evaluate the usefulness of an innovative photo-elastic stress analysis technique, to monitor the long-term response of bolted joints of Pultruded Fibre Reinforced Polymer (PFRP), which have visco-elastic properties.

The completion of the primary objective is dependent on the following secondary objective.

- to investigate the effect of a creep inhibiting chemical additive (Heloxy Modifier 107) on the time dependent birefringence of the Devcon 2-Tonn clear epoxy resin coating.

Introduction

Photoelastic Stress Analysis (PSA) has been used successfully for many years in the automotive and aerospace industries as a tool for product development.

Recent advances in optical and digital technology has provided us with a fully automated and portable polariscope unit, broadening the potential use of PSA in experimental mechanics (Lesniak *et al.*, 1997). The grey field polariscope (GFP 1000) from Stress Photonics Inc. is shown in Fig. A.1. Technological advances have given us a unit that is much easy to use and with higher measurement accuracy. The product under analysis has a photoelastic reactive coating applied to its surface. Typically, epoxy resins are brushed on allowing PSA in several hours (Calvert *et al.*, 2002). Increased sensitivity through the use of a charge coupled device camera allows a birefrigent coating of 0.25 mm thick to be used.

Epoxy resins were introduced as a photo-elastic material by Leven (1963) and have been widely accepted in the PSA industries as they fulfill the present physical and chemical requirements of an ideal photo elastic material.

- Chemically, (good birefringence) the use of acid anhydrides in the hardener develops the polymeric cross linked structure without residual stresses and birefringence. (Kobayashi, 1993)

- Physically, epoxies show a good linear stress strain relationship up to a maximum 1% proportional strain limit while producing a high modulus material, with good bond characteristics and the advantage of being in a liquid state allowing brush-on and comb coatings with thickness between 0.1 - 0.4 mm eliminates the need for correction for the relative thickness of the coating material.

These advances provide the impetus to move PSA out of the laboratory and into the field for solving a wider range of problems. Applications in civil engineering could include products of new materials and/or with complex geometries, where knowledge of the full stress/strain field is required. PSA could be used to monitor the service condition of existing structures, owing to the fact that, with

a calibrated coating applied, the portable PSA unit need only be brought to the site when monitoring is timetabled.

In contrast to mechanical engineering products, where the design life is measured in a few years and the self-weight is generally much less than the imposed loads, the design life of civil engineering products can be 50 years. Over this lifetime a structure will have to support a self-weight that can be 60% of the total loading. If PSA is going to be a monitoring tool in the field the time dependent affect of sustained loading on the photoelastic coating needs to be characterised.

Experimental Method

Measurement of birefringence

Many transparent materials become birefringent when stressed, as a result light polarized along the first principal strain direction travels faster than light polarized along the second principal strain direction. Photoelastic stress analysis systems use this effect to measure the difference in the principal strain of stressed birefringent materials.

The GFP 1000 system consists of a projector unit delivering circularly polarized light and a CCD camera with a rotating analyzer. These components of the system are shown in Fig. A.1 and the concept of photoelastic strain measurement is shown in Fig. A.2.

For each revolution of the analyzer the CCD camera captures 16 images, enabling the intensity of the returning light from the birefringent surface to be measured. Providing the stressed structure has developed birefringence in the photoelastic coating the returning light will be elliptical. Form the variation in the intensity of the returned light it is possible to calculate the axes of the elliptical light and its angle of retardation and deduce the difference in the principal

strains ε_1 and ε_2 for the stressed structure in terms of fringe orders. A conversion number is required for the PSA software to convert between units of fringe order and strain.

Specimen Preparation

Six nominal samples of 1/4 inch thick PFRP Extren© flat sheet, measuring 300×40 mm, were cut with the unidirectional fibres parallel to the longer sides. The middle 100 mm on one face was first sprayed with a reflective silver surface, to which a 0.25 mm coating of the epoxy resin/inhibitor mixture was applied. Increments of 10% (by weight) in the proportion of the Heloxy Modifier 107 provided a range of coatings with creep inhibitor concentrations between 0 and 50%, by weight. To ensure the achievement of a full-set of the photoelastic coating, a curing period in excess of 24 hrs at room temperature followed application. To provide a direct comparison with the PSA, strain gauging was located centrally on the reverse face of each specimen.

To produce a measurable change in fringe order of the reflected light a longitudinal strain gradient was imposed through the development of cantilever end-loaded flexure, as shown in Fig. A.3(a). The PSA was conducted under controlled light and temperature conditions. As only a relative value of the photoelastic measurement is required for this analysis an arbitrary conversion factor of was supplied to the software, based on previous work with the Devcon epoxy resin

Recording the photoelastic response

Using the PSA software the captured data file can be displayed, as shown in the VDU screen dump in Fig. A.3(b). A number of different shear strain components can be read off such images by moving the cursor to any point on the specimen.

Figure A.4 depicts a typical stress state consisting of normal and shear stresses which can be modeled as the superposition of three independent components as shown below. In this way the GFP software can display the differential principal strains as pure shear strains on the $\pm45°$ planes (γ_{45}) also the shear strains on the $\pm90°$ planes (γ_0). Because the state of hydrostatic strain produces no difference in Principal strains ($\varepsilon_1 - \varepsilon_2$) it is undetected by the PSA. The outputted shear strains (γ_{45} and γ_0) can be transformed in to normal strains by application of Mohr's circle of strain as shown below in Fig. A.5.

Due to the cantilever test configuration the measured stresses (ε_x and ε_y) corresponds to the Principal stresses (ε_1 and ε_2). Comparison can be made between the PSA measurement γ_{45} and $\varepsilon_1 - \varepsilon_2$, given by the strain rosette readings.

Results and comparison of photoelastic response

Due to the constant end-deflection amplitude of the test, any time dependent response of the PFRP material and/or coating is due to stress/strain relaxation. Owing to the relatively low strains (approx $700\mu\varepsilon$ or $< 7\%$) the relaxation of the PFRP material over the test duration of 2 hrs did not exceed 5%.

Figure A.6 shows the percentage decrease with time using a non-dimensional strain ratio ($\gamma_{45} \backslash \varepsilon_1 - \varepsilon_2$). The solid line shown in the figure is for the time dependent response of the pure Devcon 2-Tonn epoxy resin. This shows a total decrease in the strain ratio of over 40%. The four dashed lines are for the response of the modified coatings. It can be seen that the percentage of inhibitor significantly alters the time dependent response measured in the PSA.

A general trend in accelerating the initial relaxation process is clearly present throughout the range of modifier concentrations. After 5 minutes 89%, 95%, 97% and 97% of the relaxation observed after 2 hours was found with the 10%, 20%

30% and 40% modified coatings, respectively. For the pure epoxy coating 78% of its relaxation is seen to occur in 5 minutes, showing that it will take a long before there can be calibration for long-term monitoring. Concentrations of the inhibitor of 30% plus reduce the magnitude of the 2 hr relaxation by 50%. A non-setting coating is however obtained with 50% concentration.

Conclusions

- The time dependent birefringence of an epoxy resin coating modified with various concentrations of a creep inhibiting chemical additive has been investigated.

- Increasing the creep inhibitor above 20% by weight is found to reduce the relaxation in the coating's photoelastic response.

- The application of the inhibitor is found to accelerate the relaxation process, after which a stable response will allow quicker calibration to be made.

- Further work is required before the PSA technique reported could be routinely applied in practice.

- Owing to the significant time dependent relaxation in the birefringence of the epoxy and modified epoxy based photoelastic coatings, the author does not recommend that this technique be used where repeated and absolute strain measurements are required over a time period.
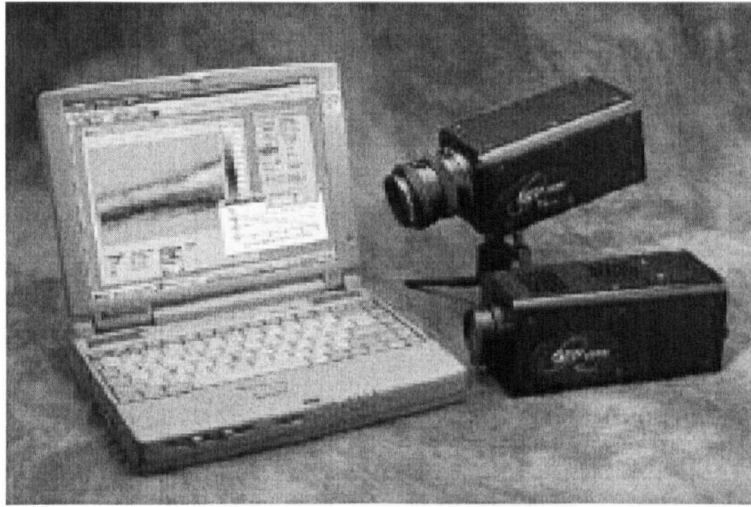
Figures

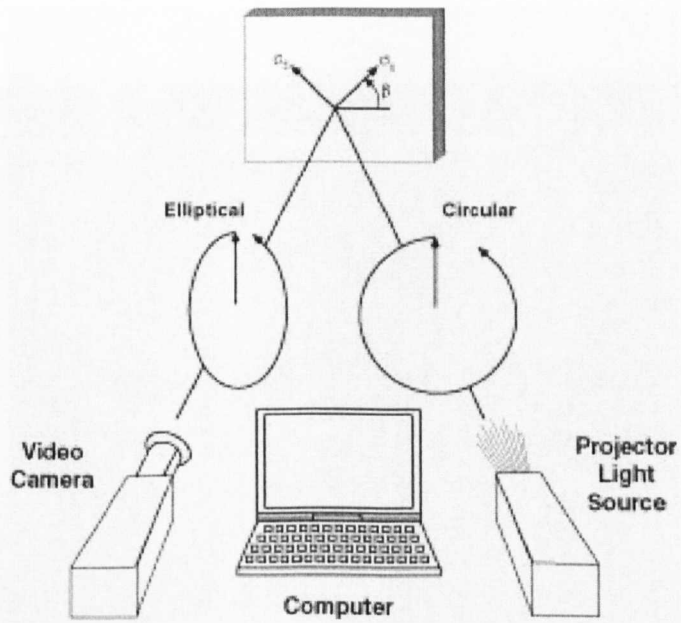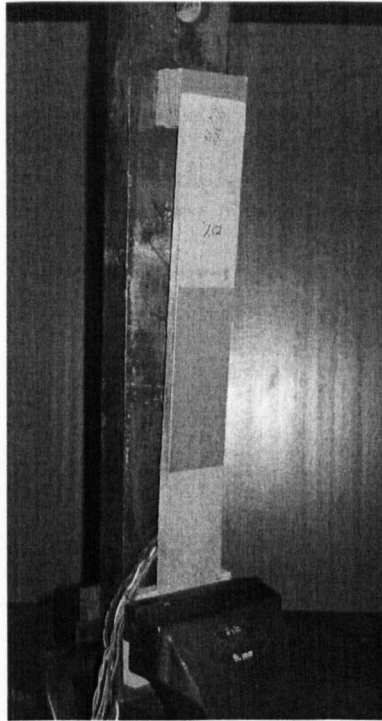Figure A.1: Stress Photonics Ltd GFP 1000, (Calvert *et al.*, 2002)

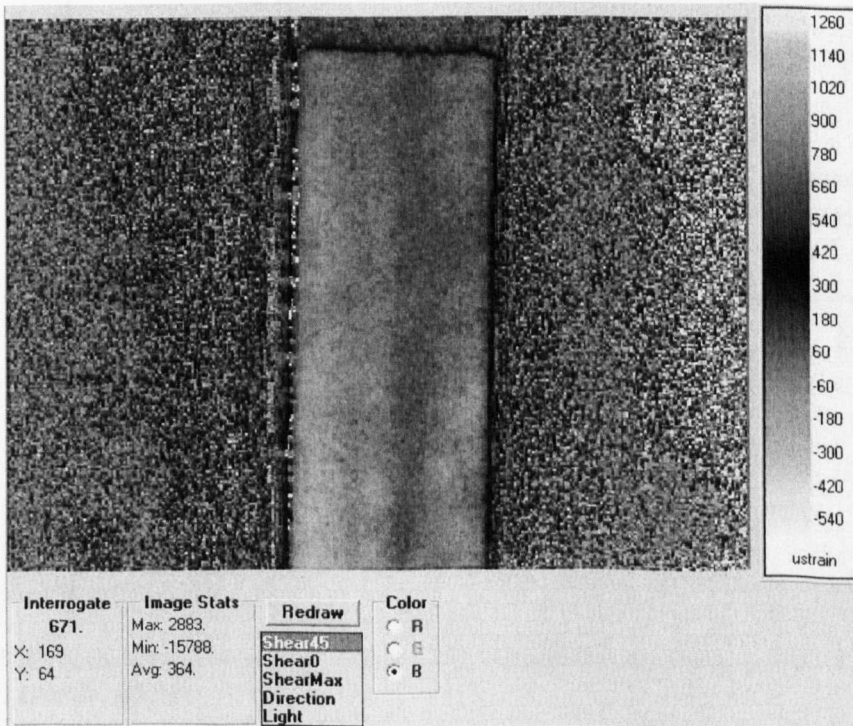Figure A.2: Principles of photoelastic measurement

(a)

(b)

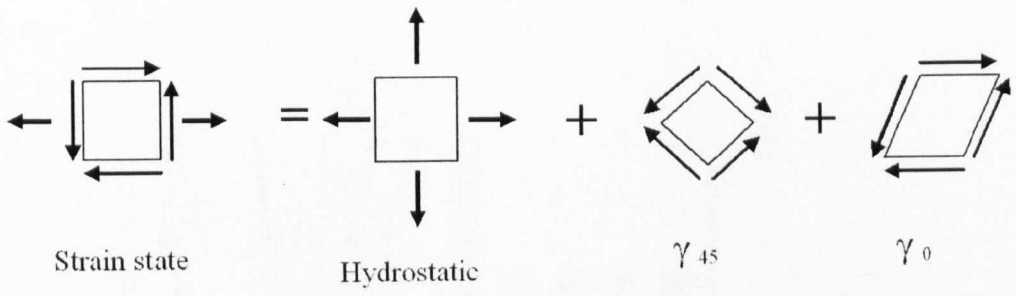Figure A.3: Experimental set-up (a) Cantilever test rig (b) VDU screen dump

Figure A.4: Components of shear strain (Lesniak, 2002)
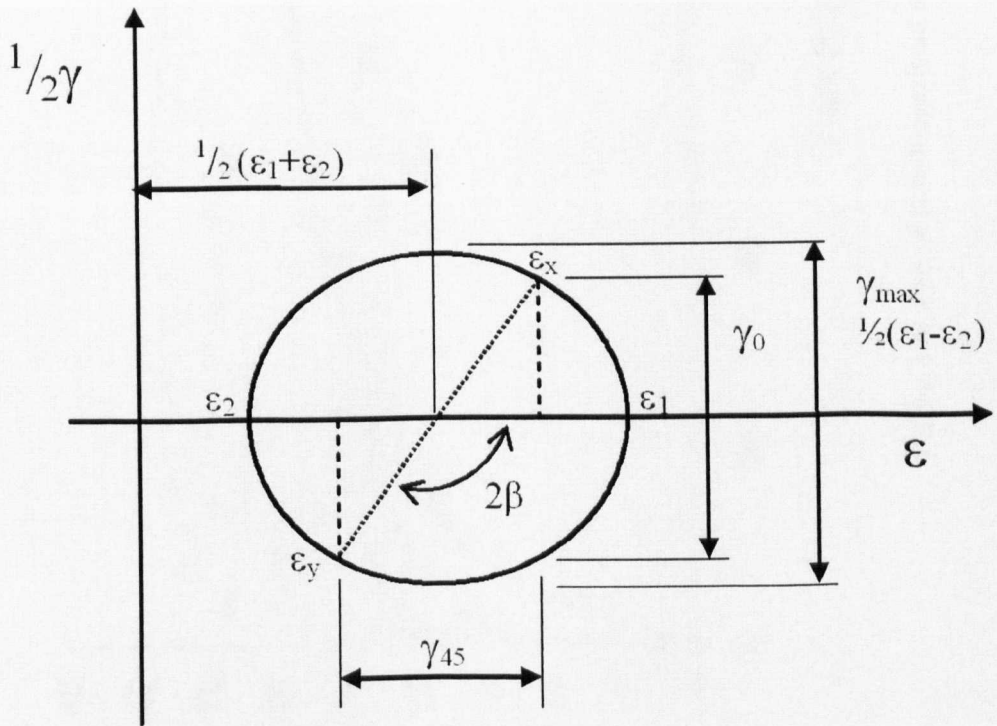
Figure A.5: Mohr's circle of strain, illustrating the equivalence of γ_{max} and $(\varepsilon_x - \varepsilon_y)$ and others (Lesniak, 2002)
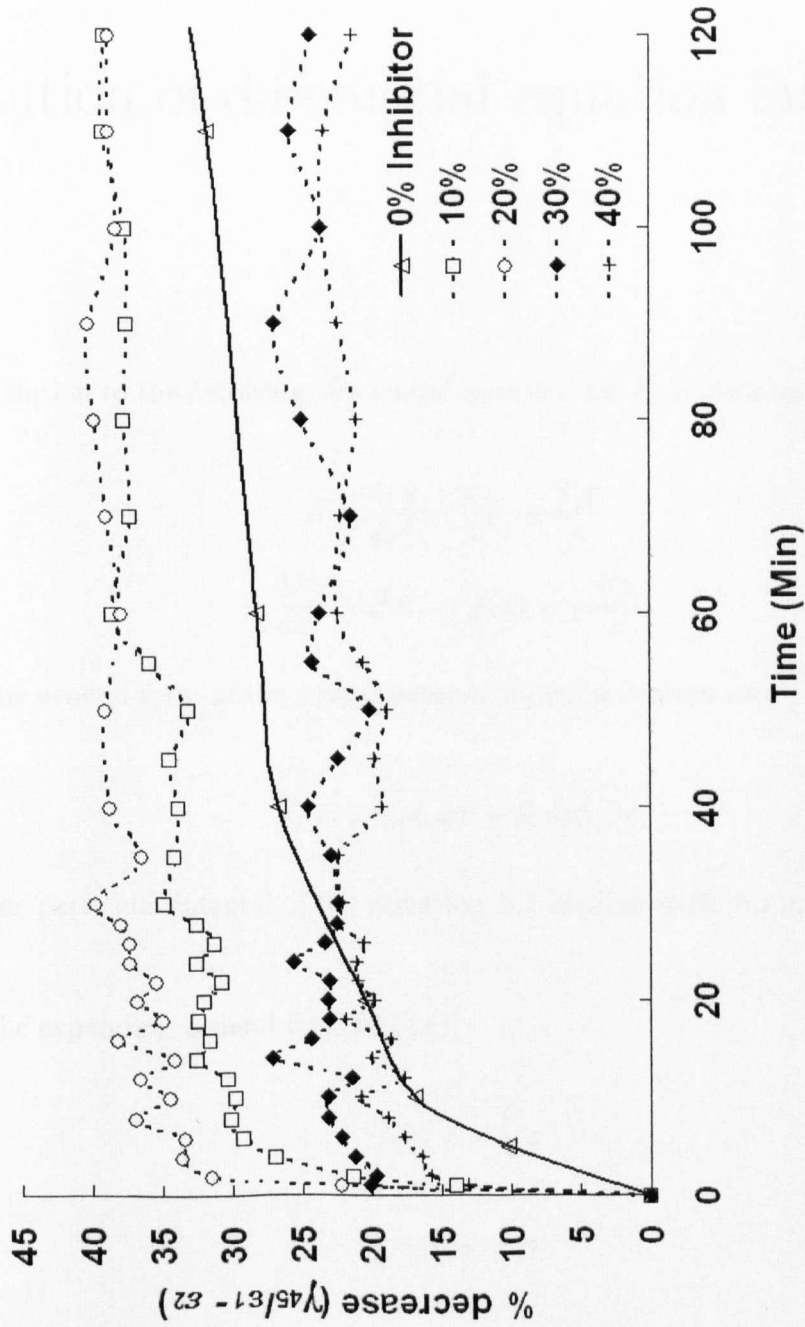
Figure A.6: Plot of non-dimensional strain ratio - Time *Min*

APPENDIX B

Solution of differential equation for F_f

The solution to the following differential equation for F_f is given in the following work.

$$0 = \frac{\mathrm{d}F_f}{\mathrm{d}x^2} - \frac{\beta}{\lambda}F_f + \frac{Px}{\lambda} \tag{B.1}$$

$$\frac{\mathrm{d}F_f}{\mathrm{d}x^2} - \psi^2 F_f = f(x) = -\frac{Px}{\lambda} \tag{B.2}$$

The general form of the complimentary function is given as:

$$F_f = A\cosh\psi x + B\sinh\psi x \tag{B.3}$$

The particular integral of the Equation A.1 is given as shown in the following steps.

The expanding general form of $f(x)$.

$$f(x) = -\frac{P}{\lambda}x \tag{B.4}$$

$$y = Cx + D \tag{B.5}$$

$$\frac{dy}{dx} = C \tag{B.6}$$

$$\frac{d^2y}{dx^2} = 0 \tag{B.7}$$

Equating coefficients of power.

$$x^2 \quad 0 = 0 \tag{B.8}$$

$$x^1 \quad \psi^2 C = \frac{P}{\lambda} \tag{B.9}$$

$$x^0 \quad -\psi^2 D = 0 \tag{B.10}$$

Therefore

$$C = \frac{P}{\lambda\psi^2} \quad D = 0 \tag{B.11}$$

Substituting C and D into Equation A.4.

$$y = \frac{P}{\lambda\psi^2}(x) + 0 \tag{B.12}$$

The general solution to the Equation A.1 is given as the summation of the complementary function (A.2) and the particular integral (A.11).

$$F_f = A\cosh\psi x + B\sinh\psi x + \frac{Px}{\lambda\psi^2} \tag{B.13}$$

A complete solution is only possible after consideration of the boundary conditions of the problem. For $x = 0$, $F_f = 0$

$$0 = A\cosh(0) + B\sinh(0) + \frac{P(0)}{\lambda\psi^2} \tag{B.14}$$

$$\therefore \ 0 = A$$

For $x = \frac{L}{2}$, $\frac{\mathrm{d}F_f}{\mathrm{d}x} = 0$

$$0 = A\psi \sinh \psi \frac{L}{2} + B\psi \cosh \psi \frac{L}{2} + \frac{P}{\lambda \psi^2} \tag{B.15}$$

$$B\psi \cosh \psi \frac{P}{2} = -\frac{P}{\lambda \psi^2} \tag{B.16}$$

$$B = -\frac{P}{\lambda \psi^3 \cosh \psi \frac{L}{2}} \tag{B.17}$$

Therefore the general solution is given by:

$$F_f = P \left(\frac{x}{\lambda \psi^2} - \frac{\sinh \psi x}{\lambda \psi^3 \cosh \psi \frac{L}{2}} \right) \tag{B.18}$$

$$F_f = \phi \left(x - \frac{\sinh \psi x}{\psi \cosh \psi \frac{L}{2}} \right) \tag{B.19}$$

References

Anon. (2003). Modern methods of house building, *Postnote-Parliamentary Office of Science and Technology* .

Anon. (2004). Guidelines for the use of metal framing, *Technical report*, Metal Framing Association, Chicago. MFMA - 103.

Anon (2005a). 60,000 Reasons to use MMC, *Modern Methods of Construction* **1**.

Anon. (2005b). Using modern methods of construction to build homes more quickly and efficiently, *Technical report*, National Audit Office.

Ansourian, P. & Roderick, J. W. (1978). Analysis of composite beams, *Journal of the Structural Division, ASCE* **104**(ST10): 1634-1645.

ASTM (2000). *ASTM D-5229: Moisture Absorption Properties and Equilibrium Conditioning of Polymer Matrix Composite Materials*.

Aurich, M. & Beber, A. J. (2002). Development of a bond model for the FEM analysis of RC beams strengthened with carbon fibre sheets, *Bond in Concrete - From research to standards*, Budapest, pp. 581-558.

Bakis, C. B., Bank, L. C., Brown, V. L., Cossenza, E., Davalos, J. F., Lesko, J. J., Machida, A., Rizkalla, S. H. & Triatafillou, T. C. (2002). Fiber-Reinforced

Polymer Composites for Construction: State-of-the-Art Review, *Journal of Composites for Construction* pp. 73 87.

Bank, L. C. (1989). Flexural and shear moduli of full-section fiber reinforced plastic (FRP) pultruded beams, *Journal of Testing and Evaluation* **17**(1): 40 45.

Bank, L. C., Cofie, E. & Gerhardt, T. D. (1992). A new test method for the determination of the flexural modulus of spirally wound paper tubes, *Journal of Engineering Materials and Technology* **114**: 84 89.

Barbero, E. & GangaRao, H. V. S. (1991). Structural applications of composites in infrastructure, Part 1, *Sampe* **27**(6): 9 - 16.

Barker, K. (2003). *The Barker Review of housing supply*, Office of the Deputy Prime Minster.

BSI. (1964). *BS 3580:1964. Guide to design considerations on the strength of screw threads.*, British Standard Institution.

BSI. (1995a). *EN1993 Eurocode 3: Design of steel structures*, British Standard Institution.

BSI. (1995b). *EN1994 Eurocode 4: Design of composite steel and concrete structures*, British Standard Institution.

BSI. (1995c). *EN1995 Eurocode 5: Design of timber structures*, British Standard Institution.

BSI. (1998). *BS 6946:1998. Specification for: Metal channel cable supports systems for electrical installations.*, British Standard Institution.

BSI. (2002). *BS EN 150 13706-2:2002 Reinforced plastics composites - Specifications for pultruded profiles - Part 2: Methods of test and general requirements*, British Standard Institution.

Buchanan, A., Honey, H. & Brian, G. (1994). Energy and carbon dioxide implications of building construction, *Energy and Buildings* **20**: 205 217.

Byers, M. & Singleton, M. (1999). *Startlink system of pultruded GRP profiles for structural systems*, Inter. Patent Application No. PCT/GB99/03382.

Calvert, G., Lesniak, J. R. & Honlet, M. (2002). Applications of modern automated photoelasticity to industrial problems, *Insight* **44**(4).

Caughey, R. A. & Scott, W. B. (1929). A practical method of for the design of I-beams haunched in concrete, *Structural Engineer* **7**(8): 275 293.

Clarke, J. L. (ed.) (1996). *Structural design of polymer composites- EUROCOMP*, E&FN Spon, London.

Creative Pultrusions Inc. (2006). *www.creativepultrusions.com.* visited March 2006.

Curtis, W. (1987). *Modern Architecture since 1900*, 2nd edn, Prentice Hall.

Dutta, P. K. (1995). Durability of FRP composites, *Fibre Reinforced Structural Plastics in Civil Engineering*, Indian Institute of Technology, McGraw-Hill, Madras, pp. 360 370.

Egan, J. (1998). *Egan Report Rethinking Construction*, Office of the Deputy Prime Minster.

Evernden, M. C. & Mottram, J. T. (2005). Characterisation of unistrut connection method with pultruded fiber reinforced polymer channels, *Journal of Materials in Civil Engineering*. Special Issue (Accepted March 2005).

Farstad, A. (ed.) (1982). *Holy Bible: The New King James Version Old Testament*, Thomas Nelson.

Fiberline Ltd. (2006). *www.fiberline.com*. visited March 2006.

Finnimore, B. (1989). *Houses from the factory: System Building and the Welfare State*, Rivers Oram Press, London.

GangaRao, H. V. S. & Sotiropoulos, S. N. (1994). Structural efficiency of connectors on pultruded FRP materials, *Proc. 39th International SAMPE Symposium*, pp. 382 390.

GangaRao, H. V. S., Vijay, P. V. & Altizer, S. D. (1995). Durability of glass composites under alkanine and prestress environment, *Fibre Reinforced Structural Plastics in Civil Engineering*, Indian Institute of Technology, McGraw-Hill, Madras, pp. 360-370.

Gaur, U. & Miller, B. (1990). Effects of environmental exposure on fiber/epoxy interfacial shear strength, *Polymer Composites* 11(4): 217.

Ghorbel & Valentini (1993). Hydrothermal effects on the physio-chemical properties of pure and glass reinforced polyester and vinylester resins, *Polymer Composites* 14: 324 334.

Gibb, A. & Goodier, C. (2005). *The value of UK market for offsite*, Promoting Off-site Production Applications, www.prOSPa.org. visited March 2005.

Green, S. D. (1996). *Smart value Management: A group decision support methodology for building design*, PhD thesis, University of Reading.

Gropius, W. (1926). *Princpiles of Bauhus Production*, Bauhaus Dessau.

Gulvanessian, H., Galgora, J. & Holicky, M. (2002). *Designers guide to EN 1990 Eurocode: Basics of structural design*, Thomas Telford, London.

Harrison, D. D. (1946). *Tomorrow's Houses*, Pilot Press Ltd, London, chapter IV An outline of Pre-fabrication.

Hayes, M. D. & Lesko, J. J. (2004). The effect of non-classical behaviours on the measurement of the Timoshenko shear stiffness, *2nd International Conference on FRP Composites in Civil Engineering (CICE 2004)*, University of Adelaide, p. 873.

Head, P. R. (1994). Cost effective advanced composite structures designed for life in the infrastructure, *Proc 22nd British Plastic Federation Composites Congres*, British Plastic Federation, London.

Head, P. R. (1995). Composite materials for bridges and structures, *Proc 1st Israeli Workshop on Composite Materials for Civil Engineering Construction*, National Building Research Institute, Technion, Israel, pp. 136 144.

Head, P. R. (1996). High performance structural materials - advanced composites, *15th Congress, International association for Bridge and Structural Engineering*, IABSE, Copenhagen.

Head, P. R. & Churchman, A. E. (1989). Design, specification and manufacture of a pultruded composite construction system, *Symposium 'Mass Production Composites'*.

Herbet, G. (1984). *The dream of the factory-made house*, MIT Press.

Hofer, K. E., Skaper, G. N., Rao, N. & Bennett, L. C. (1986). Effect of moisture on fatigue and residual strength loses of various composites, *Proc. 41st Annual*

Conference, Reinforced Plastics/Composite Institue, Society of the Plastics Industry, pp. Session 7 B, 1 7.

Hollaway, L. (1993). *Polymer composites for civil and structural engineering*, Balckie Academic & Professional, Glasgow.

Hutchings, J. F. (1998). *Builders Guide to Modular Construction*, Mc Graw Hill.

Kaiser, H. J. (1945). Prefabricated Plastic Houses, *Technical report*, H. J. Kaiser Company.

Karbhari, V. M., Chin, J. W. & Reynaud, D. (2000). Critical gaps in durability for FRP composites in civil infrastructure, *Proc. 45th International Symposium and Exhibition, Society for the Advancement of Material and Process Engineering*, Vol. 45, SAMPE, pp. 549–563.

Karbhari, V. M. & Xie, M. (1998). Investigation of Bond between Composites: Use of Peel Test, *Journal of Composite Materials* **32**(21).

Keller, T., Castro, J., Dooley, S. & Dubois, V. (2001). Use of fibre reinforced polymers in bridge construction, *Technical report*, Swiss Federal Institute of Technology, Composite construction Laboratory CCLab, Lausanne.

Khennane, A. & Melchers, R. E. (2000). Fiber reinforced polymer for infrastructure application, durability and life predictibility- A Review, *Technical report*, Dept of Civil, Surveying and Environmental Engineering, University of Newcastle, New South Wales, Australia.

Kishima, T., Watanabe, T. & Mesiarashi, S. (2004). Bending properties of secondary bonded pultruded I-shaped FRP beams, *Proc. International Conference on FRP Composites in Civil Engineering (CICE 2004)*, University of Adleliade, p. 837.

Knowles, P. R. (1971). *Composite steel and reinforced concrete structures*, Buuterworths, London.

Kobayashi, A. S. (ed.) (1993). *Handbook on Experimental Mechanics*, 2nd edn, John Wiley & Sons.

Kuenzi, E. W. & Wilkinson, T. L. (1971). Composite timber beams- Effect of adhesive or fastener rigidity, Forest Prod. Lab. Rep. 152, *Technical report*, U.S.D.A. Forest Service.

Kulak, G. L., Fisher, J. W. & Struik, J. H. A. (2000). *Guide to design criteria for bolted and riveted joints*, 2nd edn, American Institute of Steel Construction, chapter 4.

Lane, A. (2002). *An experimental investigation of buckling mode interaction in PFRP columns*, PhD thesis, University of Warwick, UK.

Latham, M. (1994). *The Latham Report: Review of Procurement and Contractual Arrangements in the UK Construction Industry*, Department of the Environment.

Lawson, R. M., Grubb, P. J., Prewer, J. & Trebilcock, P. J. (1999). Modular construction using light steel framing: An architects guide, *Technical report*, Steel Construction Institute Publications, Berkshire.

Lawson, R. M., Ogden, R. G., Pedreschi, R., Grubb, P. J. & Popo-Ola, S. O. (2005). Developments in prefabricated systems in light steel and modular construction, *The Structural Engineer*. Evening meeting.

LeCuyer, A. (2003). *Steel and Beyond: New Strategies for Metals in Architecture*, BirkhSuser.

Leggart, A. (1984). *GRP and Buildings: A design guide for architects and engineers*, Buttersworth, London.

Leonard, L. (1990). Rebuilding the infrastructure with advanced composites, *Advanced Composites* pp. 43 7.

Lesniak, J. R. (2002). *GFP1000 User Manual- Appendix A*, Stress Photonics.

Lesniak, J. R., Zickel, M. J., Welch, C. S. & Johanson, D. F. (1997). An innovative polariscope for photoelastic stress analysis, *SEM Conference, Seattle, USA*.

Leven, M. M. (1963). *Photoelasticity*, Pergamon, New York, chapter Epoxy resins for photoelastic use.

Liao, Y. T. (1989). A study of glass fiber-epoxy composite interface, *Polymer Composites* **10**(6): 424.

Milburn, J. & Bowler, K. (2005). A review of off-site manufacturing, *Offsite Construction* .

Miles, J. (2003). Opportunity of a lifetime, *Ingenia: The Royal Academy of Engineering* .

Mita Ltd. (2006). *www.mita.co.uk.* visited March 2006.

Mottram, J. T. (1991). Structural properties of pultruded E-glass fibre-reinforced polymeric box beam, *Structural Engineer* **69**(11): 211 220.

Mottram, J. T. (1993). Short- and long-term structural properties of pultruded beam assemblies fabricated using adhesive bonding, *Composite Structures* **25**: 387 395.

Mottram, J. T. (2004a). Friction and load transfer in bolted joints of pultruded fiber reinforced plastic profiles, *Proc. 2nd International Conference on FRP Composites in Civil Engineering, CICE 2004*, Univeristy of Adelaide.

Mottram, J. T. (2004b). Shear modulus of standard pultruded FRP material, *Journal of Composites for Construction* **8**(2): 141 147.

Mottram, J. T. & Turvey, G. J. (2003). Physical test data for the appraisal of design procedures for bolted joints in pultruded FRP structural shapes and system, *Progress in Structural Engineering and Materials* **5**(4): 195 222.

Nagaraj, V. & GangaRao, V. H. S. (1997). Static behaviour of pultruded GFRP beams, *Journal of Composites for Construction* **2**(1): 120 129.

Nanni, S., Matsubara & Hasuo (1992). Durability of braided epoxy impregnated Aramid FRP rods, *in* K. W. Neale & P. Labossiere (eds), *Advanced Composite Materials in Bridges and Structures*, CSCE, Montreal.

NCE (1992). Bridges. link to a tee, *New Civil Engineer, London* pp. 20 3.

Newmark, N. M., Seis, C. P. & Viest, I. M. (1952). Test and analysis of composite beams with incomplete interaction, *Proc. of the Society of Experimental Stress analysis*, Vol. 1, pp. 75 92.

Norris, C. B., Ericksen, W. S. & Kommers, W. J. (1952). Flexural rigidity of a rectangular strip of sandwich construction - Comparison between mathematical and results of tests, Forest Prod. Lab. Rep. 1505A, *Technical report*, U.S.D.A. Forest Service.

Oehlers, D. J. & Bradford, M. A. (1995). *Composite steel and composite structural members - Fundamental behavior*, Elsevier Science Ltd.

Pan, W., Gibb, A. & Dainty, A. (2005). Practices and strategies of leading UK house builders on Offsite-MMC, *Offsite Construction* .

Pawley, M. (1990). *Buckminster Fuller: How much does that building weigh?*, Trefoil Publications Ltd, London.

Pearce, A. (2006). Discussion: Is there a future in Modern Methods of Construction. Futurebuild Conference, London.

Pervsner, N. (1986). *Pioneers of Modern Design*, Peregrine Books.

Prian, L. & Barkatt, A. (1998). Chemical, thermochemical, and mechanical studies of FRP degradation in corrosive environments, *Proc. International Annual Conference and Corrosion Show*, Vol. 1, Houston, p. 455.

Prian, L. & Barkatt, A. (1999). Degradation mechanism of fiber-reinforced plastics and its implications to prediction of long-term behavior, *Journal of Material Science* **34**: 3977 3989.

Quattlebaum, J. B., Kent, A., Harries, K. A. & Petrou, F. M. (2005). Comparison of three flexural retrofit systems under monotonic and fatigue loads, *Journal of Bridge Engineering, ASCE* **10**(6): 731 740.

Ray, J. C., Lamanna, G. I. & Bank, L. C. (2001). Rapidly installed fiber-reinforced polymer (FRP) plates for upgrade of reinforced concrete bridges for the military, *High Performnce Materials in Bridges*, Kona Hawaii.

Roberts, T. M. & Marsi, H. M. K. J. A. H. (2003). Section properties and buckling behavior of pultruded FRP profiles, *Journal of Reinforced Plastics and Composites* **22**(14): 1305 1317.

SERC (1994). State Environmental Resource Center: Innovative Manufacturing Initiative 'Construction as a Manufacturing process', *New Builder* .

Sims, G. D. & Johnson, A. F. (1987). Mechanical and Structural Properties of a GRP Pultruded Section, *Composite Structures* **8**: 173 187.

Singleton, M. (2006). Private communication. Feburary, 2006.

Smith, S. T. & Teng, J. G. (2001). Interfacial stresses in plated beams, *Engineering Structures* **23**: 857 871.

Sotiropoulos, S. N., GangaRao, H. V. S. & Mongi, A. N. K. (1996). Theoretical and experimental evaluation of FRP components and systems, *Journal of Structural Engineering, ASCE* **120**(2): 464 485.

Stansfield, K. (2005). Meeting the housing numbers challenge with MMC, *The Structural Engineer*, pp. 16 17.

Starr, T. (2000). *Pultrusion for Engineers*, Woodhead Publishing Ltd.

Strongwell (2006). *www.strongwell.com*. visited March 2006.

Sun, H. T., Chang, F. K. & Qing, X. (2002). The response of composite joints with bolt clamping loads, Part 2: Model verification, *Journal of Composite Materials* **36**(1): 69 93.

Taljesten, B. (1997). Strengthening of beams by plate bonding, *Journal of Materials in Civil Engineering, ASCE* **9**(4): 206 212.

The Oxford English Dictionary (2006). *www.oed.com*, Oxford University Press.

Timoshenko, S. (1955). *Strength of Materials; Part 1: Elementary Theory and Problems*, Van Nostrand, New York.

Turvey, G. J. (2001). Evaluation of the structural performance of box beams fabricated from a system of pultruded profiles, *Proc. 1st International Conference on Composites in Construction, (CCC 2001)*, pp. 171 176.

Unistrut (2006). *www.unistrut.com*. visited March 2006.

Wagner, H. D., Maron, G. & Roman, I. (1982). Analysis of several loading methods for simultaneous determination of young's and shear modulus in composites, *Fibre Science and Technology* (16): 61   65.

Waschmann, K. (1939). *Building the Wooden House*, Birkhauser.

Yam, L. C. P. (1981). *Design of Composite Steel-Concrete Structures*, Surrey University Press.

Yeomans, D. (1997). *Conctruction Since 1900: Materials*, Batsford.